

12. 667

NATIONAL ADVISORY COMMITTEE
FOR AERONAUTICS

TECHNICAL NOTE

No. 1327

JUN 16 1947

WIND-TUNNEL INVESTIGATION OF THE EFFECT OF POWER
AND FLAPS ON THE STATIC LATERAL CHARACTERISTICS
OF A SINGLE-ENGINE LOW-WING AIRPLANE MODEL

By Vito Tamburello and Joseph Weil

Langley Memorial Aeronautical Laboratory
Langley Field, Va.



Washington

June 1947

NACA LIBRARY
LANGLEY MEMORIAL AERONAUTICAL
LABORATORY
Langley Field, Va.

NATIONAL ADVISORY COMMITTEE FOR AERONAUTICS

TECHNICAL NOTE NO. 1327

WIND-TUNNEL INVESTIGATION OF THE EFFECT OF POWER
AND FLAPS ON THE STATIC LATERAL CHARACTERISTICS
OF A SINGLE-ENGINE LOW-WING AIRPLANE MODEL

By Vito Tamburello and Joseph Weil

SUMMARY

As part of a comprehensive investigation of the effect of power, flaps, and wing position on static stability, tests were made in the Langley 7- by 10-foot tunnel to determine the lateral-stability characteristics with and without power of a model of a typical low-wing single-engine airplane with flaps neutral, with a full-span single slotted flap, and with a full-span double slotted flap.

Power decreased the dihedral effect regardless of flap condition, and the double-slotted-flap configuration showed the most marked decrease. The usual effect of power in increasing the directional stability was also shown. Deflection of the single slotted flap produced negative dihedral effect, but increased the directional stability. The effects of deflecting the double slotted flap were erratic and marked changes in both effective dihedral and directional stability occurred. The addition of the tail surfaces always contributed directional stability and generally produced positive dihedral effect.

INTRODUCTION

Recent trends in aeronautics have been toward the development of airplanes with increased power and increased wing loadings. The realization of these advances, however, has introduced new and serious problems in the stability and control characteristics of the airplane. Increased engine power has been shown

to produce large slipstream effects and trim changes, whereas increased wing loadings have presented the problem of obtaining higher lift for take-off and landing without impairing stability and control.

A comprehensive investigation was undertaken at the Langley Laboratory in 1941 to determine the effects of power, full-span flaps, and the vertical position of the wing on the stability and control characteristics of a model of a typical single-engine airplane. The present work includes the lateral-stability and control characteristics of the model as a low-wing airplane. The results of the longitudinal-stability investigation with the model as a low-wing airplane are presented in reference 1.

COEFFICIENTS AND SYMBOLS

The results of the tests are presented as standard NACA coefficients of forces and moments. Rolling-, yawing-, and pitching-moment coefficients are given about the center-of-gravity location shown in figure 1 (26.7 percent of the mean aerodynamic chord). The data are referred to the stability axes, which are a system of axes having their origin at the center of gravity and in which the Z-axis is in the plane of symmetry and perpendicular to the relative wind, the X-axis is in the plane of symmetry and perpendicular to the Z-axis, and the Y-axis is perpendicular to the plane of symmetry. The positive directions of the stability axes, of the angular displacements of the airplane and control surfaces, and of the hinge moments are shown in figure 2.

C_L	lift coefficient (L/qS)
C_X	longitudinal-force coefficient (X/qS)
C_Y	lateral-force coefficient (Y/qS)
C_l	rolling-moment coefficient (L/qSb)
C_m	pitching-moment coefficient (M/qSc')
C_n	yawing-moment coefficient (N/qSb)

- C_{H_r} rudder hinge-moment coefficient. $(H_r/qb_r\bar{c}_r^2)$
 T_c' effective thrust coefficient based on wing area
 (T_{eff}/qS)
 Q_c torque coefficient $(Q/\rho V^2 D^3)$
 V/nD propeller advance-diameter ratio
 η propulsive efficiency $(T_{eff}V/2\pi nQ)$
 Lift = -Z
 $\left. \begin{array}{l} X \\ Y \\ Z \end{array} \right\}$ forces along axes, pounds
 $\left. \begin{array}{l} L \\ M \\ N \end{array} \right\}$ moments about axes, pound-feet
 H_r rudder hinge moment, pound-feet
 T_{eff} propeller effective thrust, pounds
 Q propeller torque, pound-feet
 q free-stream dynamic pressure, pounds per square
 foot $\left(\frac{\rho V^2}{2}\right)$
 S wing area (9.44 sq ft on model)
 c airfoil section chord, feet
 c' wing mean aerodynamic chord (M.A.C.) (1.36 ft on
 model)
 \bar{c}_r rudder root-mean-square chord back of hinge line
 (0.353 ft on model)
 b wing span, unless otherwise designated (7.458 ft
 on model)
 b_r rudder span along hinge line (1.508 ft on model)
 V air velocity, feet per second

D	propeller diameter (2.00 ft on model)
n	propeller speed, revolutions per second
and	
ρ	mass density of air, slugs per cubic foot
α	angle of attack of fuselage center line, degrees
ψ	angle of yaw, degrees
δ	control-surface deflection with respect to chord line, degrees
β	propeller blade angle at 0.75 radius (25° on model)
Γ_{eff}	effective dihedral, degrees
$C_{l\psi}$	rate of change of rolling-moment coefficient with angle of yaw ($\partial C_l / \partial \psi$)
$C_{n\psi}$	rate of change of yawing-moment coefficient with angle of yaw ($\partial C_n / \partial \psi$)
$C_{Y\psi}$	rate of change of lateral-force coefficient with angle of yaw ($\partial C_Y / \partial \psi$)
Subscripts:	
e	elevator
r	rudder
av	average
trim	trim condition

MODEL AND APPARATUS

The tests were made in the Langley 7- by 10-foot tunnel, which is described in references 2 and 3. The model was a modified $\frac{1}{5}$ -scale model of a fighter airplane

and is shown in figure 1. No landing gear was used for the tests. The wing was fitted with a 40-percent-chord double slotted flap that covered 93 percent of the span and was designed from data in reference 4. For the flap-neutral tests, the flap was retracted and the gaps were faired to the airfoil contour with modeling clay. The rear portion of the flap was deflected 30° for the single-slotted-flap tests, and for tests with the double slotted flap both parts of the flap were deflected 30° . (See detail of flaps in fig. 1.) For the flap-deflected conditions, the gap between the inboard ends of the flap (directly below the fuselage) was sealed with Scotch cellulose tape.

A more detailed drawing of the tail assembly is shown in figure 3. The horizontal tail had an inverted Clark Y section and was equipped with a fixed leading-edge slot. The reasoning behind the horizontal tail design is treated in reference 1. When the model was tested with the flaps neutral, the slot was sealed.

The vertical tail (fig. 3) was offset $1\frac{1}{2}^\circ$ to the left to help counteract the asymmetry in yawing moment due to slipstream rotation.

Power for the 2-foot-diameter, three-blade, right-hand, metal propeller was obtained from a 56-horsepower water-cooled induction motor mounted in the fuselage nose. The motor speed was measured by means of an electric tachometer. The dimensional characteristics of the propeller are given in figure 4.

Rudder hinge moments were measured by means of an electric strain gage mounted in the fin.

TESTS AND RESULTS

Test Conditions

The tests were made in the Langley 7- by 10-foot tunnel at dynamic pressures of 12.53 pounds per square foot for the power-on tests with the double slotted flap and 16.37 pounds per square foot for all other tests. These dynamic pressures correspond to airspeeds of about 70 and 80 miles per hour, respectively. The test

Reynolds numbers were about 875,000 and 1,000,000, based on the wing mean aerodynamic chord of 1.36 feet. Because of the turbulence factor of 1.6 for the tunnel, effective Reynolds numbers (for maximum lift coefficients) were about 1,400,000 and 1,600,000, respectively.

Corrections

All power-on data have been corrected for tare effects caused by the model support strut. The power-off data, however, have not been corrected for tare effects because they have been found to be relatively small and erratic on similar models, especially with flaps deflected. Jet-boundary corrections have been applied to the angles of attack, longitudinal-force coefficients, and tail-on pitching-moment coefficients. The corrections were computed as follows:

$$\Delta\alpha = 57.3 \delta_w \frac{S}{C} C_L \text{ (degrees)}$$

$$\Delta C_X = -\delta_w \frac{S}{C} C_L^2$$

$$\Delta C_m = -57.3 \left(\frac{\delta_T}{\sqrt{q_t/q}} - \delta_w \right) \frac{S}{C} \frac{\partial C_m}{\partial i_t} C_L$$

where

δ_w jet-boundary-correction factor at wing (0.1125)

δ_T total jet-boundary-correction factor at tail
(varies between 0.200 and 0.210)

S model wing area (9.44 sq ft)

C tunnel cross-sectional area (69.59 sq ft)

$\partial C_m / \partial i_t$ change in pitching-moment coefficient per degree
change in stabilizer setting as determined
in tests

q_t/q ratio of effective dynamic pressure over the
horizontal tail to free-stream dynamic
pressure

All jet boundary corrections were added to the test data.

Test Procedure

A propeller calibration was made by measuring the longitudinal force with the model at zero yaw, zero angle of attack, flaps neutral, and tail removed for a range of propeller speed. The effective thrust coefficient was then computed from the relation

$$T_c' = C_X(\text{propeller operating}) - C_X(\text{propeller removed})$$

The motor torque was also measured and the propeller efficiency computed. The results of the propeller calibration ($\beta = 25^\circ$) are shown in figure 5. Figure 6 illustrates the relation between T_c' and C_L , which is representative of a constant-power operating curve for a constant-speed propeller. For simplicity, a straight line variation of T_c' with C_L was used ($T_c' = 0.161C_L$). The propeller speed required to simulate this thrust condition was determined from figures 5 and 6. The approximate amount of thrust horsepower represented is given in figure 7 for various model scales and wing loadings. The value of T_c' for the tests with the propeller windmilling was about -0.005.

At each angle of attack for power-on yaw tests the propeller speed was held constant throughout the yaw range. Because the lift and thrust coefficients vary with yaw when the propeller speed and angle of attack are held constant, the thrust coefficient is strictly correct only at zero yaw.

Lateral-stability derivatives were obtained from pitch tests at angles of yaw of $\pm 5^\circ$ by assuming a straight-line variation between these points. The effective dihedral angle was determined from the derivative $C_{L\psi}$

by considering $\Gamma_{\text{eff}} = \frac{C_{L\psi}}{0.0002}$.

Presentation of Results

An outline to the figures presenting the results of the investigation is given as follows:

Figure

Effect of power on $C_{L\psi}$, $C_{n\psi}$, and $C_{Y\psi}$:	
Flap neutral	8
Single slotted flap deflected	9
Double slotted flap deflected	10
Increments in $C_{L\psi}$, $C_{n\psi}$, and $C_{Y\psi}$ resulting from:	
Power	11
Flap deflection	12
Tail surfaces	13
Aerodynamic characteristics in yaw:	
Flap neutral	14
Single slotted flap deflected	15
Double slotted flap deflected	16
Effect of wing and fuselage modifications on aerodynamic characteristics in yaw with the single slotted flap deflected	
	17
Rudder control characteristics:	
Flap neutral	18
Single slotted flap deflected	19
Double slotted flap deflected	20

DISCUSSION

Effective-Dihedral Derivative ($C_{L\psi}$)

The variation of effective-dihedral derivative ($C_{L\psi}$) with lift coefficient (figs. 8 to 10) was generally smooth for all conditions with the exception of the double-slotted-flap configuration. The irregularity of the curves for this condition is attributed to unsteady lift increments of the flap on the right and left wing panels. (See reference 1.)

Effect of power.- For all configurations tested, except those with the double slotted flap, the variation of effective dihedral with lift coefficient was approximately linear for power-off conditions and there was

almost no variation for the tail-off configurations. With power on, however, the effective dihedral generally decreased with increasing lift coefficient for both constant power and constant thrust conditions (figs. 8 to 10). Unusually large variations of effective dihedral (14° to -25°) were obtained with the double-slotted-flap configuration.

The incremental values of effective dihedral ($\Delta C_{L\psi}$) resulting from a change from windmilling propeller to constant power are shown in figure 11. These data show that increasing power caused a decrease in effective dihedral. This decrease was greater as the lift coefficient was increased except for the double-slotted-flap configuration for which the unsteady lift increments of the flap probably caused a different trend. Part of the decrease in effective dihedral with power resulted from an increase in slipstream velocity over the trailing wing during sideslip, which tended to produce rolling moments in a direction that would give a decrease in effective dihedral. The increase in slipstream velocity over the wing-fuselage juncture probably magnified the wing-fuselage interference, which on the low-wing airplane caused a reduction in dihedral effect (reference 5) and thus caused an additional decrease in effective dihedral with power.

The reduction in effective dihedral caused by power (model with the tail on) ranged from 0° to 3° throughout the lift range for the flap-neutral case, from 1° to 5° for the single slotted flap, and from 11° to 19° for the double slotted flap.

Effect of flap deflection.- The effect of deflecting the single slotted flap on effective dihedral is shown in figure 12. Inasmuch as the double-slotted-flap configuration was not tested at lift coefficients low enough to make a direct comparison with the flap-neutral condition, the increments between single- and double-slotted-flap deflection are also indicated in figure 12 to show the effect of the double slotted flap.

Deflecting the single slotted flap always produced negative effective dihedral. With the tail on, the reduction of $C_{L\psi}$ caused by flap deflection was slightly less. The change in effective dihedral caused by flap deflection was almost independent of the power condition

used. The analysis in reference 6 indicates that part of the reduction in effective dihedral when the flaps are deflected can be attributed to the swept-forward position of the flaps.

Deflecting the double slotted flap has an erratic but pronounced effect on $C_{L\psi}$. The effective dihedral is reduced with power on but is increased with power off. This increase with power off is thought to be a result of the unsteady flow conditions obtained with the double slotted flap.

Effect of tail surfaces.- The effect of the tail surfaces on the effective dihedral is summarized in figure 13. The data show that the tail surfaces almost always contributed a positive dihedral effect; the increment was slightly greater with the power on. It should be noted that the rolling moment contributed by the vertical tail is dependent upon the distance from the X-axis (fig. 2) to the center of pressure of the vertical tail. For a given lift coefficient, therefore, it follows that the double-slotted-flap condition would show the greatest positive increment in $C_{L\psi}$ and the flap-neutral condition the least. This trend is shown to occur for the flap neutral and for the single slotted flap and, in the higher lift range, for the double slotted flap. Similar reasoning can be followed to explain the variation of $\Delta C_{L\psi}$ with lift coefficient. Further, inasmuch as the increment in $C_{L\psi}$ resulting from the tail is a function of tail lift, it is obvious that, if the rudder deflection for trim at the various angles of sideslip were considered, $\Delta C_{L\psi}$ would be somewhat reduced.

Effect of modifications.- In an attempt to reduce the large loss in effective dihedral that occurs in the flap-down power-on condition, several modifications were made to the model, tested with the single-slotted-flap configuration.

One change consisted in removing the flap center section beneath the fuselage, its span being equivalent to 9.7 percent of the flap span (fig. 1). This modification with constant power, however, gave only slightly less negative effective dihedral whereas, with power off, it decreased the effective dihedral somewhat. (See fig. 17(a).) The other modification consisted in

placing a spoiler beneath the fuselage as shown in figure 17(b). Again no noticeable improvement was evident for the critical constant-power condition (fig. 17(b)).

Directional-Stability Derivative ($C_{n\psi}$)

Effect of power.- The effects of power on the directional stability derivative ($C_{n\psi}$) are presented in figure 11. With the tail on, power always increased the directional stability for any flap configuration whereas with the tail removed, power produced both a small stabilizing and destabilizing tendency. The contribution of power to $C_{n\psi}$ for the model with tail on varied throughout the lift range from about 0 to -0.0011 for the flap-neutral configuration, -0.0010 to -0.0032 with the single slotted flap and -0.0004 to -0.0017 with the double slotted flap.

The effect of the windmilling propeller was to cause a destabilizing shift of about 0.00020 in $C_{n\psi}$ for most conditions. With the tail on and with the double slotted flaps deflected, the effect was considerably greater (see fig. 10).

Effect of flap deflection.- Deflection of the single slotted flap was found to increase the directional stability. (See fig. 12.) The data indicate that this increase is augmented when power is on and further increased when the tail surfaces are in place. The contribution of $\Delta C_{n\psi}$ due to single-slotted-flap deflection (model with tail on) ranges from -0.0015 to -0.0012 with the windmilling propeller and from -0.0022 to -0.0019 for the constant-power condition. It is shown in reference 5 that the increase in $-C_{n\psi}$ is partly caused by the favorable wing-fuselage interference on low wing designs, and is further increased by deflecting the flaps.

Deflecting the double slotted flap also increased the directional stability for all conditions except the power-on condition for the model with tail on for which a considerable destabilizing increment is shown.

Effect of tail surfaces.- The tail surfaces, as expected, always provide directional stability $-C_{n\psi}$ (See fig. 13.) For the windmilling condition, the tail contributions remained almost constant throughout the lift range for the flap-neutral and single-slotted-flap configurations. With constant power, however, the increment in $C_{n\psi}$ was found to increase as C_L increased. The increment, moreover, was always greater with power on than with power off.

It has been shown (reference 5) that the effect of wing-fuselage interference on fin effectiveness is favorable for low-wing designs. An explanation of this favorable interference is offered in reference 7. It is sufficient to say that for a low-wing airplane the vertical tail is mainly in a region of stabilizing sidewash.

The effect of tail configuration on the characteristics in yaw are contained in figures 14 to 16. Inasmuch as no rudder-free tests were made for the single-slotted-flap configuration, the rudder-free characteristics were estimated from cross plots of the rudder-hinge-moment and yawing-moment curves. Less directional stability existed in all cases when the rudder was free than when held fixed. No rudder lock occurred for any of the configurations tested although such a tendency was present. It is interesting to note that in the double-slotted-flap configuration with tail removed, the magnitude of $C_{n\psi}$ contributed by the flap is sufficient to cause a stable yawing-moment curve with the propeller removed and, to a lesser degree, with the propeller windmilling. (See figs. 16(a) and (b).)

Directional Control and Trim

Effect of power on rudder control and hinge-moment characteristics.- A summary of some of the principal control and hinge-moment parameters obtained from the results of the yaw tests (figs. 18 to 20) is given in table I.

The progressively reduced rudder effectiveness $\partial\psi/\partial\delta_r$ for the windmilling condition with single- and double-slotted-flap deflection is caused by the increased directional stability, which may be attributed to the flaps. With power on, the value of $\partial\psi/\partial\delta_r$ was considerably lower than with power off for the single-slotted-flap condition. It is apparent in this instance that the increase in directional stability caused by power was greater than that caused by the increase in q at the tail.

For the flap-neutral configuration only slight changes occurred in the hinge-moment parameters $\partial C_{h_r}/\partial\psi$ and $\partial C_{h_r}/\partial\delta_r$ with power. The thrust coefficient is low for this condition (low C_L) and therefore power effects would also be expected to be low. For the other flap conditions, the effect of power is to increase the values of the hinge-moment parameters. This effect is especially marked on values of $\partial C_{h_r}/\partial\psi$ for the double-slotted-flap condition.

Effect of power on trim.- A factor of prime importance to the pilot is the trim change with power. The dashed curve for $C_y = 0$ on the yawing-moment curves (figs. 18 to 20) indicates points on the C_n -curve at which the lateral force is zero. The point at which the curve for $C_y = 0$ intersects the C_n -axis gives the rudder deflection and yaw angle necessary to maintain straight flight with zero bank. The changes in rudder deflection required to trim with the wings level when power is applied and the corresponding changes in yaw angle are as follows:

Flap	α (deg)	$C_{L_{av}}$	$\Delta\delta_{r_{trim}}$ (deg)	$\Delta\psi_{trim}$ (deg)
Neutral	1.2	0.3	-2	0.1
Single slotted	9.7	2.1	-23.5	6.0
Double slotted	7.3	2.9	-28	6.5

These results show that although the trim changes caused by power are rather large, control could probably be maintained. The trim changes result from change of twist imparted to the slipstream by the propeller and are dependent upon blade-angle setting and other propeller characteristics. The use of a skewed thrust axis would

provide an ideal way to reduce the magnitude of the directional trim changes.

CONCLUSIONS

Tests were conducted on a powered model equipped with full-span single slotted and double slotted flaps to investigate the effects of power, flap deflection, and tail surfaces on the lateral stability and control characteristics. The following conclusions can be drawn from the data presented.

1. Effect of power:

(a) Power produced negative effective dihedral which generally increased with the lift coefficient.

(b) Application of power increased the directional stability of the complete model. Greater stability was realized as the lift coefficient increased.

2. Effect of flaps:

(a) Single-slotted-flap deflection produced negative effective dihedral, which was virtually independent of the power condition.

(b) Deflection of the single slotted flap produced positive increments of directional stability. The increase in directional stability was less pronounced as the lift coefficient increased.

(c) The effects of double-slotted-flap deflection were erratic and marked changes in both effective dihedral and directional stability occurred.

3. Effect of tail surfaces:

(a) The tail surfaces contributed positive effective dihedral except through part of the lift range in the double-slotted-flap configuration. No consistent variation with lift coefficient of the increment due to the presence of the tail existed among the configurations tested.

(b) Positive increments of directional stability were provided by the tail surfaces. These increments varied slightly throughout the lift range for the windmilling condition and increased with lift coefficient for the constant-power condition.

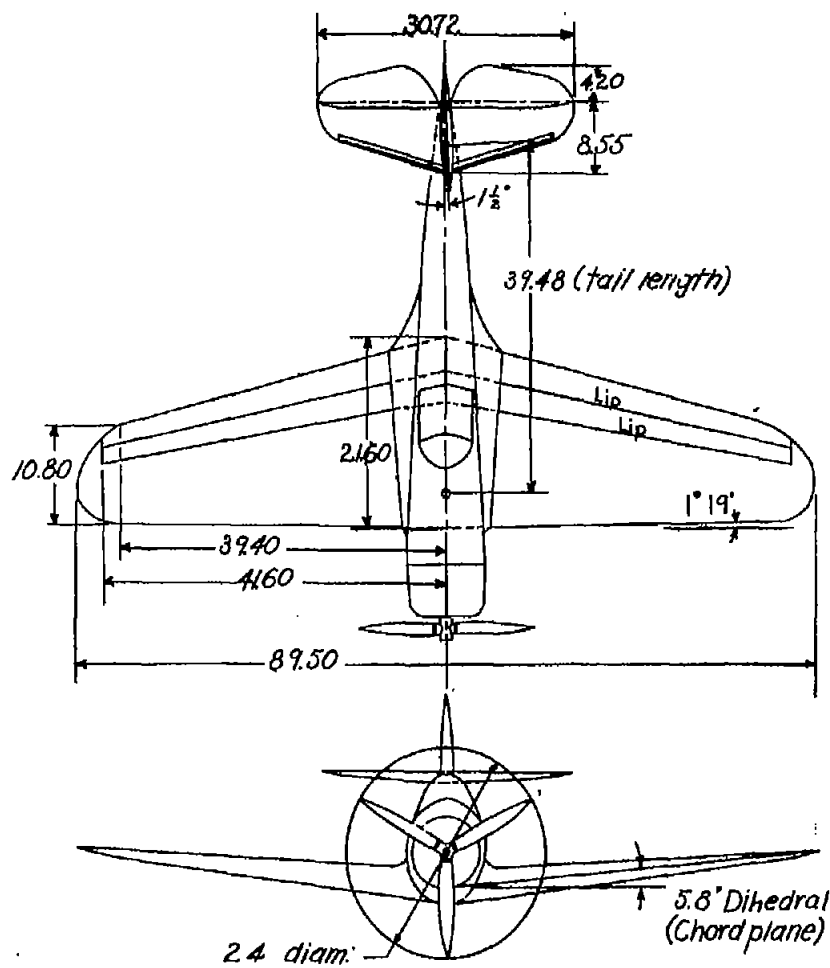
Langley Memorial Aeronautical Laboratory
National Advisory Committee For Aeronautics
Langley Field, Va., April 19, 1946

REFERENCES

1. Wallace, Arthur R., Rossi, Peter F., and Wells, Evalyn G.: Wind-Tunnel Investigation of the Effect of Power and Flaps on the Static Longitudinal Stability Characteristics of a Single-Engine Low-Wing Airplane Model. NACA TN No. 1239, 1947.
2. Harris, Thomas A.: The 7 by 10 Foot Wind Tunnel of the National Advisory Committee for Aeronautics. NACA Rep. No. 412, 1931.
3. Wenzinger, Carl J., and Harris, Thomas A.: Wind-Tunnel Investigation of an N.A.C.A. 23012 Airfoil with Various Arrangements of Slotted Flaps. NACA Rep. No. 664, 1939.
4. Harris, Thomas A., and Recant, Isidore G.: Wind-Tunnel Investigation of NACA 23012, 23021, and 23030 Airfoils Equipped with 40-Percent-Chord Double Slotted Flaps. NACA Rep. No. 723, 1941.
5. House, Rufus O., and Wallace, Arthur R.: Wind-Tunnel Investigation of Effect of Interference on Lateral-Stability Characteristics of Four NACA 23012 Wings, an Elliptical and a Circular Fuselage, and Vertical Fins. NACA Rep. No. 705, 1941.
6. Tucker, Warren A.: Wind-Tunnel Investigation of Effect of Wing Location, Power, and Flap Deflection on Effective Dihedral of a Typical Single-Engine Fighter-Airplane Model with Tail Removed. NACA TN No. 1061, 1946.
7. Pass, H. R.: Analysis of Wind-Tunnel Data on Directional Stability and Control. NACA TN No. 775, 1940.

TABLE I - SUMMARY OF RUDDER-CONTROL AND HINGE-MOMENT PARAMETERS

Flap	Power	α (deg)	C_L	$\frac{\partial C_n}{\partial \delta_r}$	$C_{n\psi}$	$C_{n\psi}$ (Tail off)	$\frac{\partial \psi}{\partial \delta_r}$	$\frac{\partial C_{h_r}}{\partial \psi}$	$\frac{\partial C_{h_r}}{\partial \delta_r}$
Neutral	Windmilling	1.2	0.3	-0.0010	-0.0018	0.0006	-0.56	-0.0020	-0.0055
Single slotted	Windmilling	9.7	2.0	-.0011	-.0025	.0005	-.44	-.0009	-.0048
Double slotted	Windmilling	7.3	2.6	-.0011	-.0029	-.0001	-.38	-.0035	-.0059
Neutral	Constant power	1.2	.3	-.0011	-.0019	.0007	-.58	-.0019	-.0047
Single slotted	Constant power	9.7	2.2	-.0017	-.0055	.0005	-.31	-.0080	-.0101
Double slotted	Constant power	7.3	3.1	-.0019	-.0053	0	-.36	-.0140	-.0117



Geometric characteristics

Wing area, sq ft	9.44
MAC, ft.	1.36
C.G. (percent MAC)	26.70
<i>Wing section</i>	
Root	NACA 2215
Tip	NACA 2209
Wing incidence, deg.	1.0

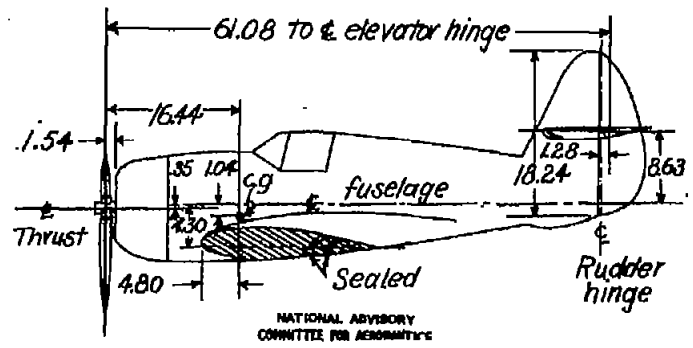
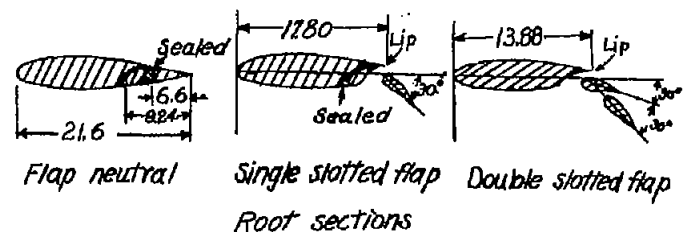


Figure 1.- Three-view drawing of model as a low-wing airplane.
All dimensions in inches.

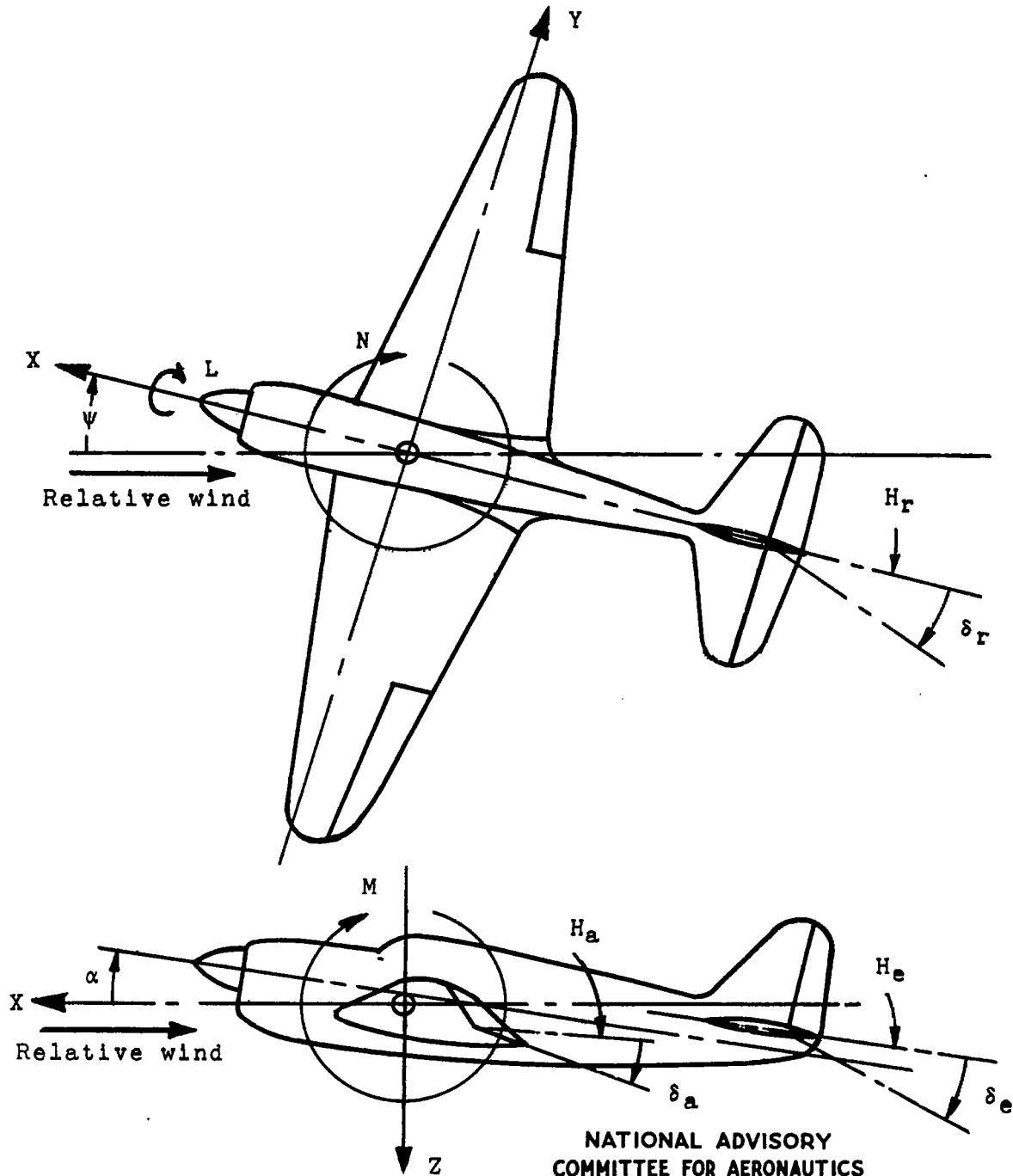
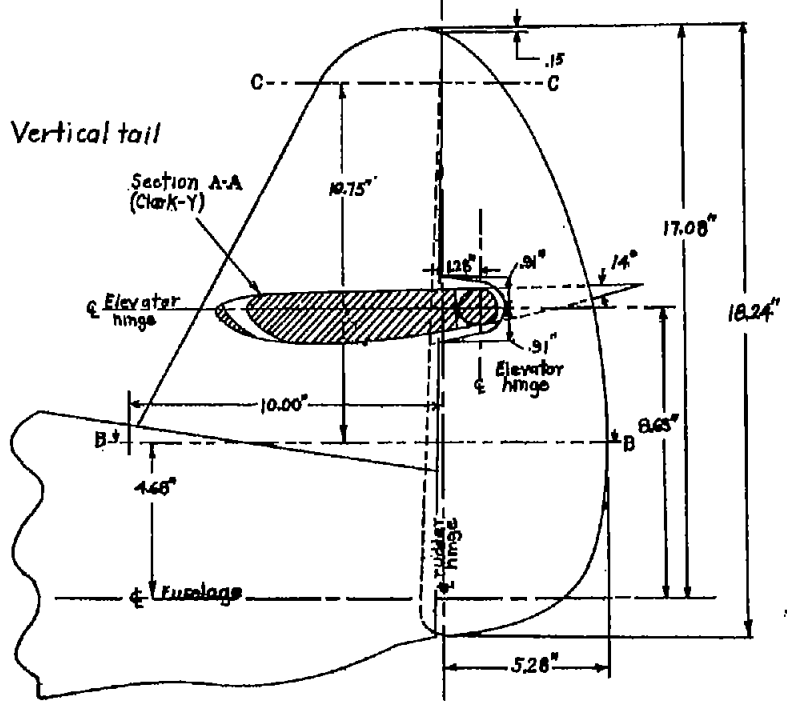
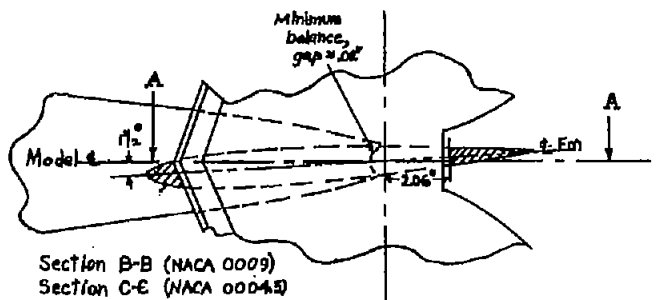
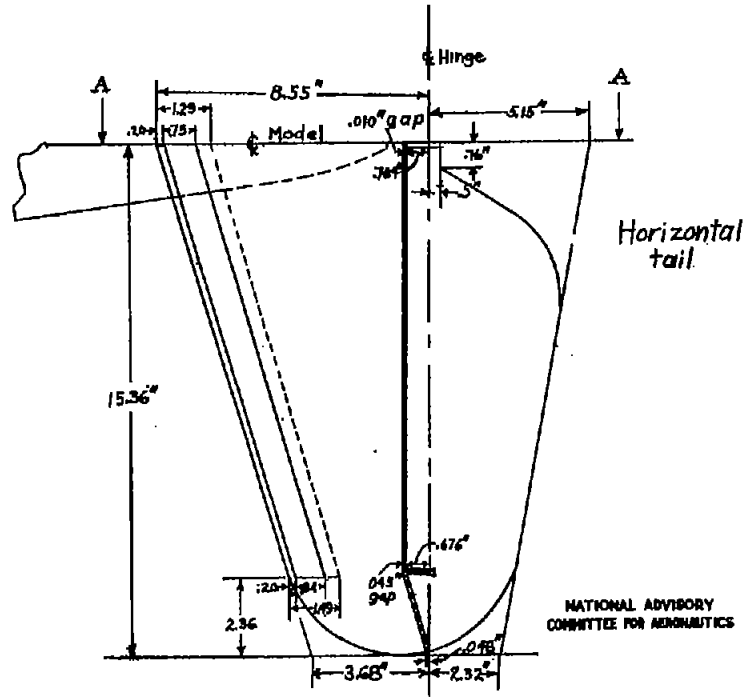


Figure 2 .- System of axes and control-surface hinge moments and deflections. Positive values of forces, moments, and angles are indicated by arrows. Positive values of tab hinge moments and deflections are in the same directions as the positive values for the control surfaces to which the tabs are attached.

Elevator area, sq ft . . .	0.671
Elevator rms chord, ft . . .	0.264
Rudder area, sq ft . . .	0.506
Rudder rms chord, ft . . .	0.353
Horizontal tail area, sq ft . . .	1.92
Vertical tail area, sq ft . . .	1.25
Elevator span, ft . . .	2.542
Rudder span, ft . . .	1.508



(a) Vertical tail.



(b) Horizontal tail.

Figure 3.- Model tail assembly.

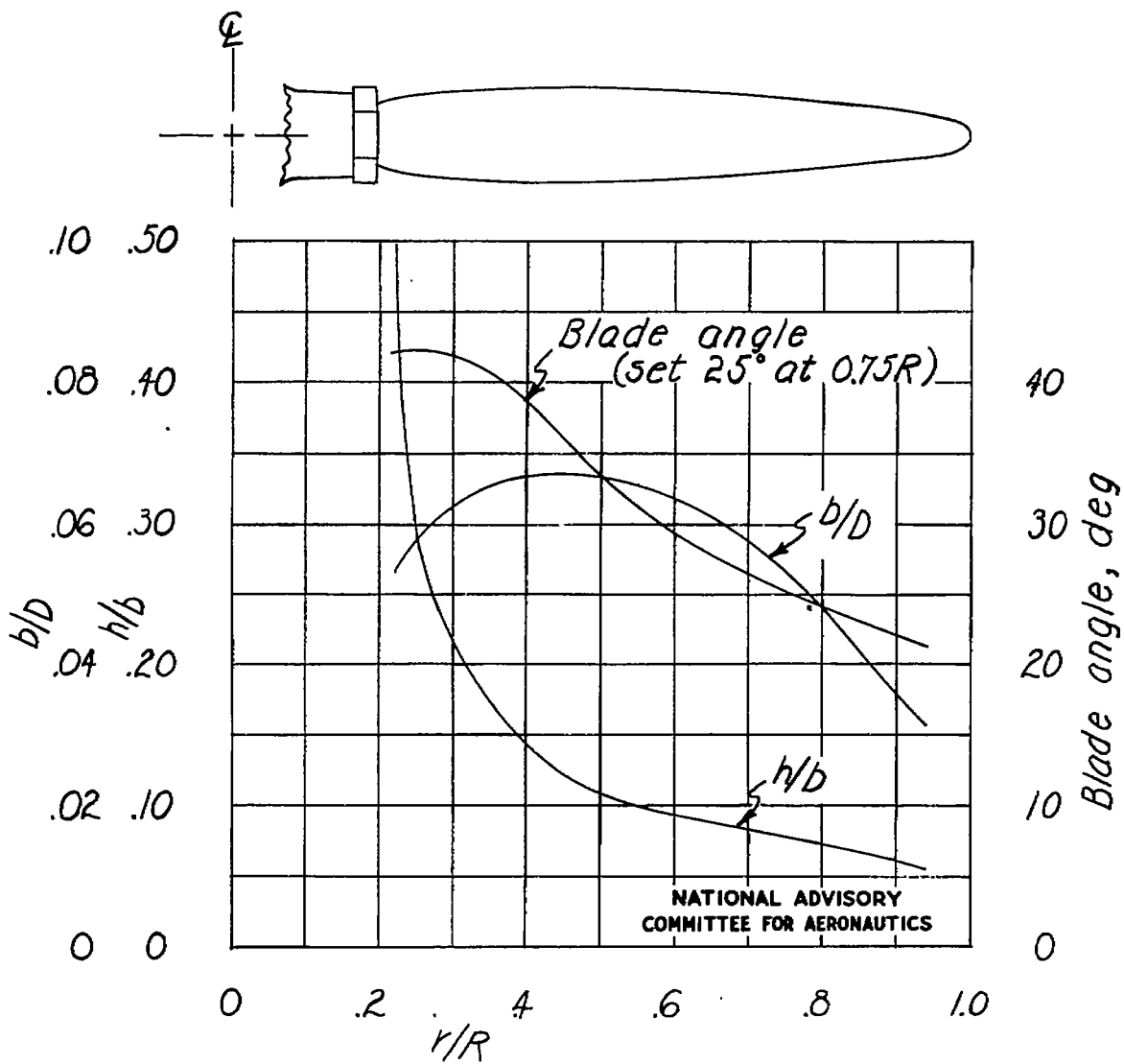


Figure 4.- Plan form and blade-form curves for the model propeller. D, diameter; R, radius to tip; r, station radius; b, section chord; h, section thickness; RAF 6 airfoil section.

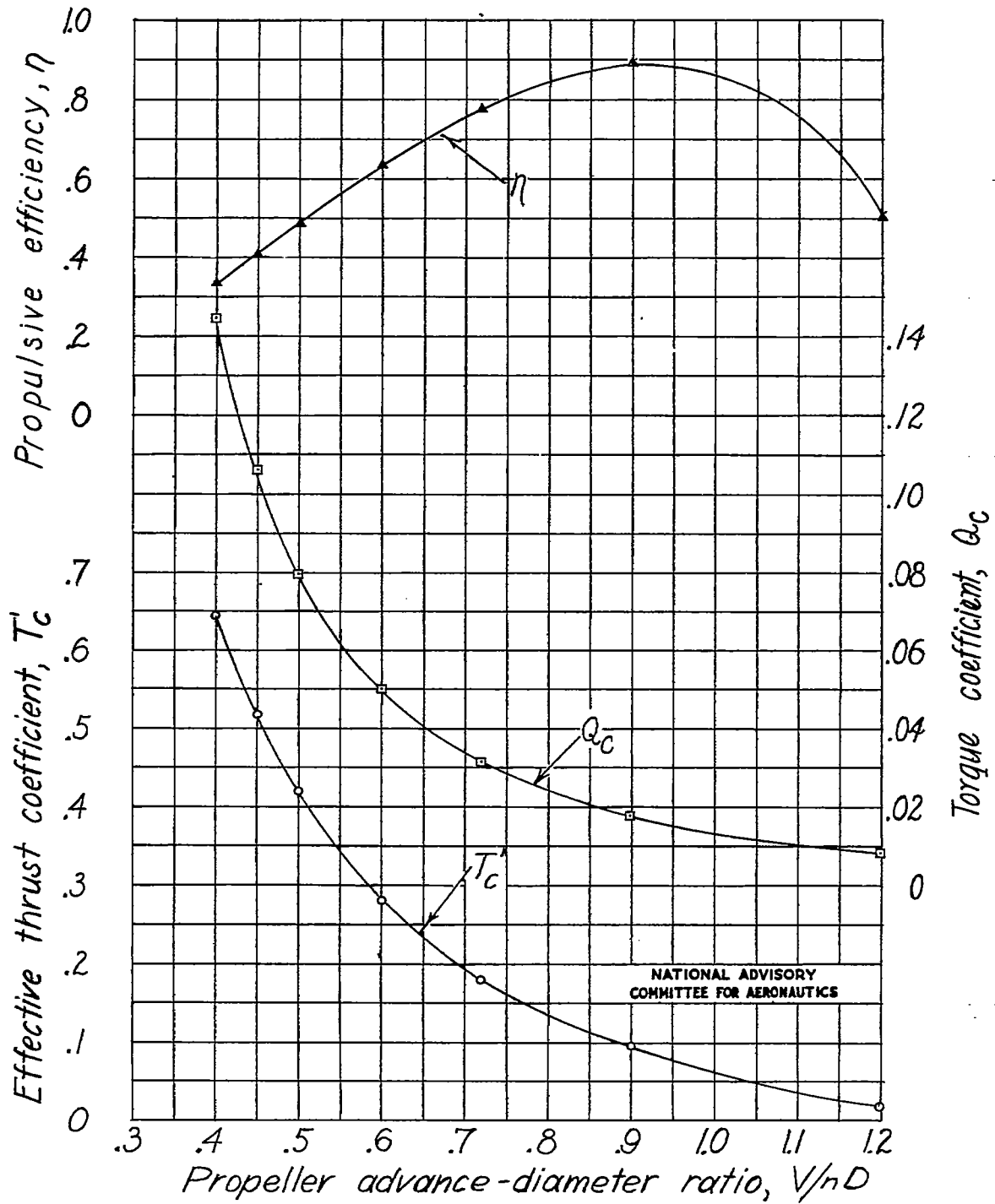


Figure 5.- Effective thrust coefficient, torque coefficient, and efficiency as functions of propeller advance-diameter ratio for the model of the low-wing airplane tested. $D = 2.0$ ft; $\beta = 25^\circ$.

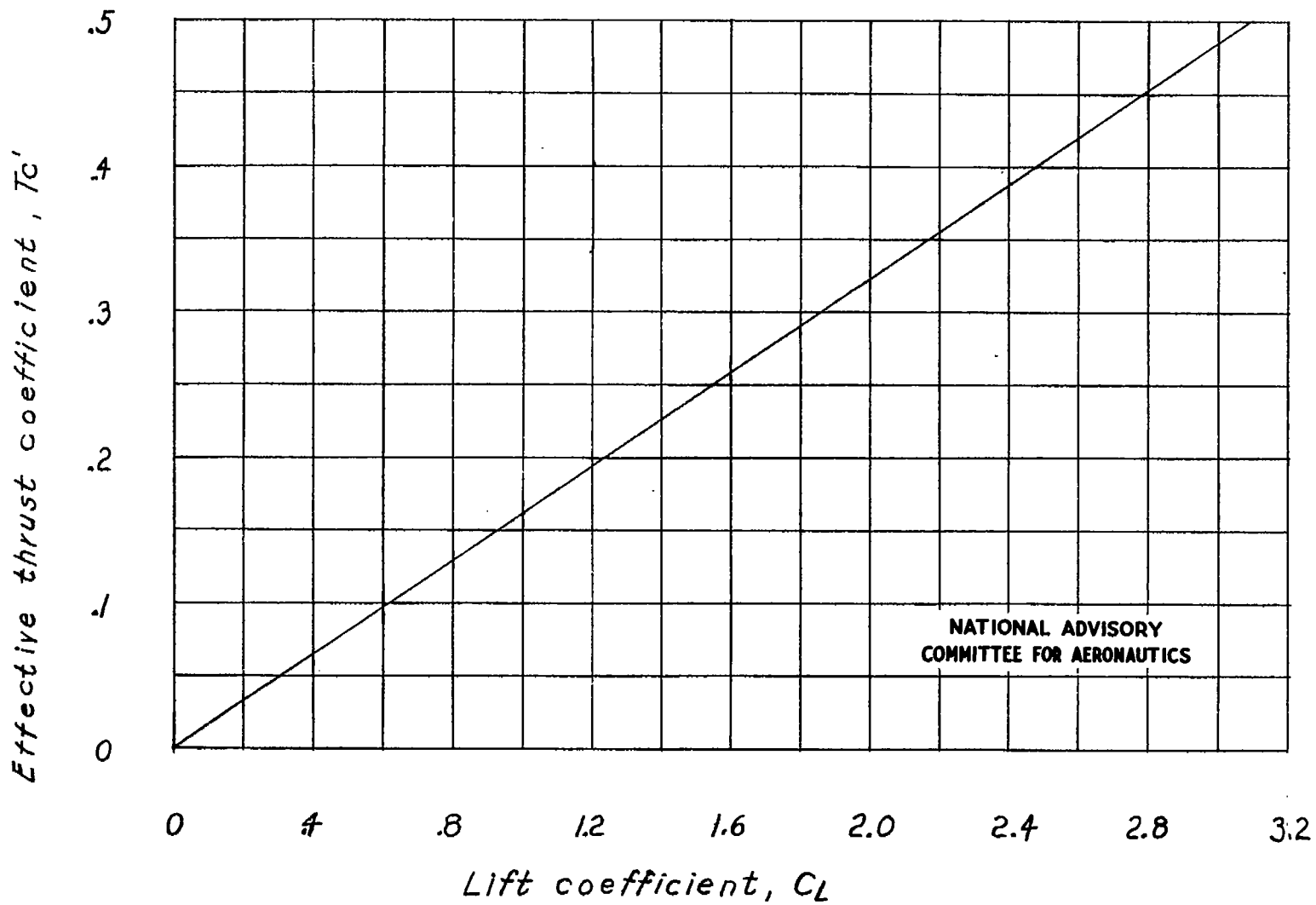


Figure 6.- Variation of effective thrust coefficient with lift coefficient for constant-power tests.

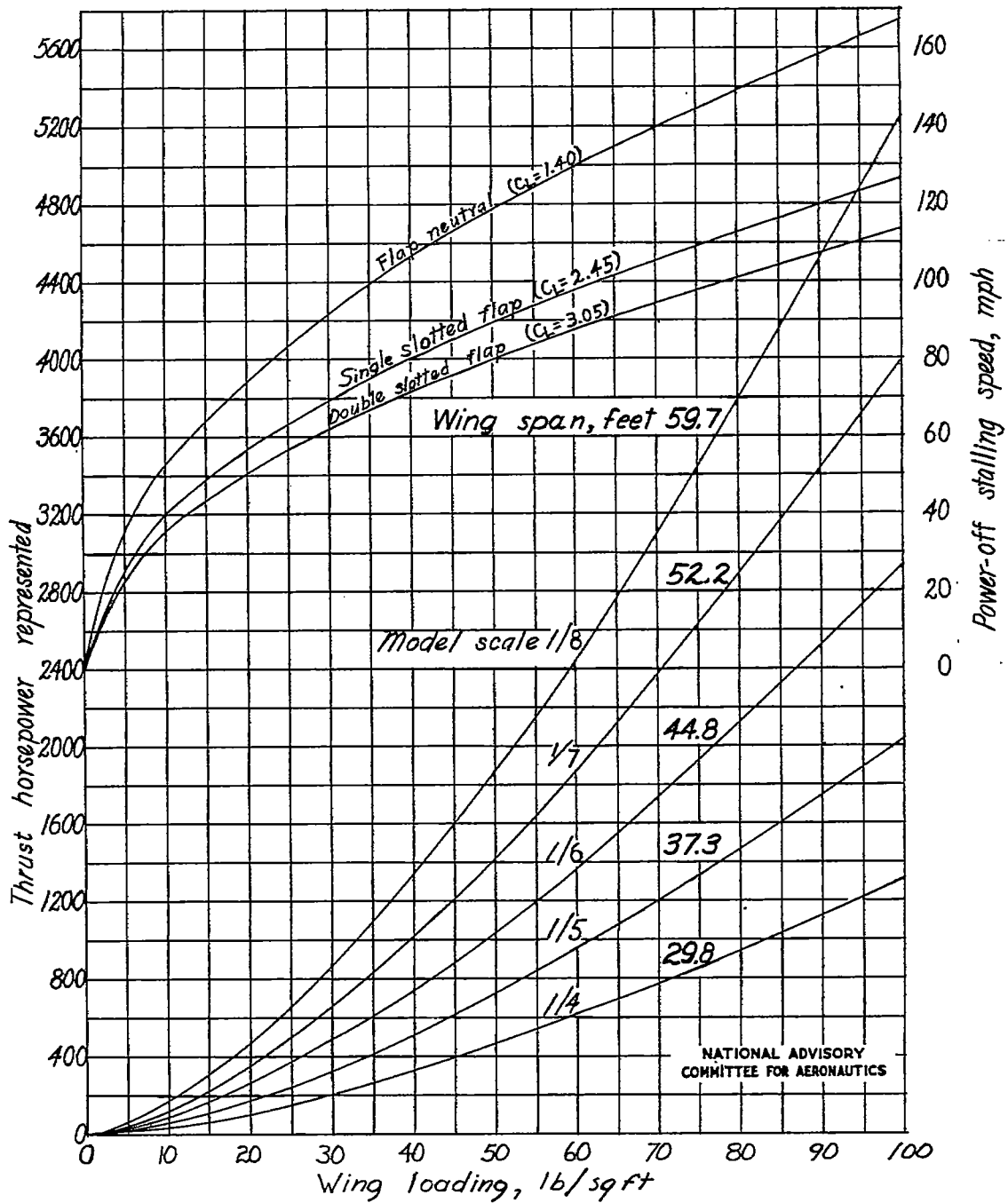
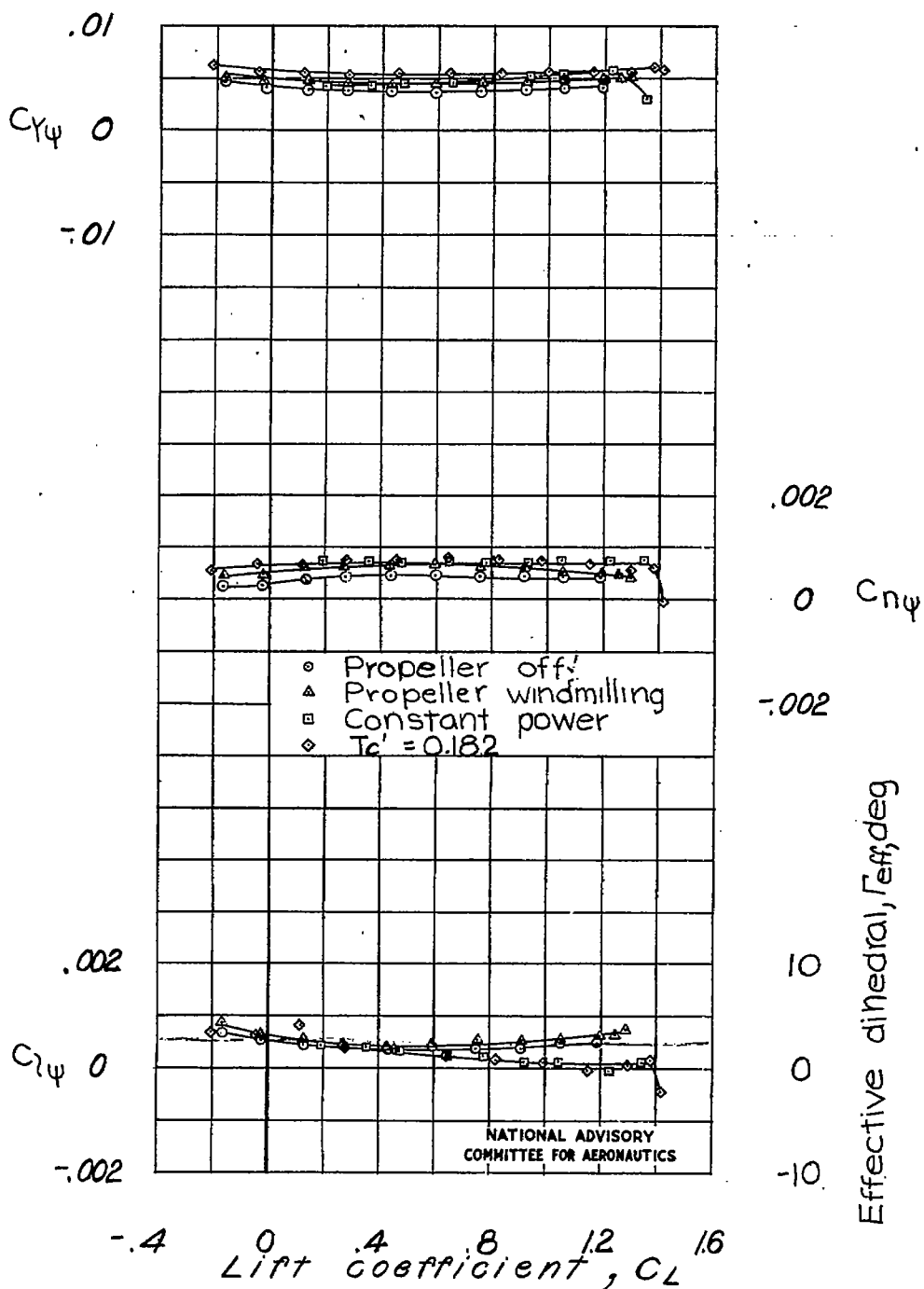
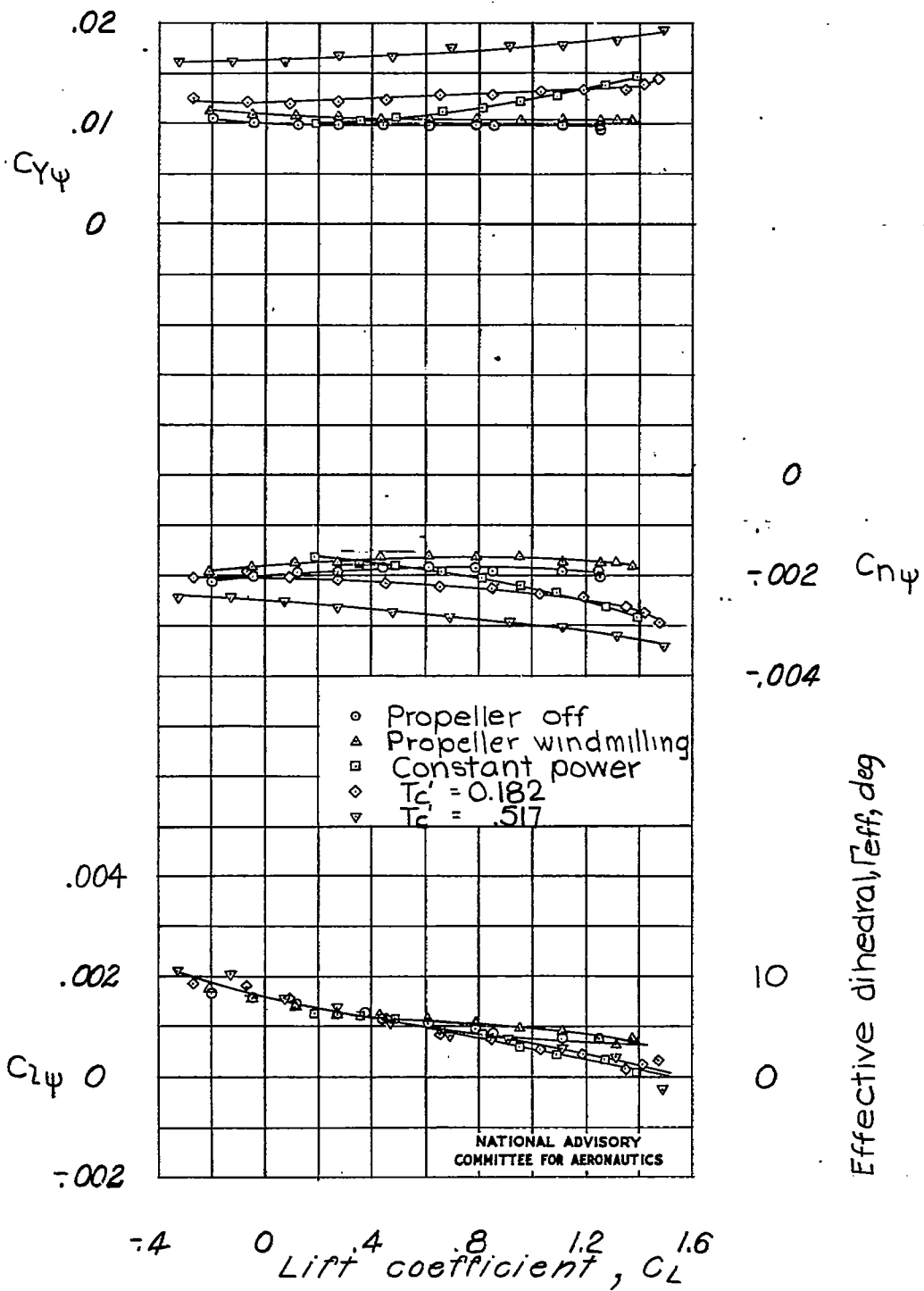


Figure 7.- Variation of approximate horsepower represented and stalling speeds with airplane wing loading.



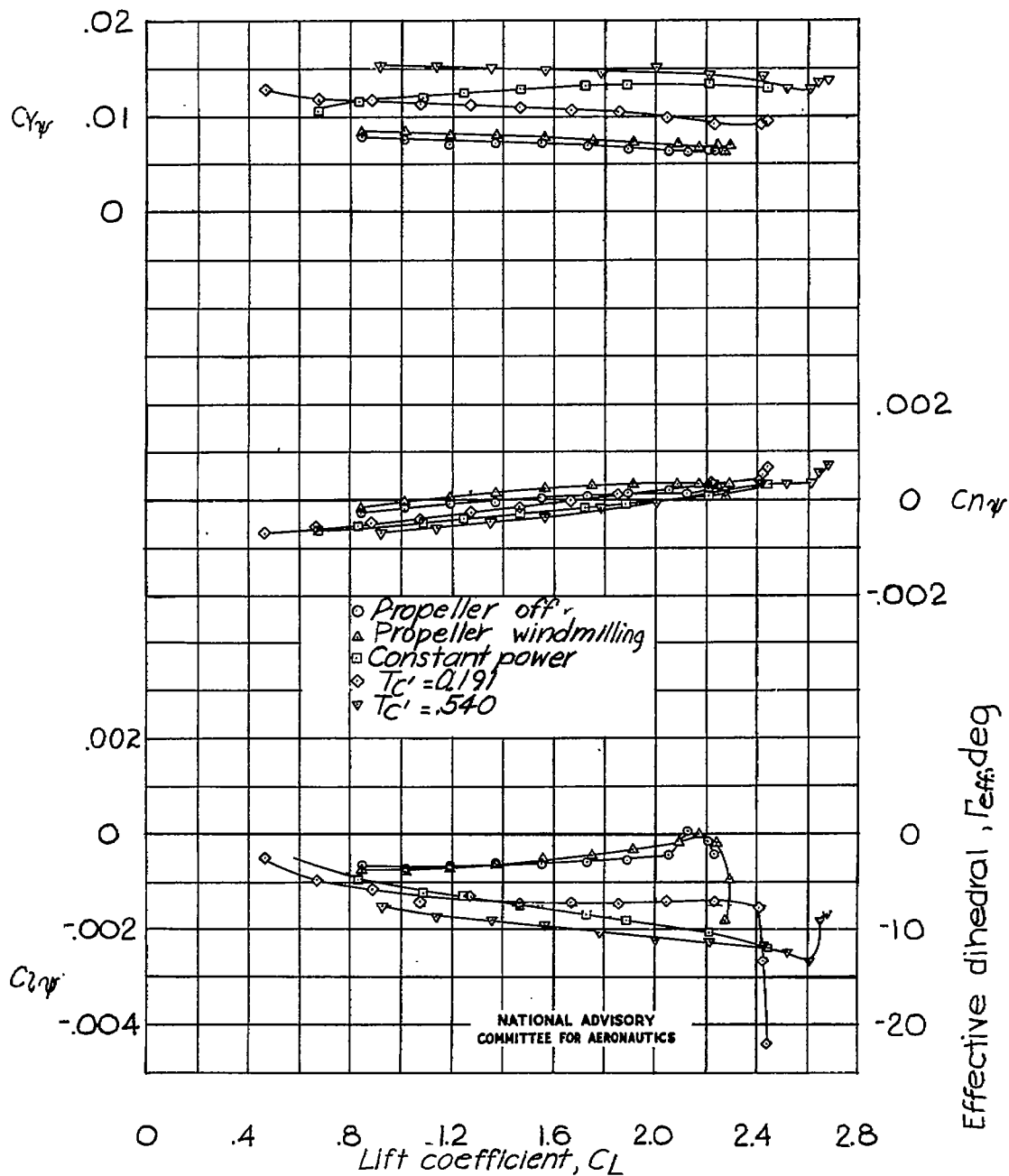
(a) Tail off.

Figure 8.- Effect of power on the variation of $C_{L\psi}$, $C_{N\psi}$, and $C_{Y\psi}$ with lift coefficient for the model as a low-wing airplane with flap neutral.



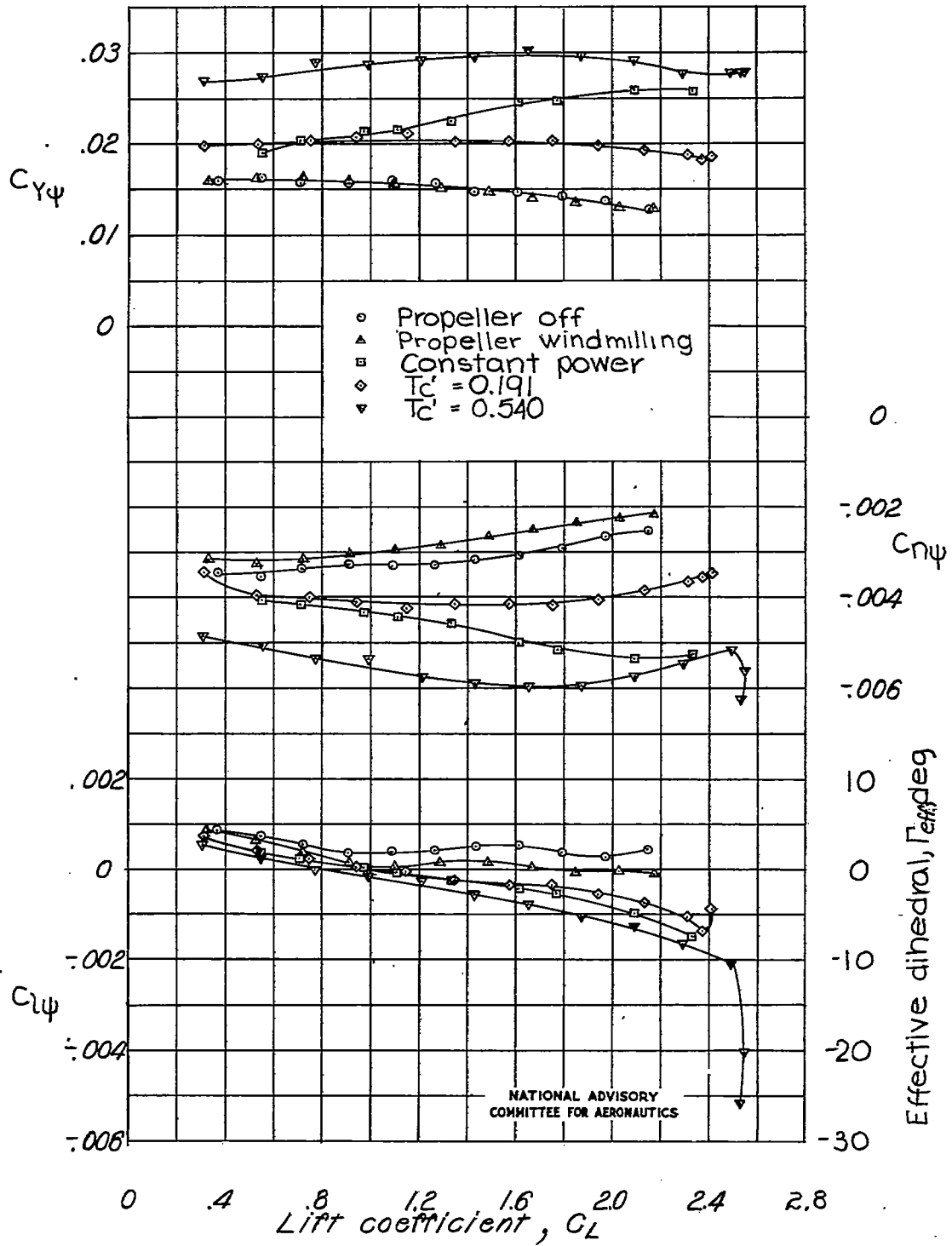
(b) Tail on.

Figure 8.- Concluded.



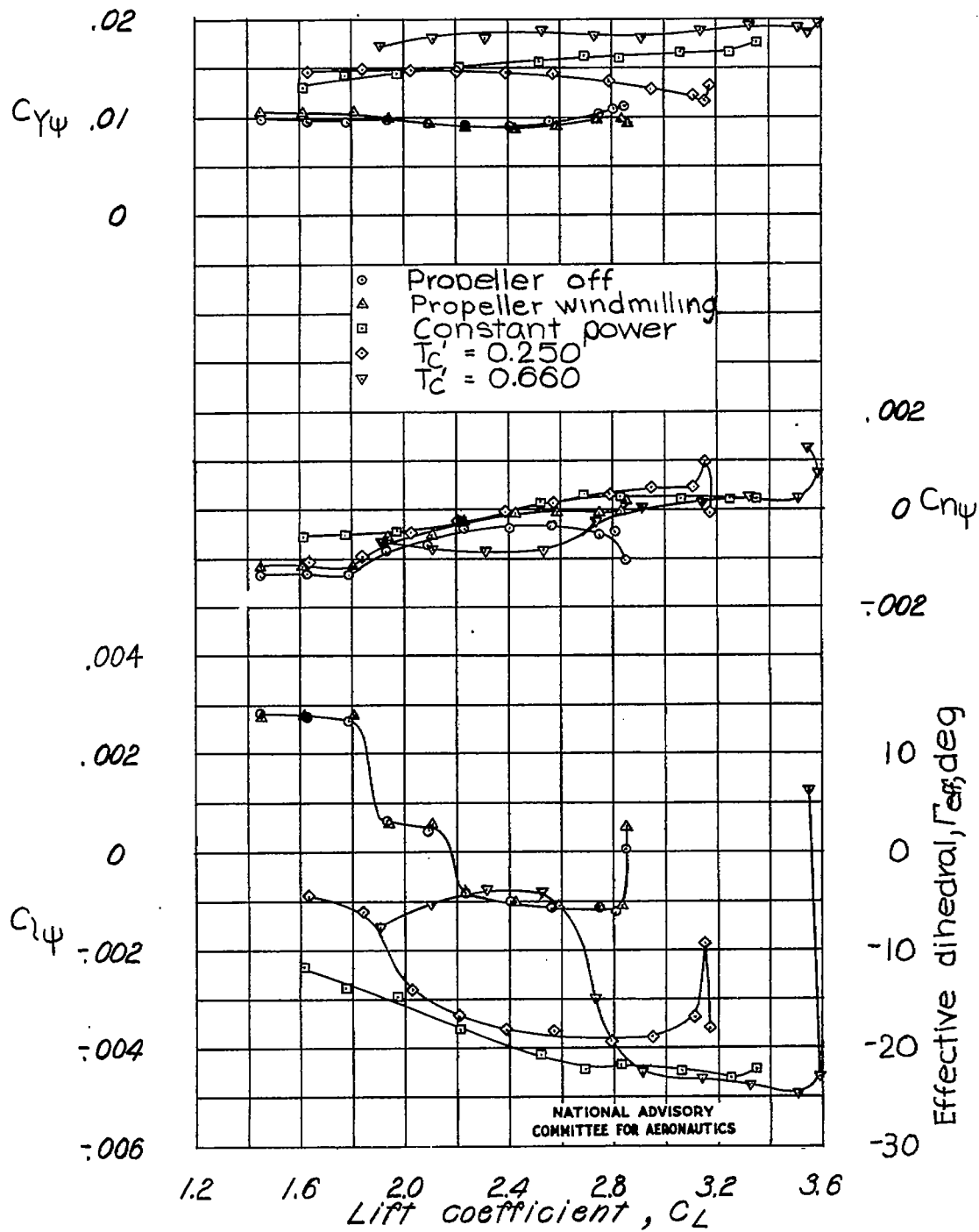
(a) Tail off.

Figure 9.- Effect of power on the variation of $C_{L\psi}$, C_{nr} , and C_{ny} with lift coefficient for the model as a low-wing airplane with full-span single slotted flap.



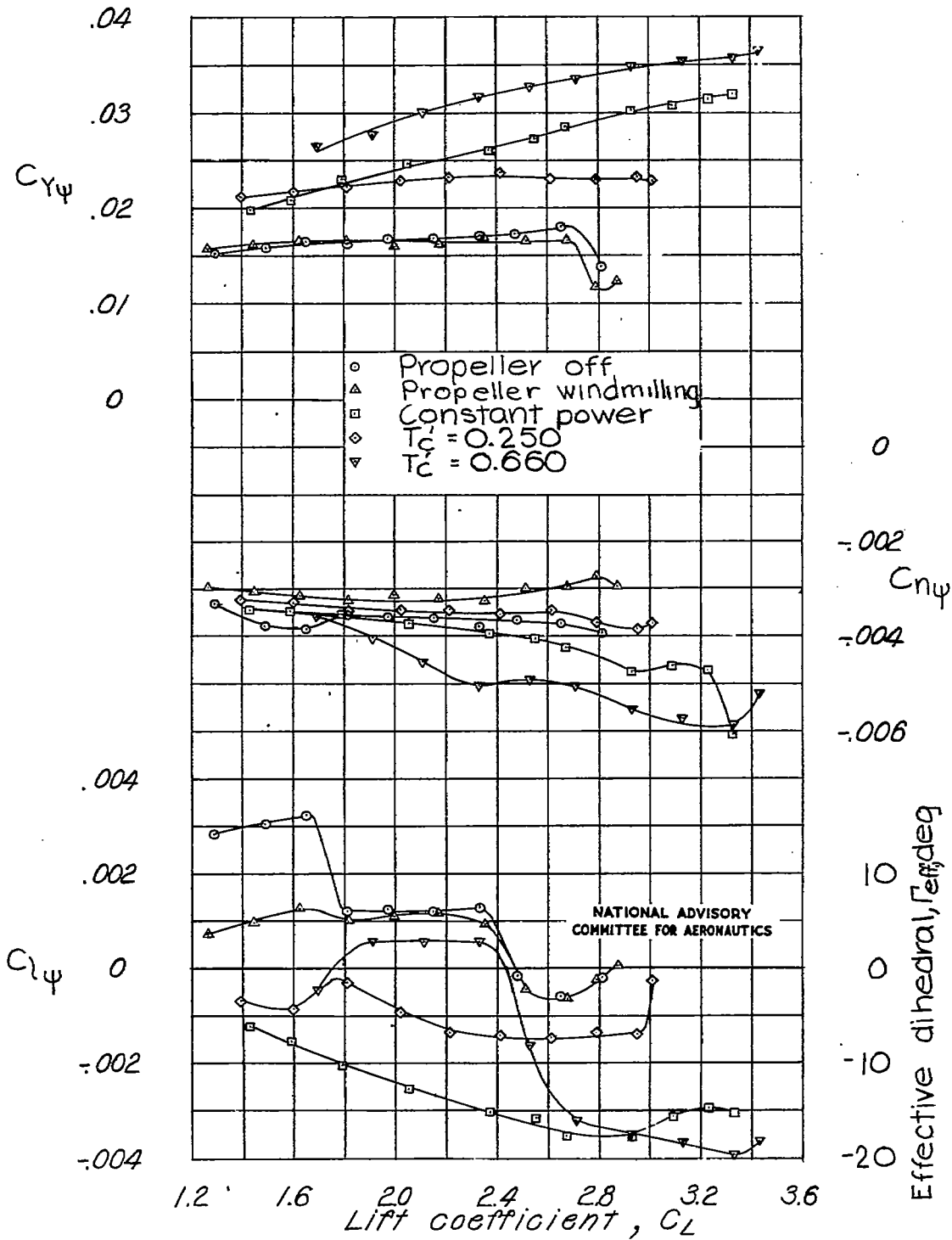
(b) Tail on.

Figure 9.- Concluded.



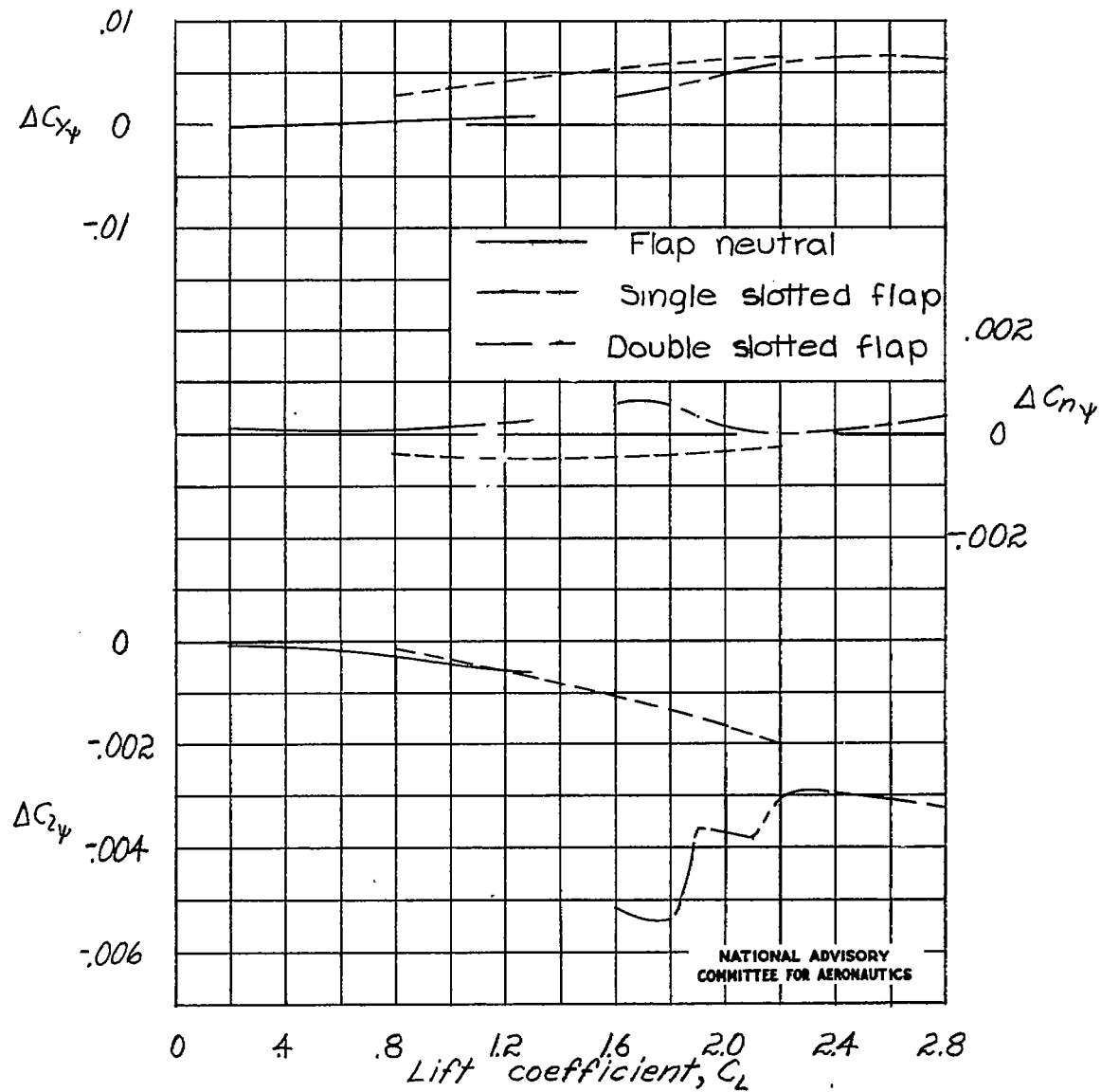
(a) Tail off.

Figure 10.- Effect of power on the variation of $C_{L\psi}$, $C_{N\psi}$, and $C_{Y\psi}$ with lift coefficient for the model as a low-wing airplane with full-span double slotted flap.



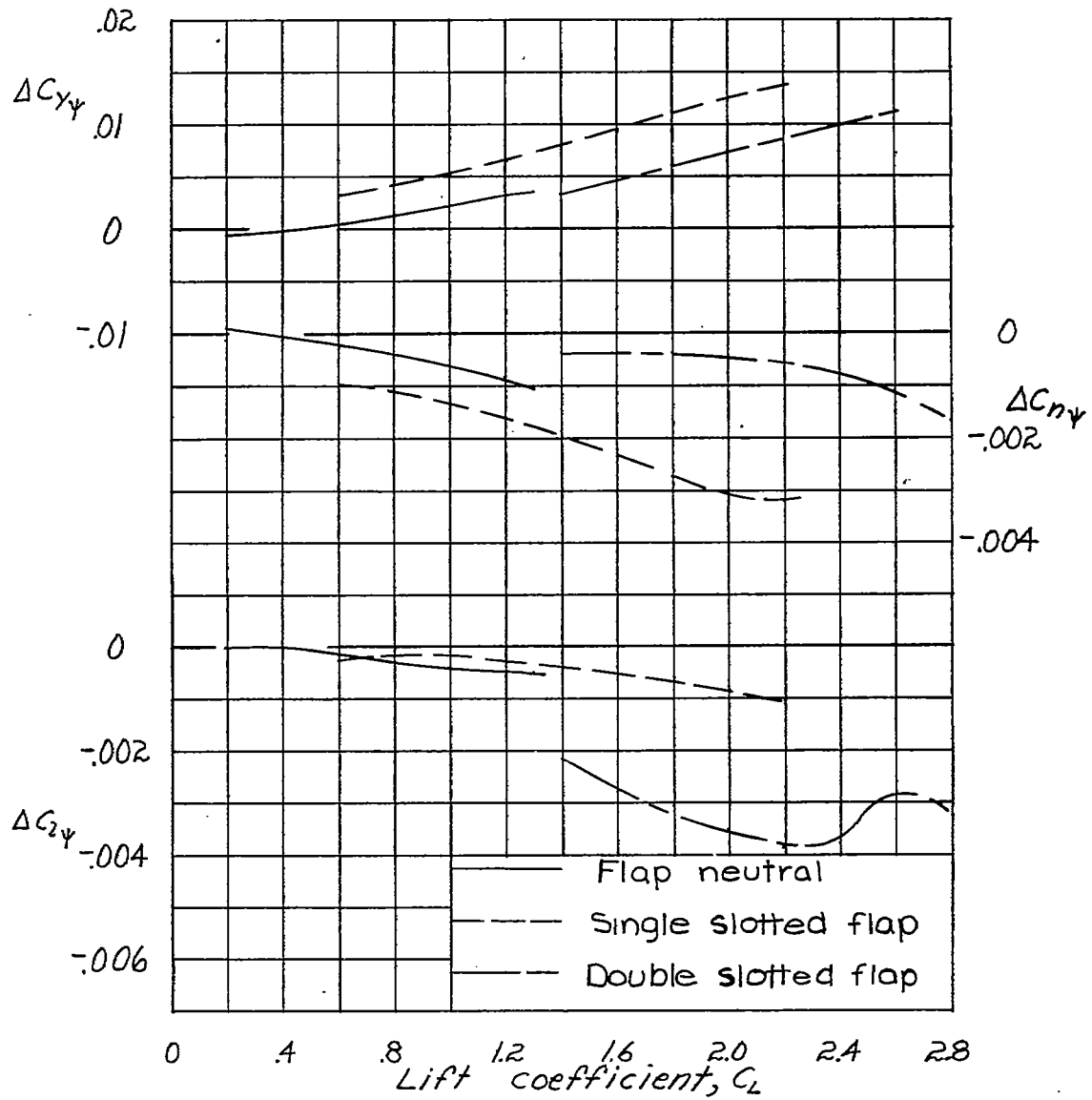
(b) Tail on.

Figure 10.- Concluded.



(a) Tail off.

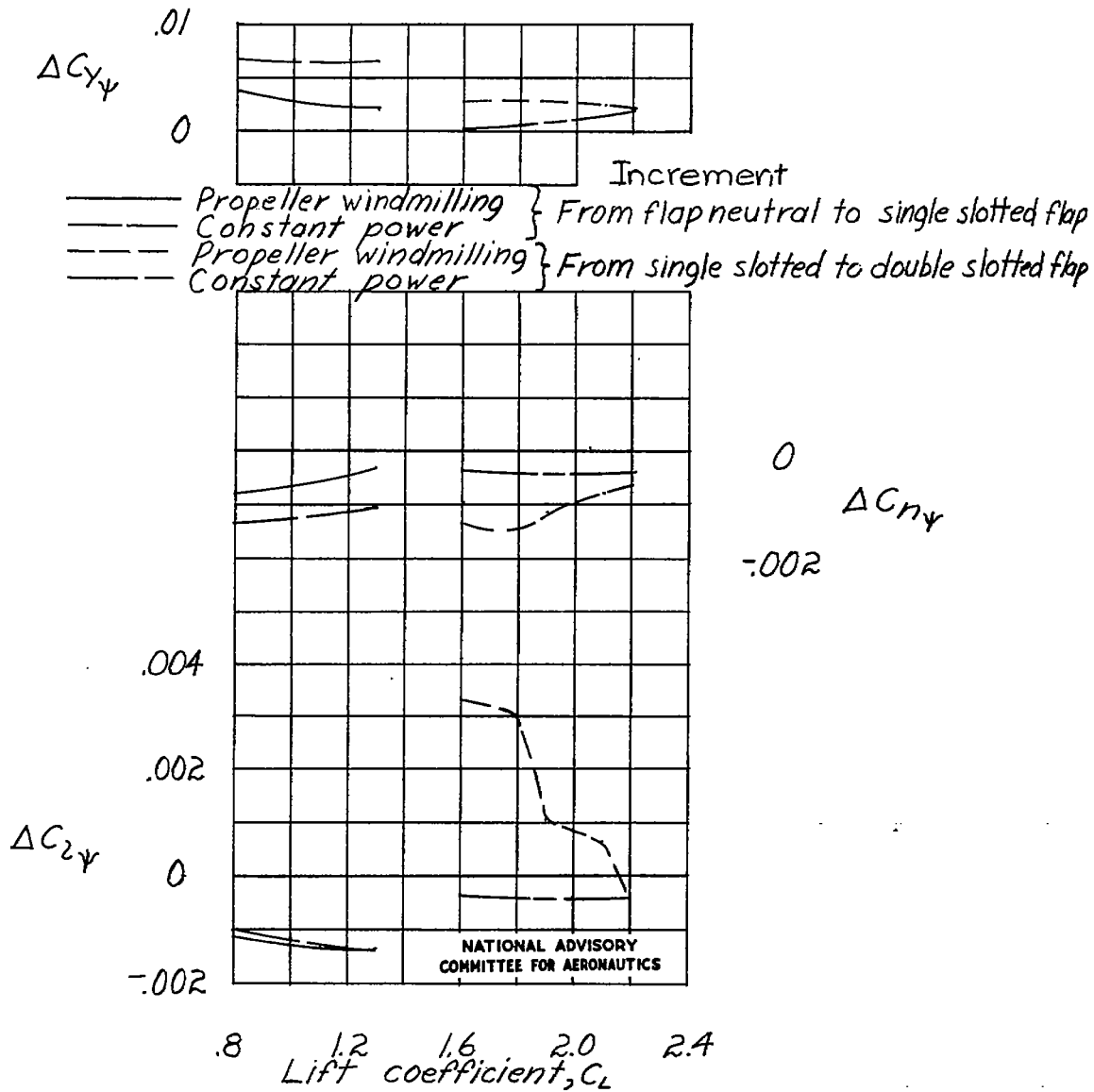
Figure 11.- Increments in $C_{l\psi}$, $C_{n\psi}$, and $C_{Y\psi}$ resulting from a change from windmilling propeller to constant power for the model as a low-wing airplane.



NATIONAL ADVISORY
COMMITTEE FOR AERONAUTICS

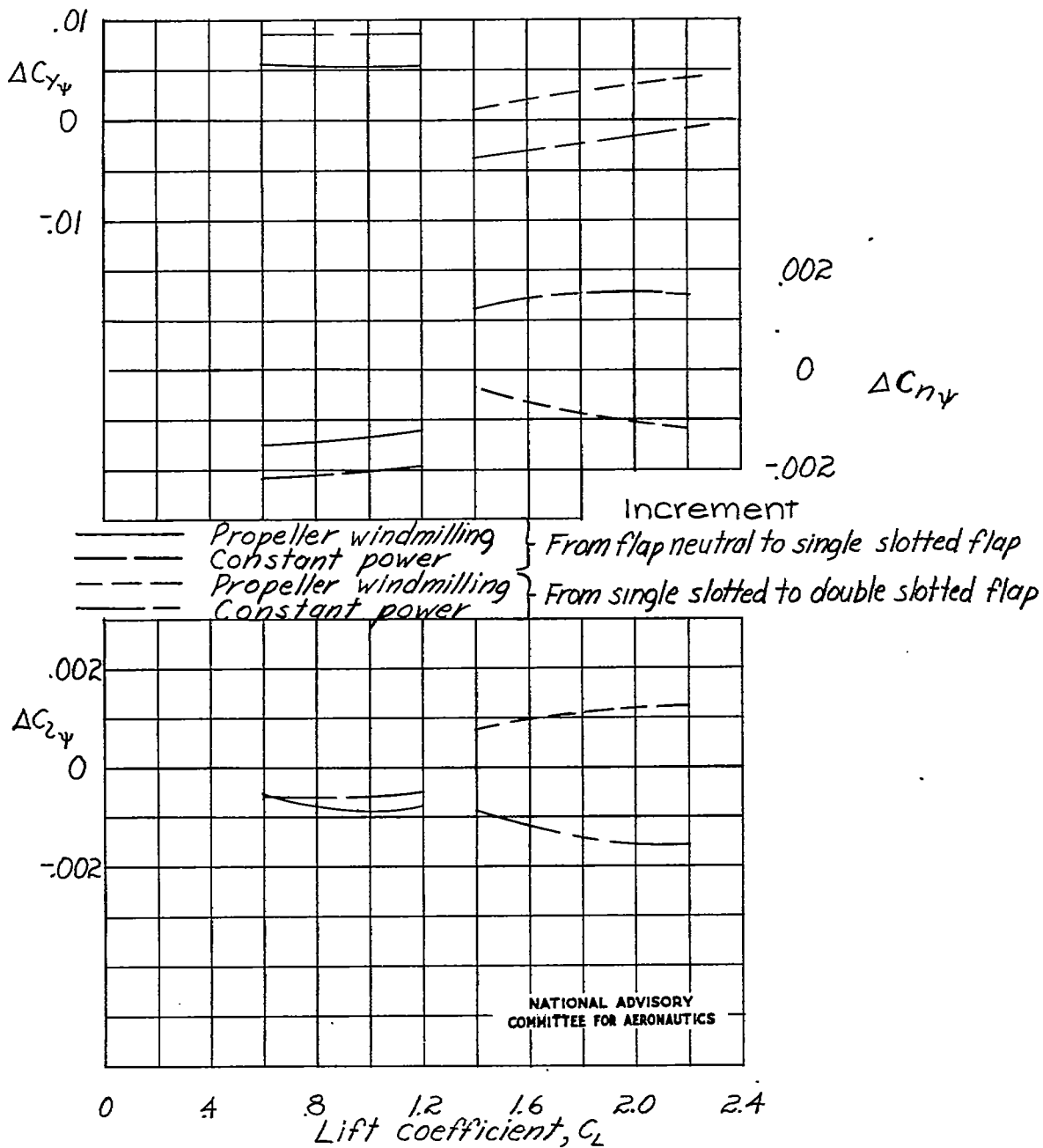
(b) Tail on.

Figure 11.- Concluded.



(a) Tail off.

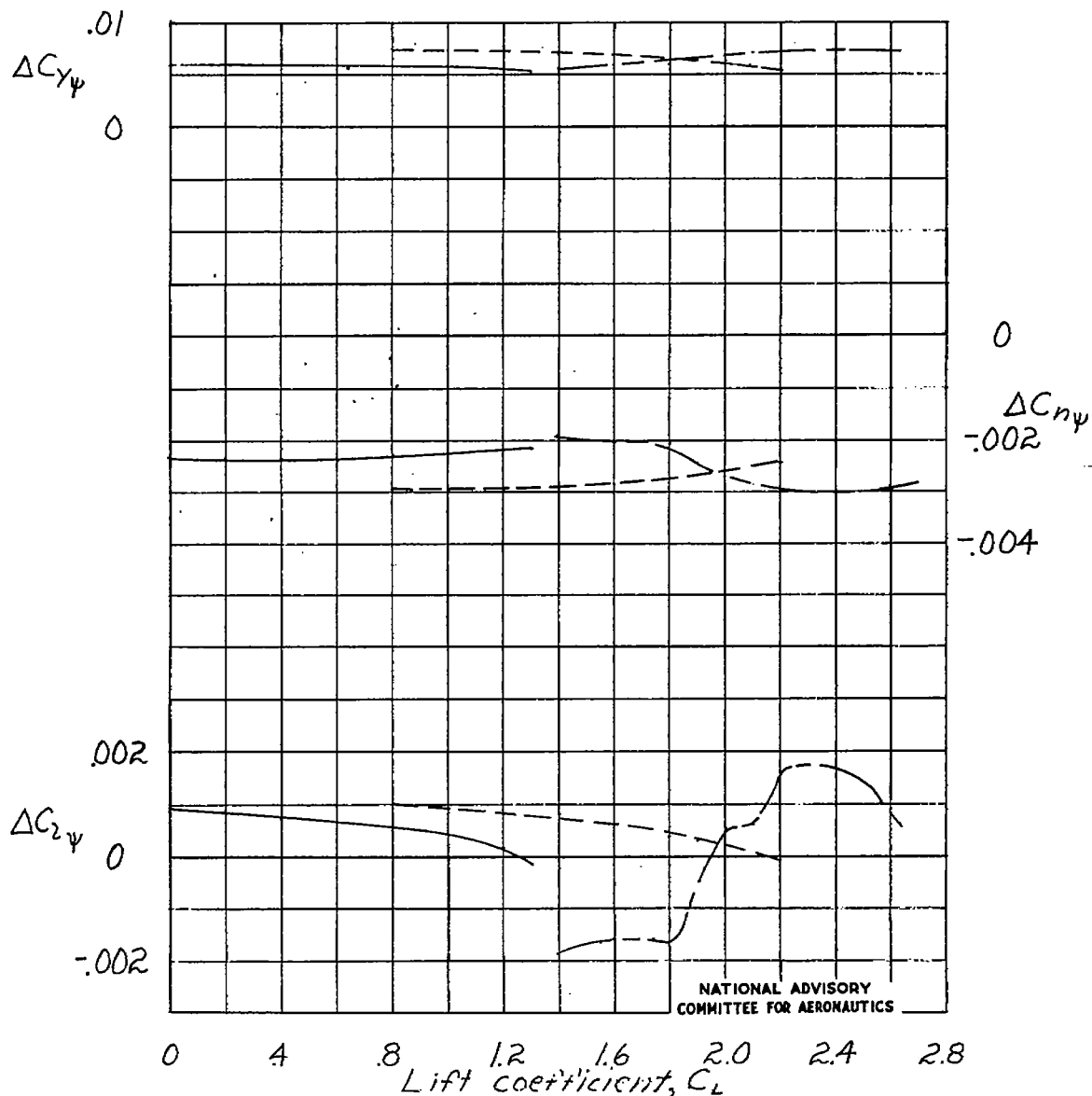
Figure 12.- Increments in $C_{l\psi}$, $C_{n\psi}$, and $C_{y\psi}$ resulting from flap deflection for the model as a low-wing airplane.



(b) Tail on.

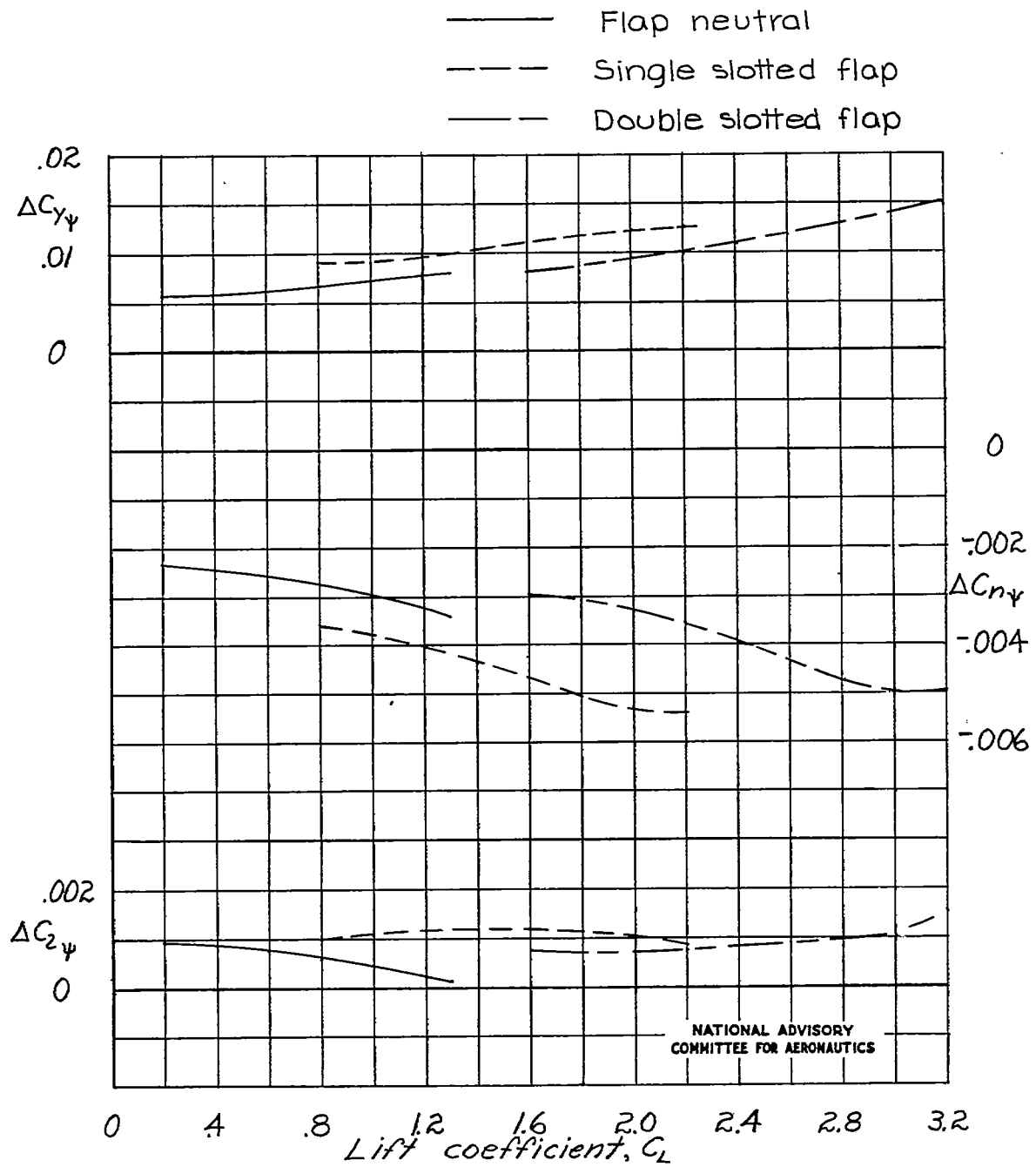
Figure 12.- Concluded.

— Flap neutral
 - - - Single slotted flap
 — — Double slotted flap



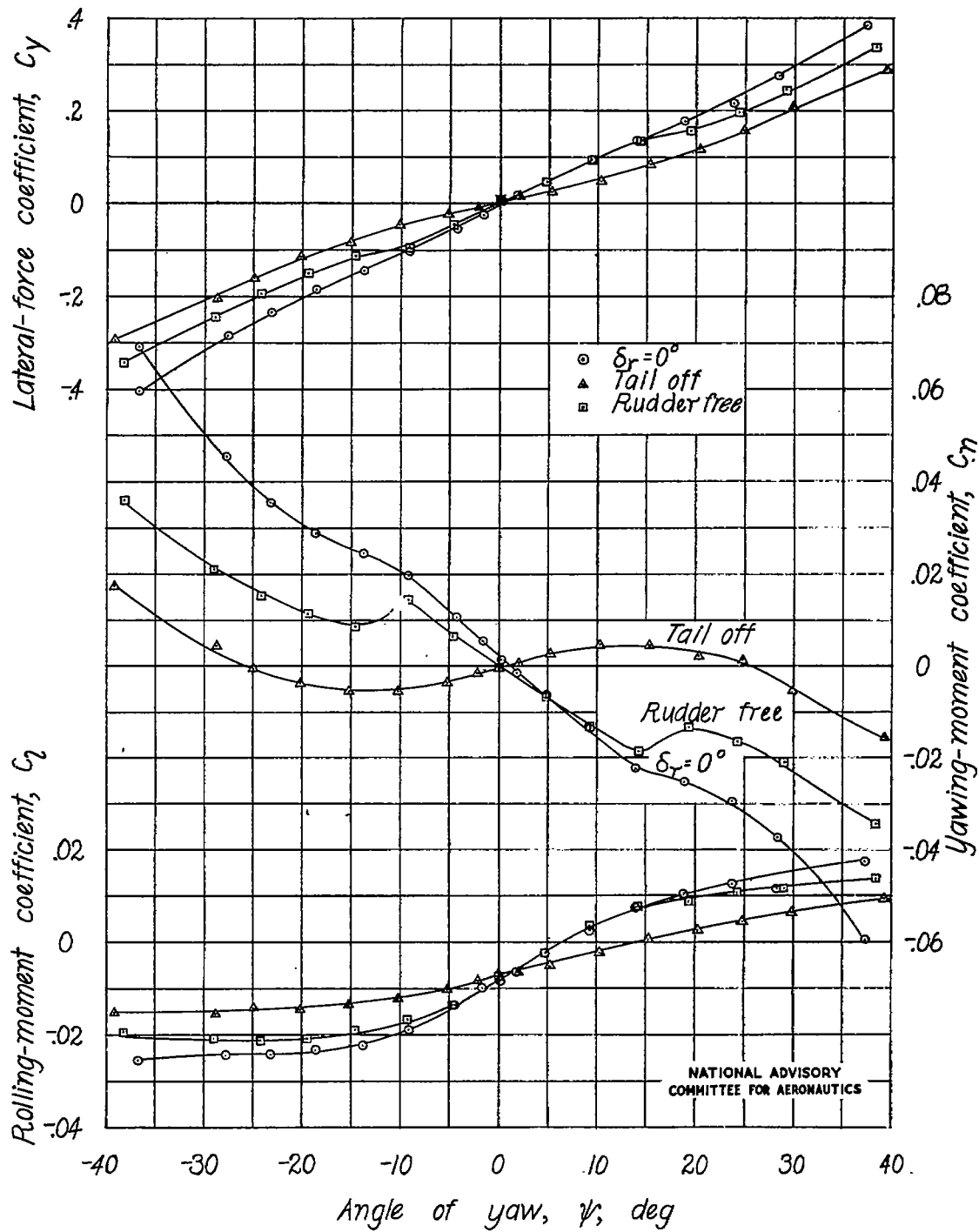
(a) Propeller windmilling.

Figure 13.- Increments in $C_{l\psi}$, $C_{n\psi}$, and $C_{y\psi}$ contributed by the tail surfaces for the model as a low-wing airplane.



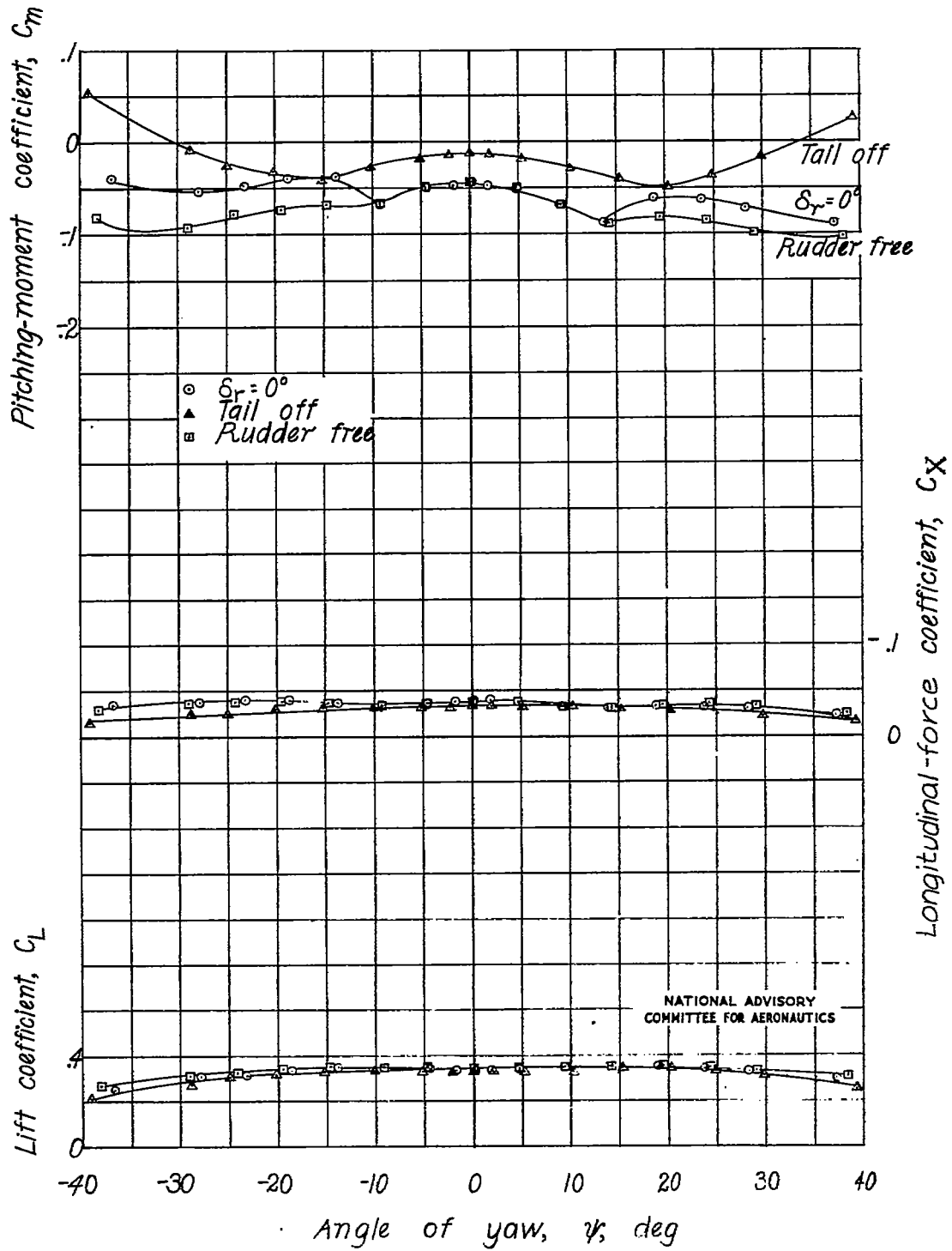
(b) Constant power.

Figure 13.- Concluded.



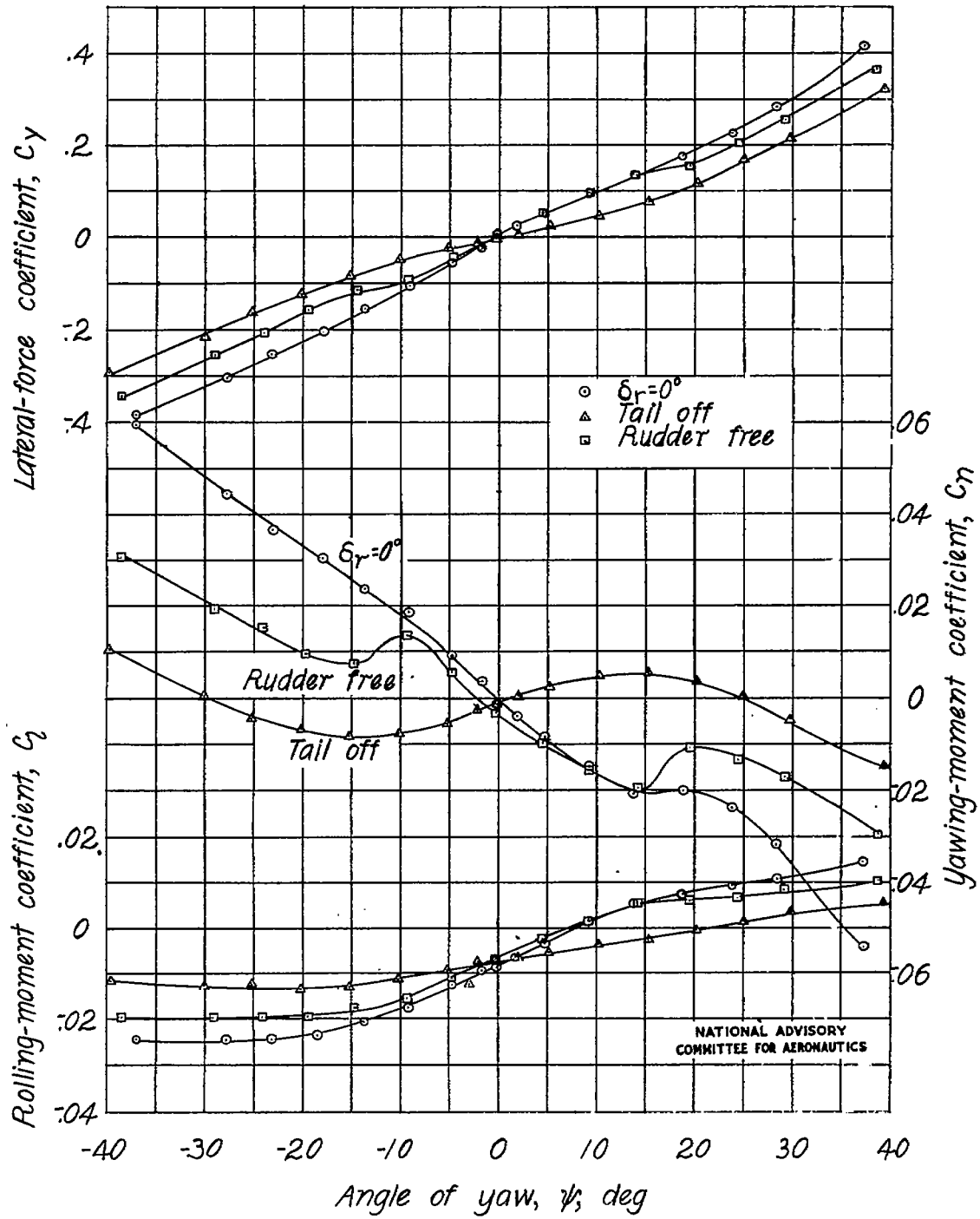
(a) Propeller windmilling.

Figure 14.- Aerodynamic characteristics in yaw of the model as a low-wing airplane with flap neutral. $\alpha \approx 1.2^\circ$.



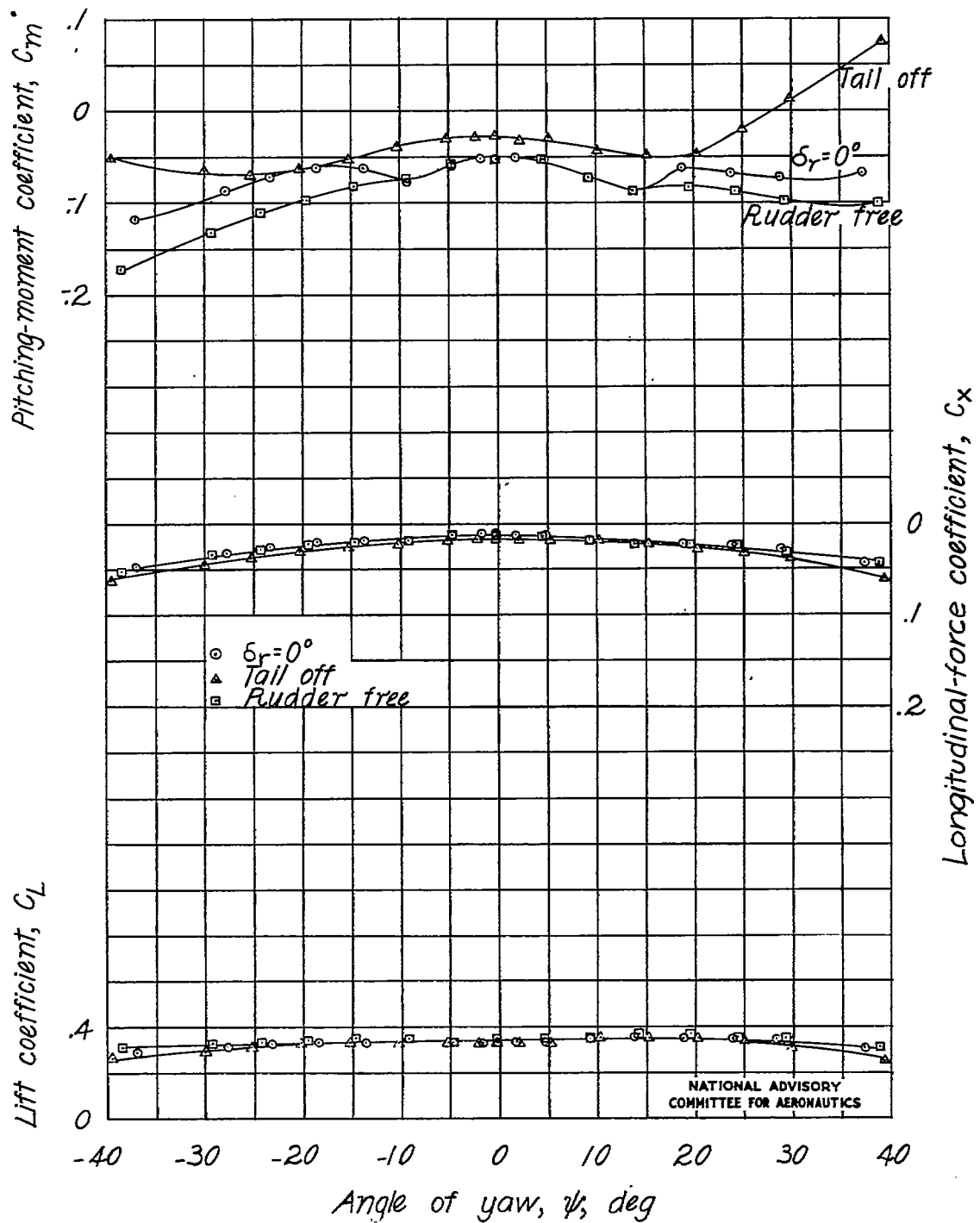
(a) Concluded.

Figure 14.- Continued.



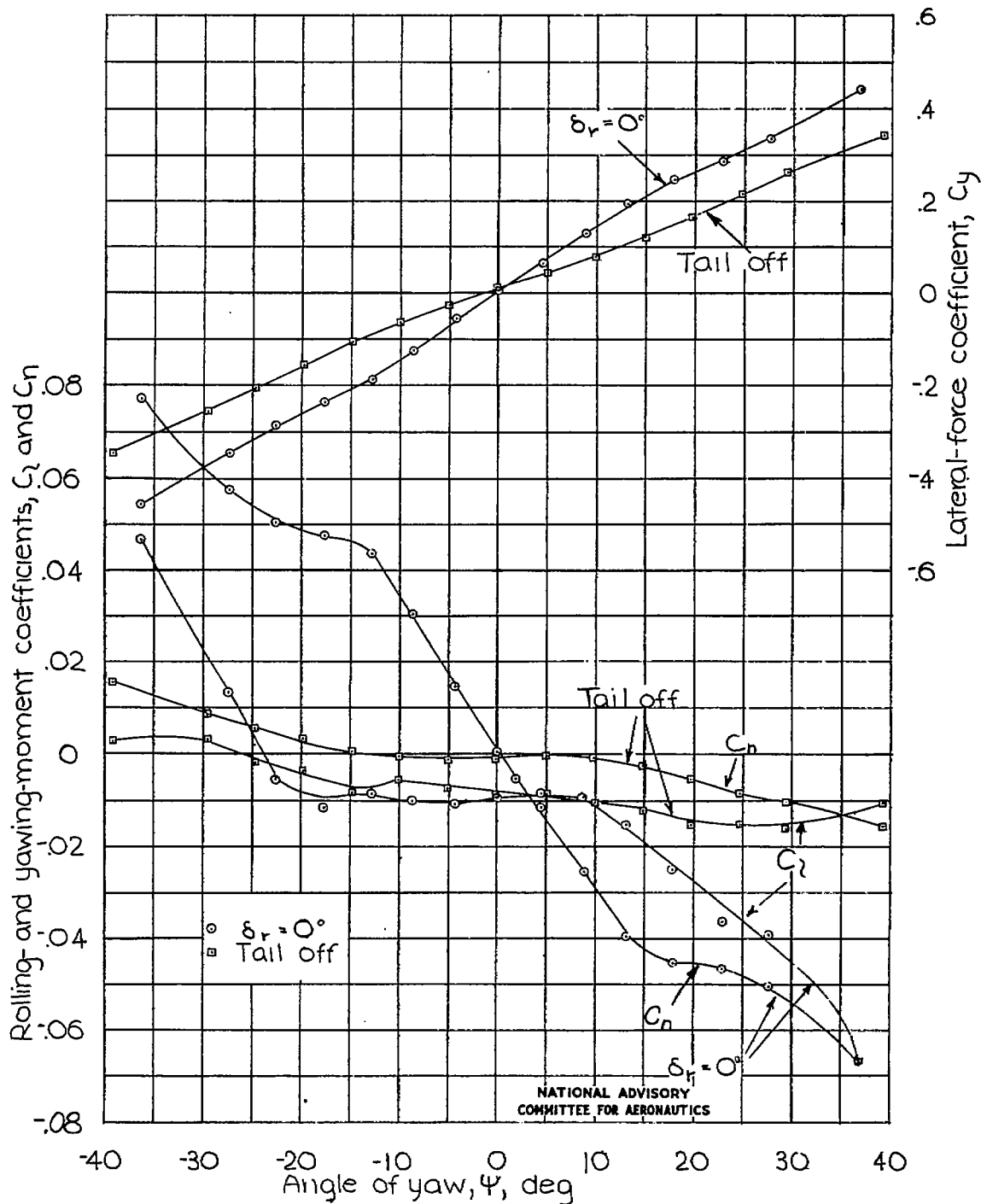
(b) Constant power.

Figure 14.- Continued.



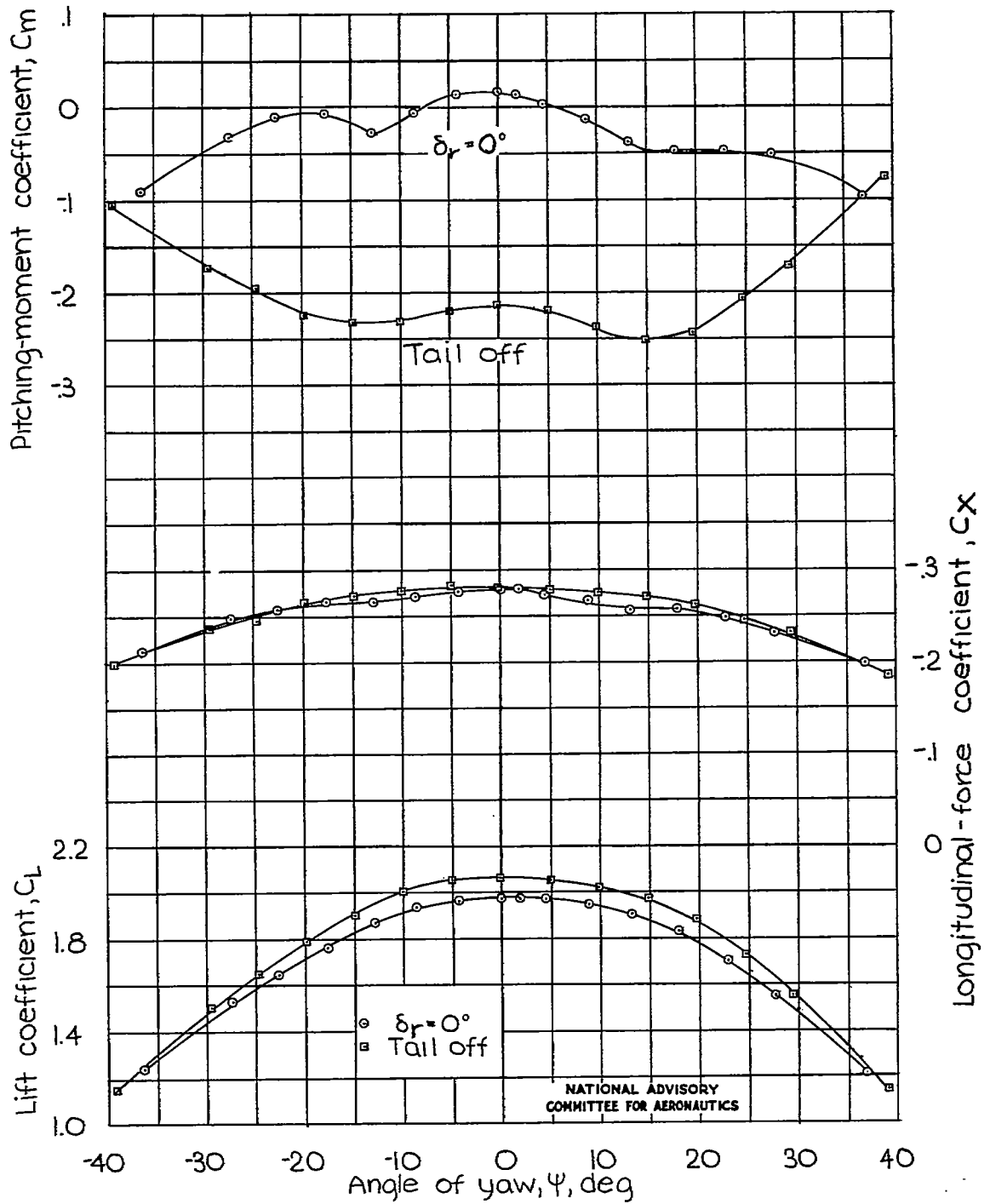
(b) Concluded.

Figure 14.- Concluded.



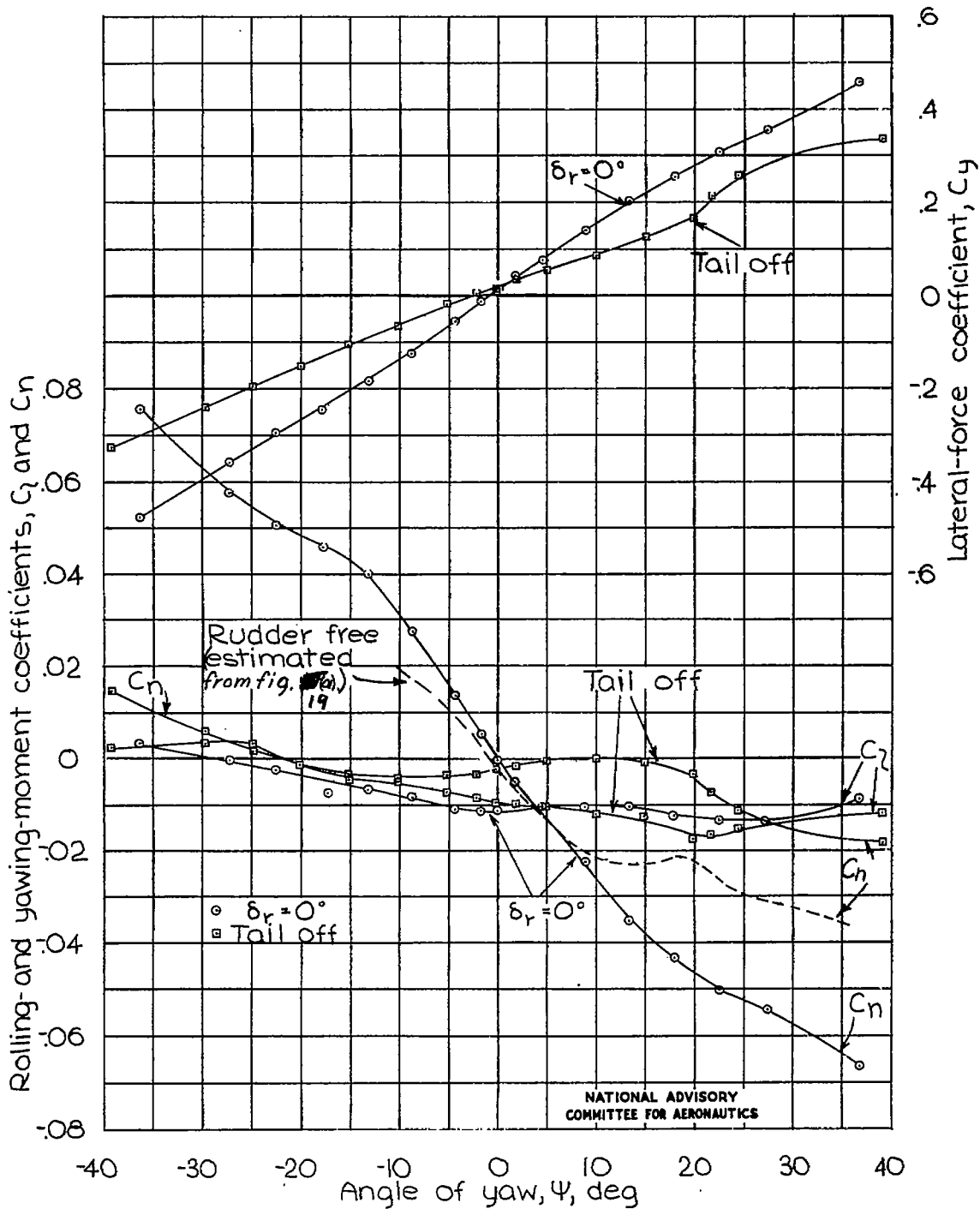
(a) Propeller off.

Figure 15.- Aerodynamic characteristics in yaw of the model as a low-wing airplane with a full-span single slotted flap. $\alpha \approx 9.7^\circ$.



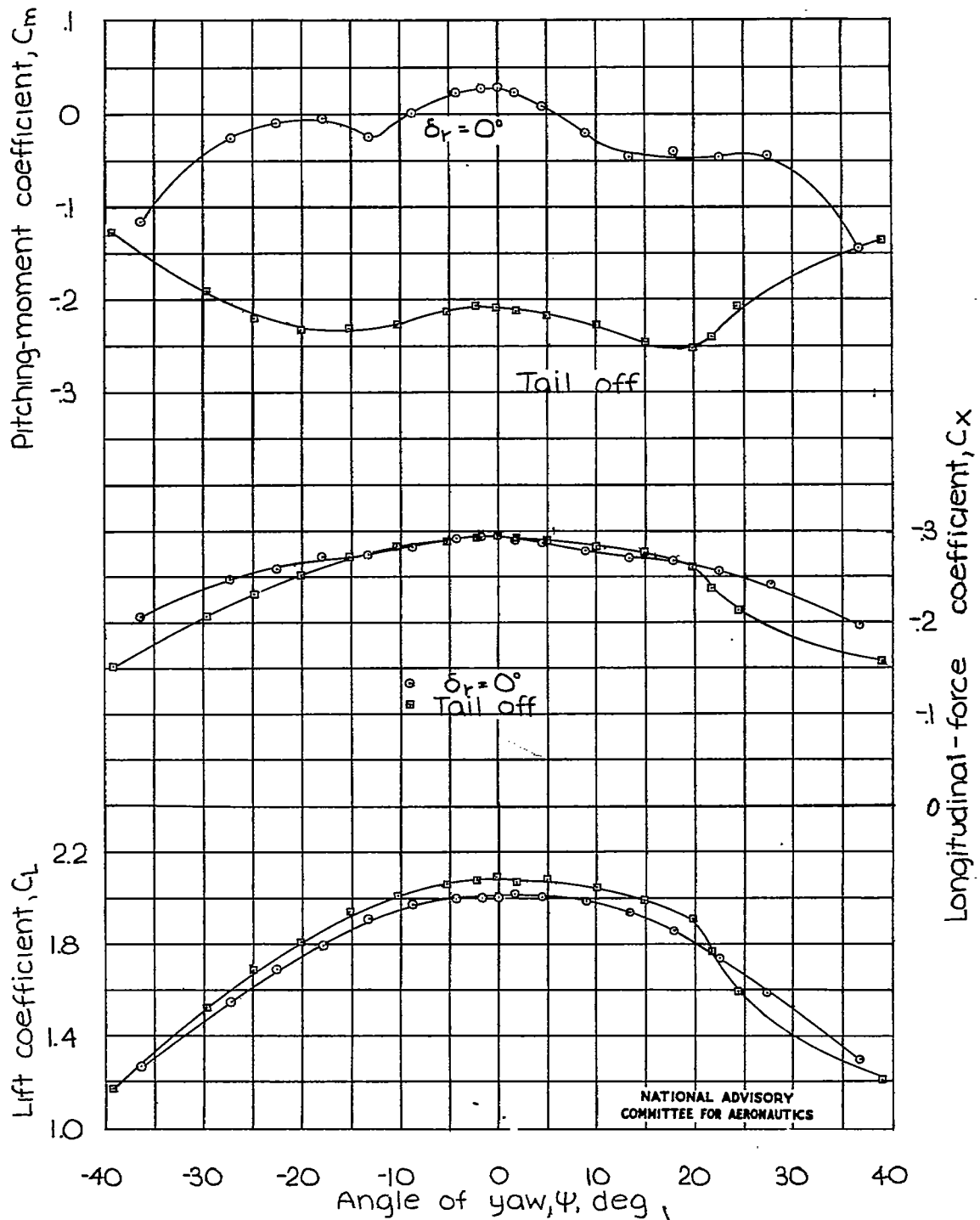
(a) Concluded.

Figure 15.- Continued.



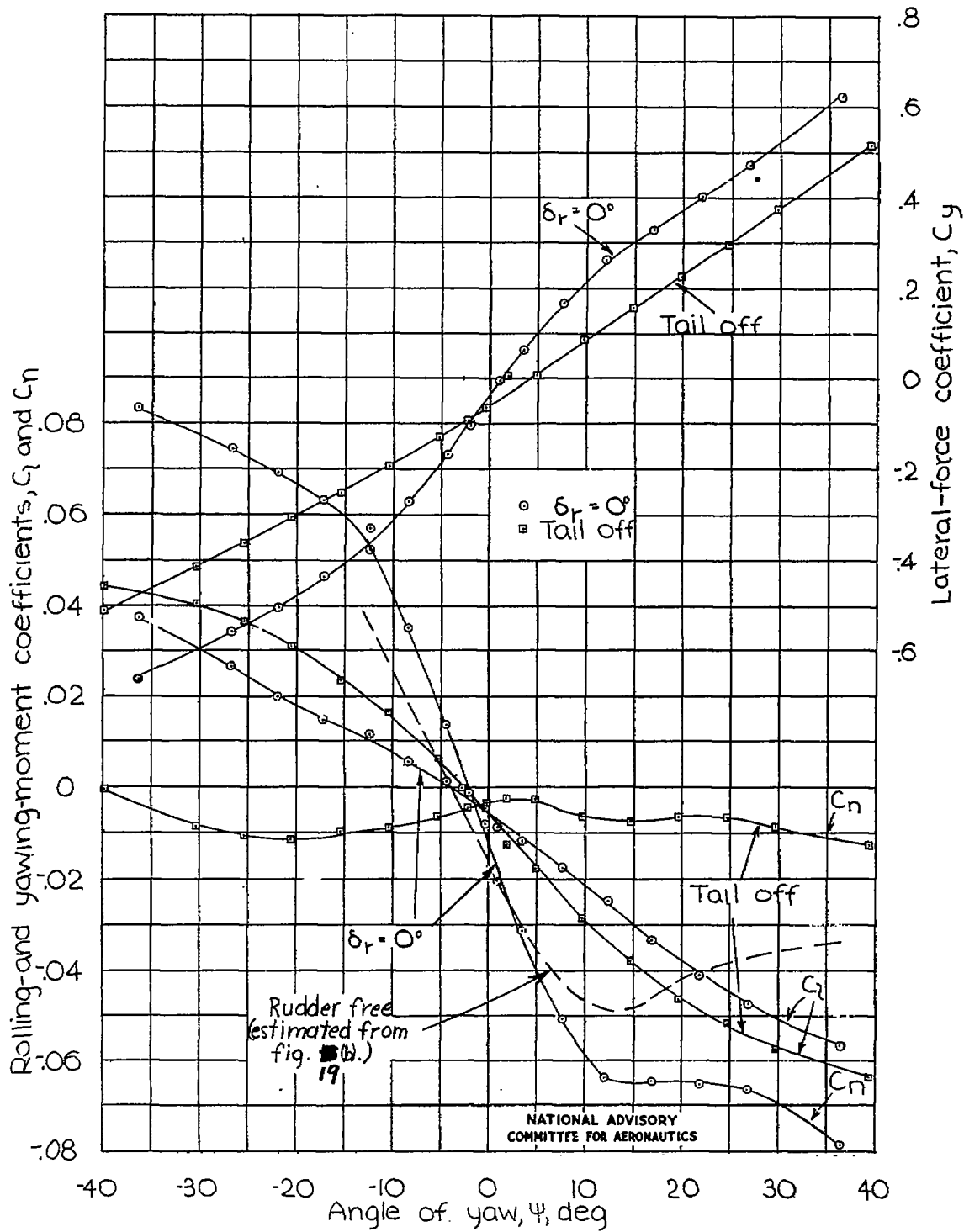
(b) Propeller windmilling.

Figure 15.- Continued.



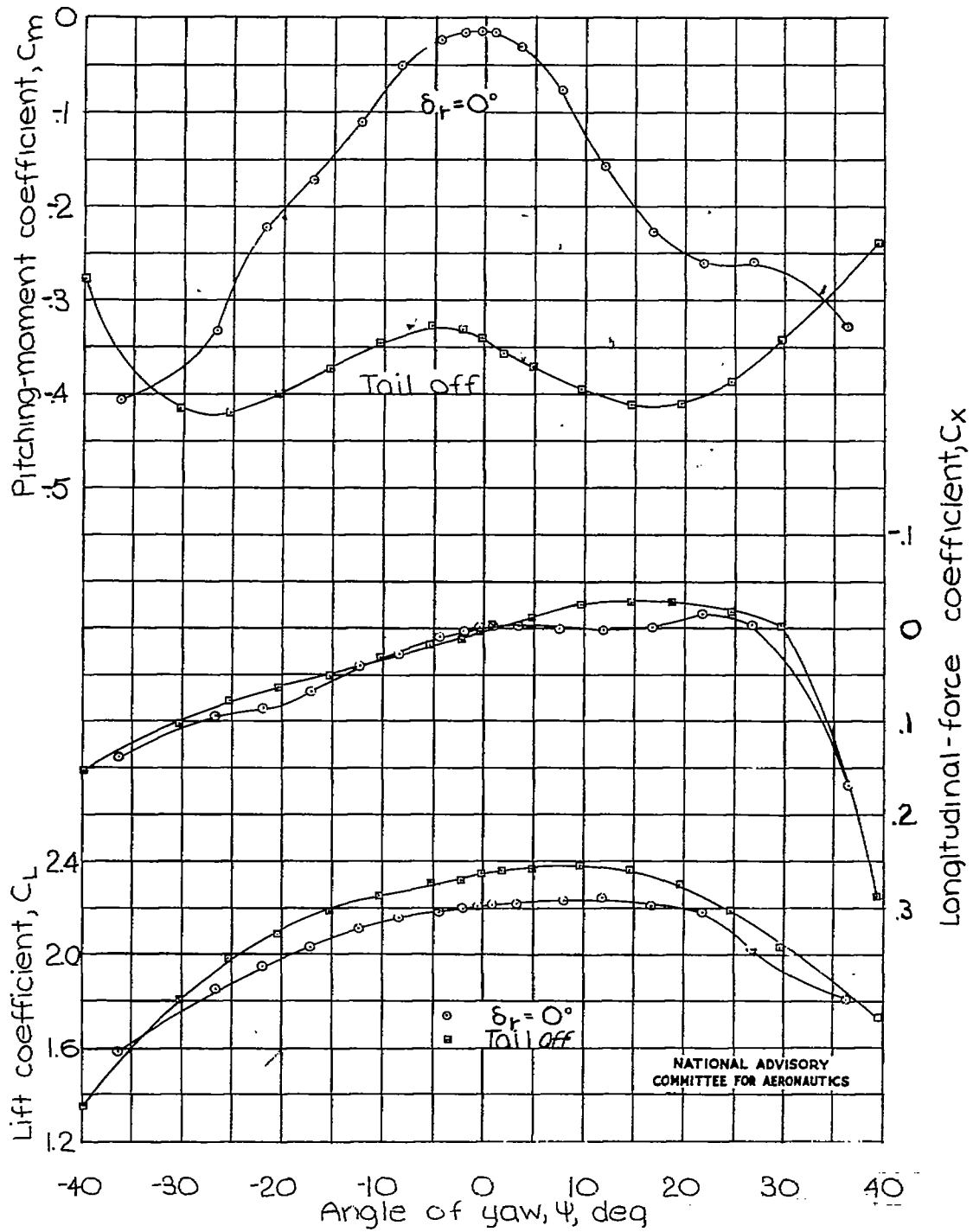
(b) Concluded.

Figure 15.- Continued.



(c) Constant power.

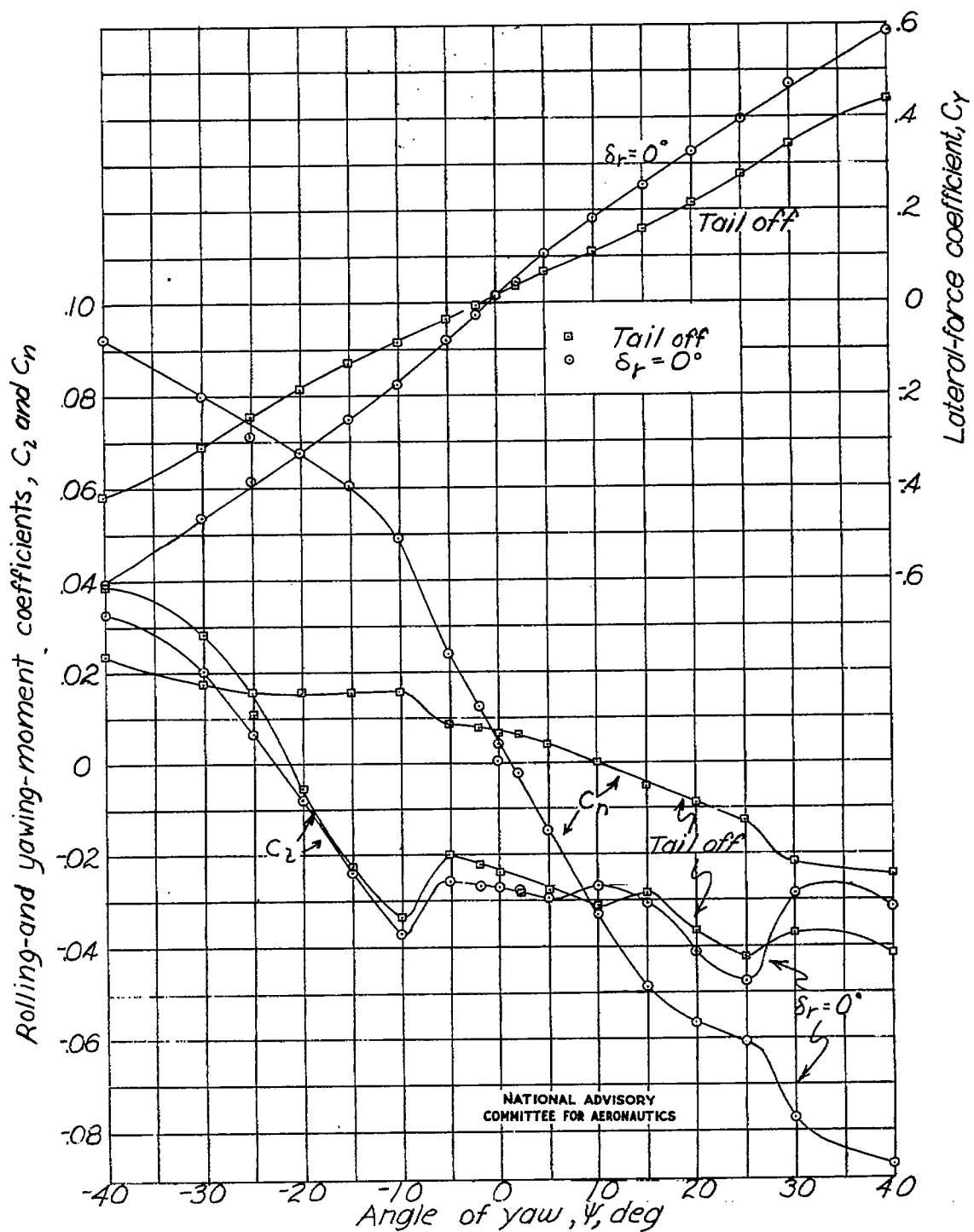
Figure 15.- Continued.



(c) Concluded.

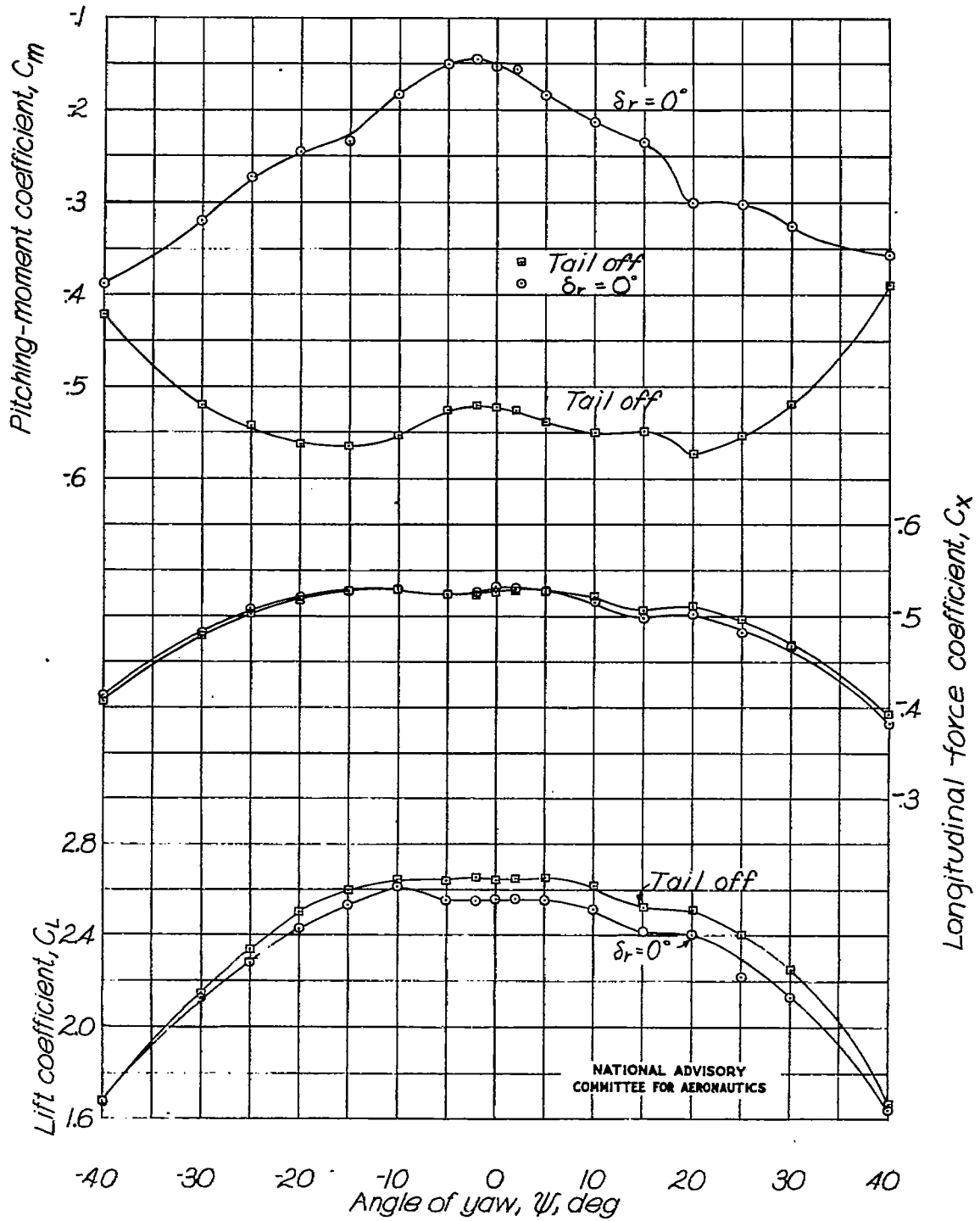
Figure 15.- Concluded.

NATIONAL ADVISORY
COMMITTEE FOR AERONAUTICS



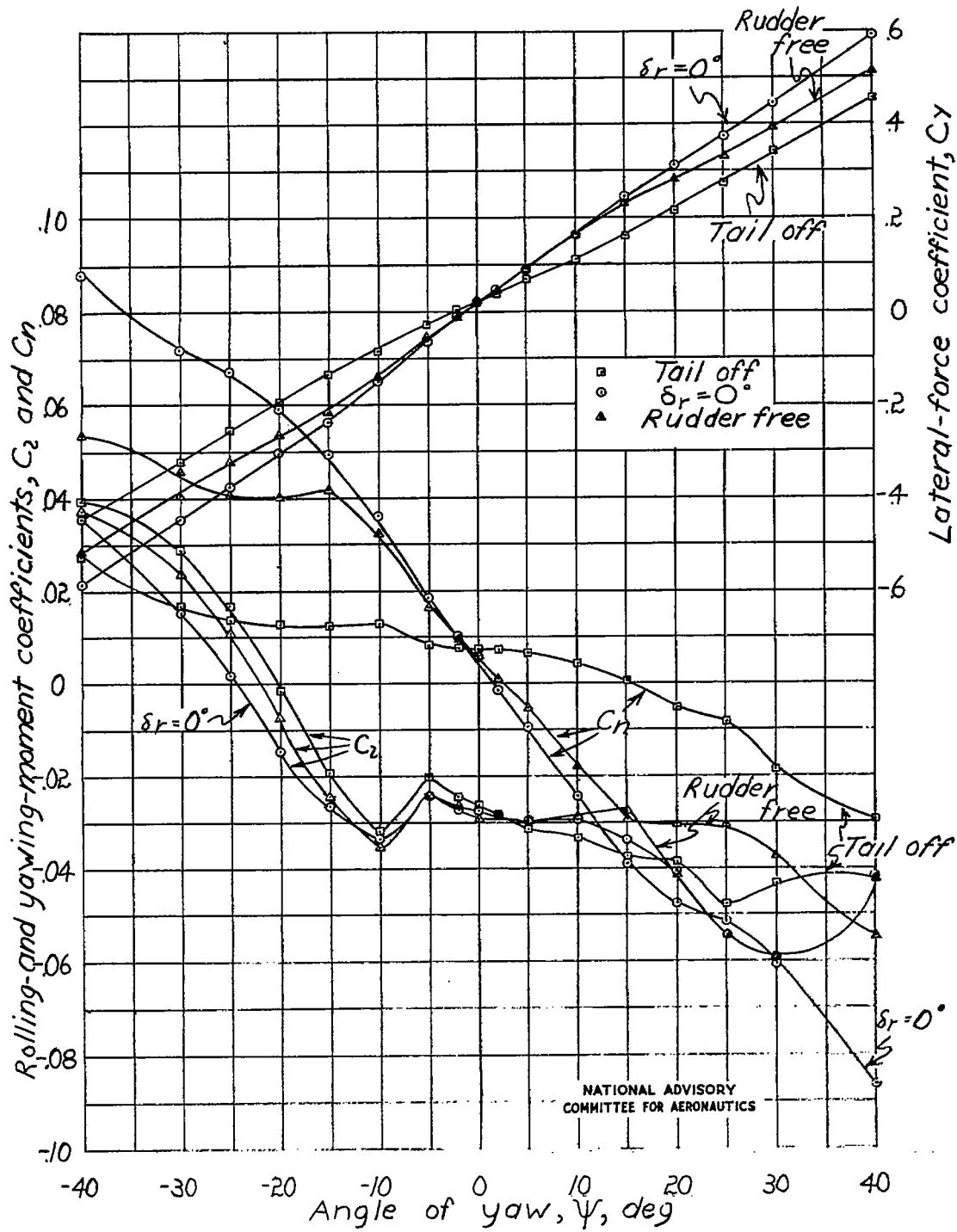
(a) Propeller off.

Figure 16.- Aerodynamic characteristics in yaw of the model as a low-wing airplane with full-span double slotted flap. $\alpha \approx 7.0^\circ$.



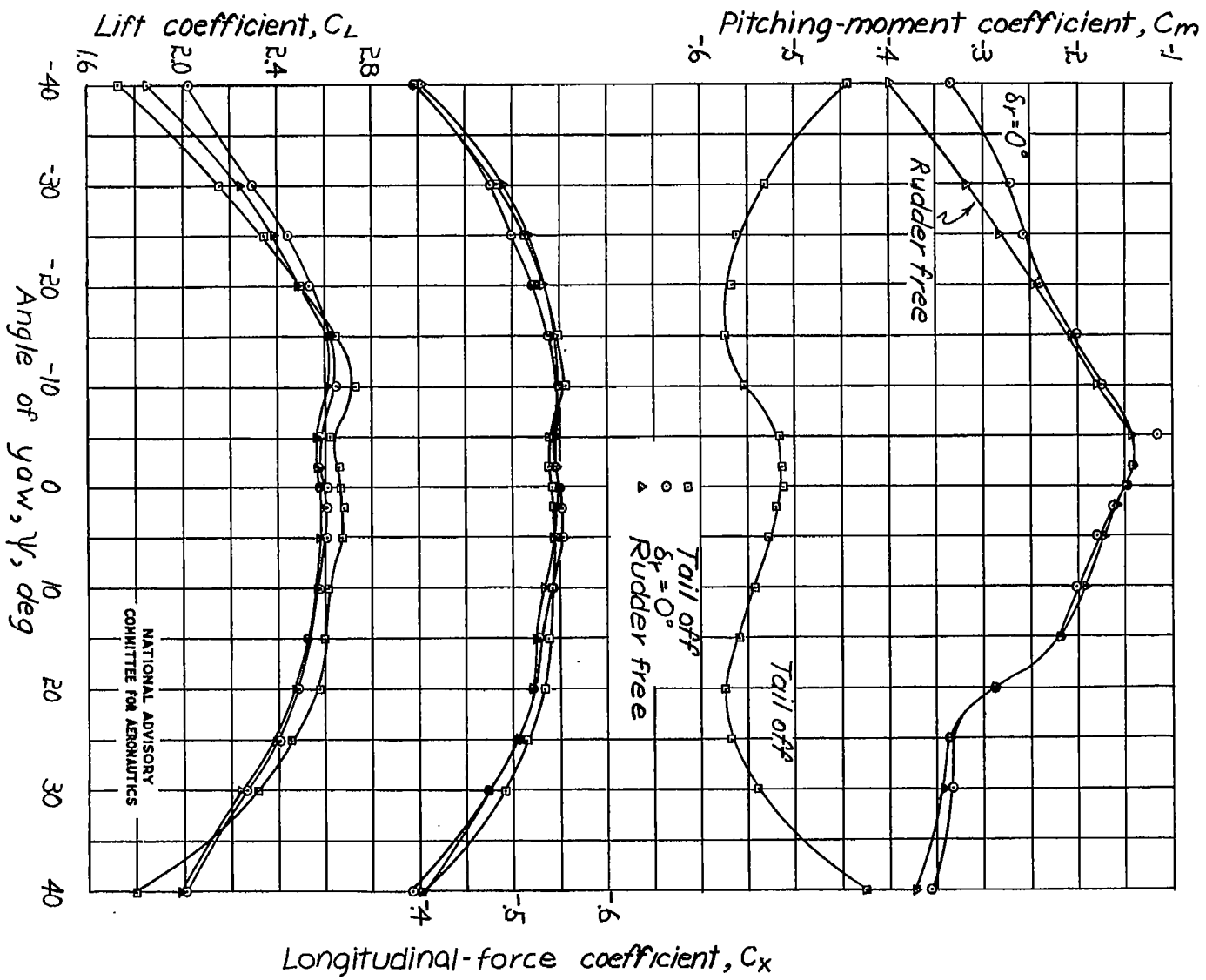
(a) Concluded.

Figure 16.- Continued.



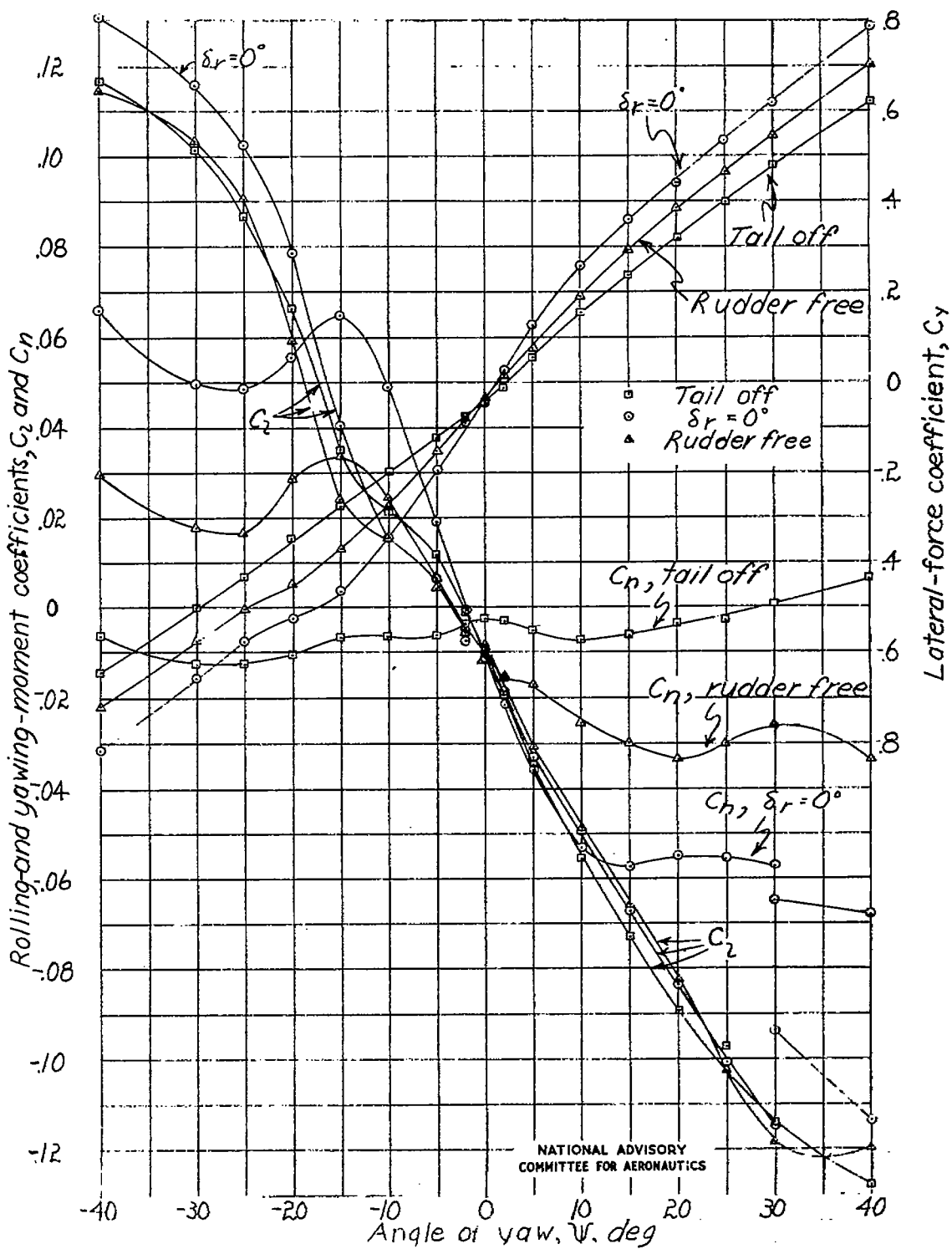
(b) Propeller windmilling.

Figure 16.- Continued.



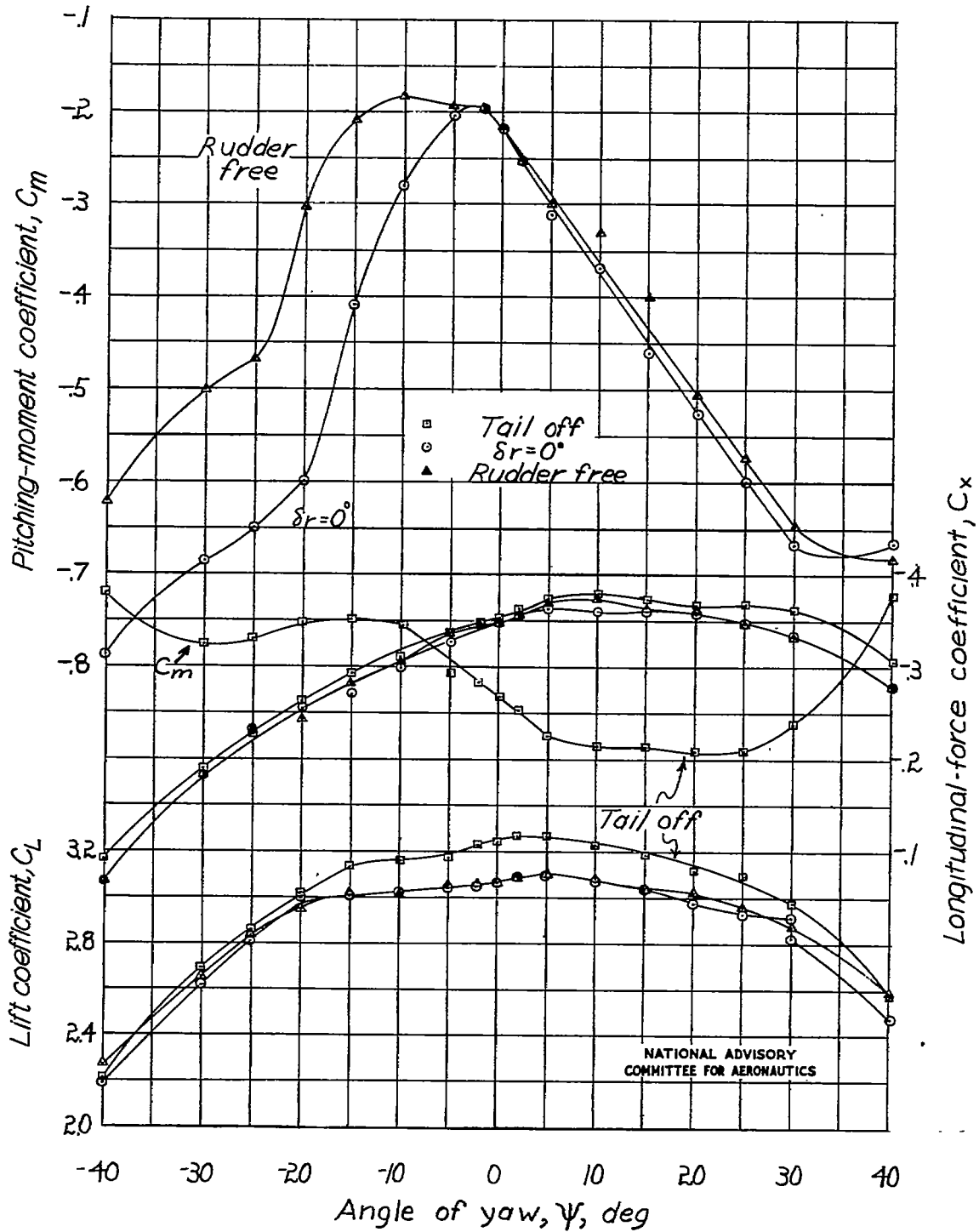
(b) Concluded.

Figure 16.- Continued.



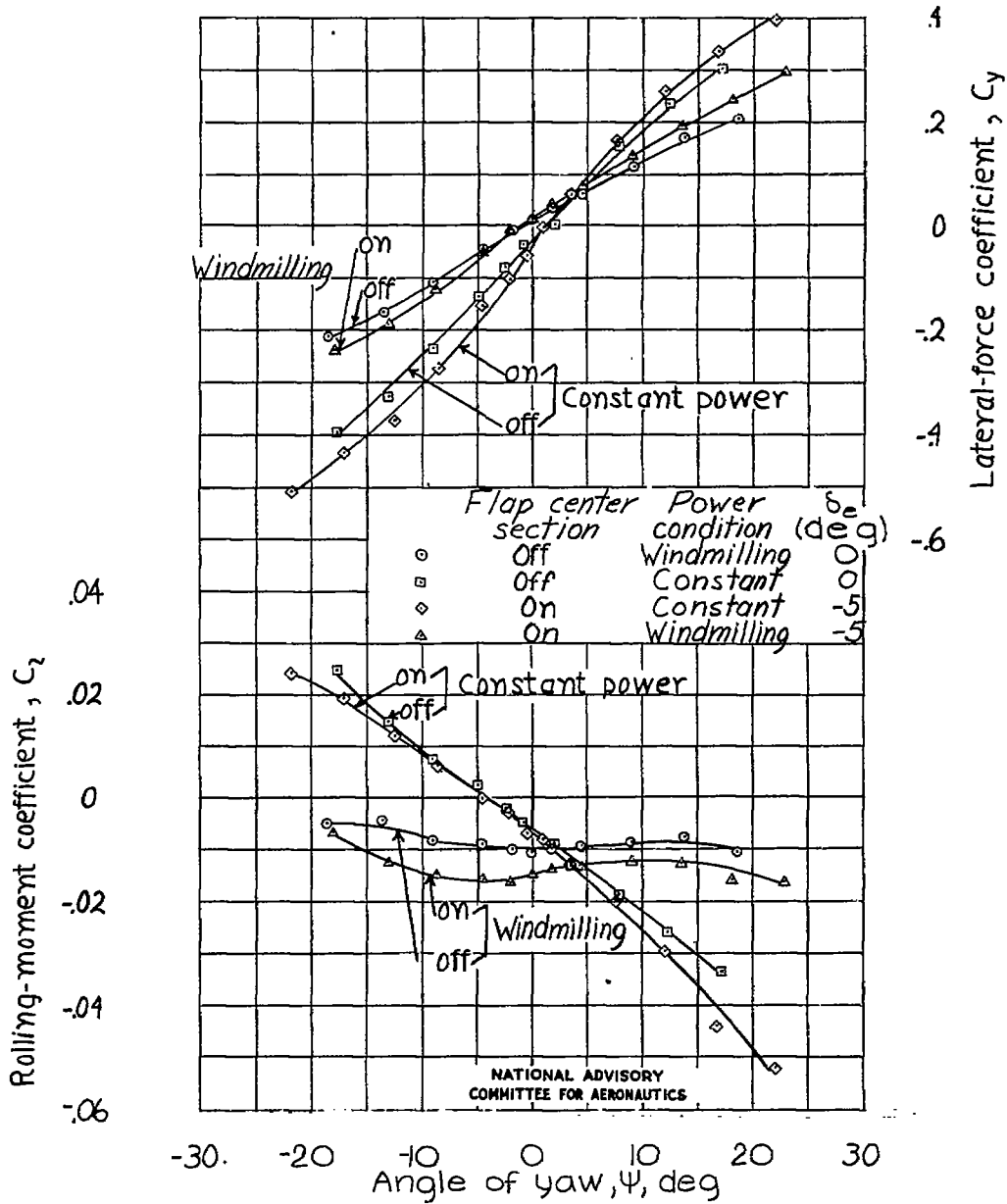
(c) Constant power.

Figure 16.- Continued.



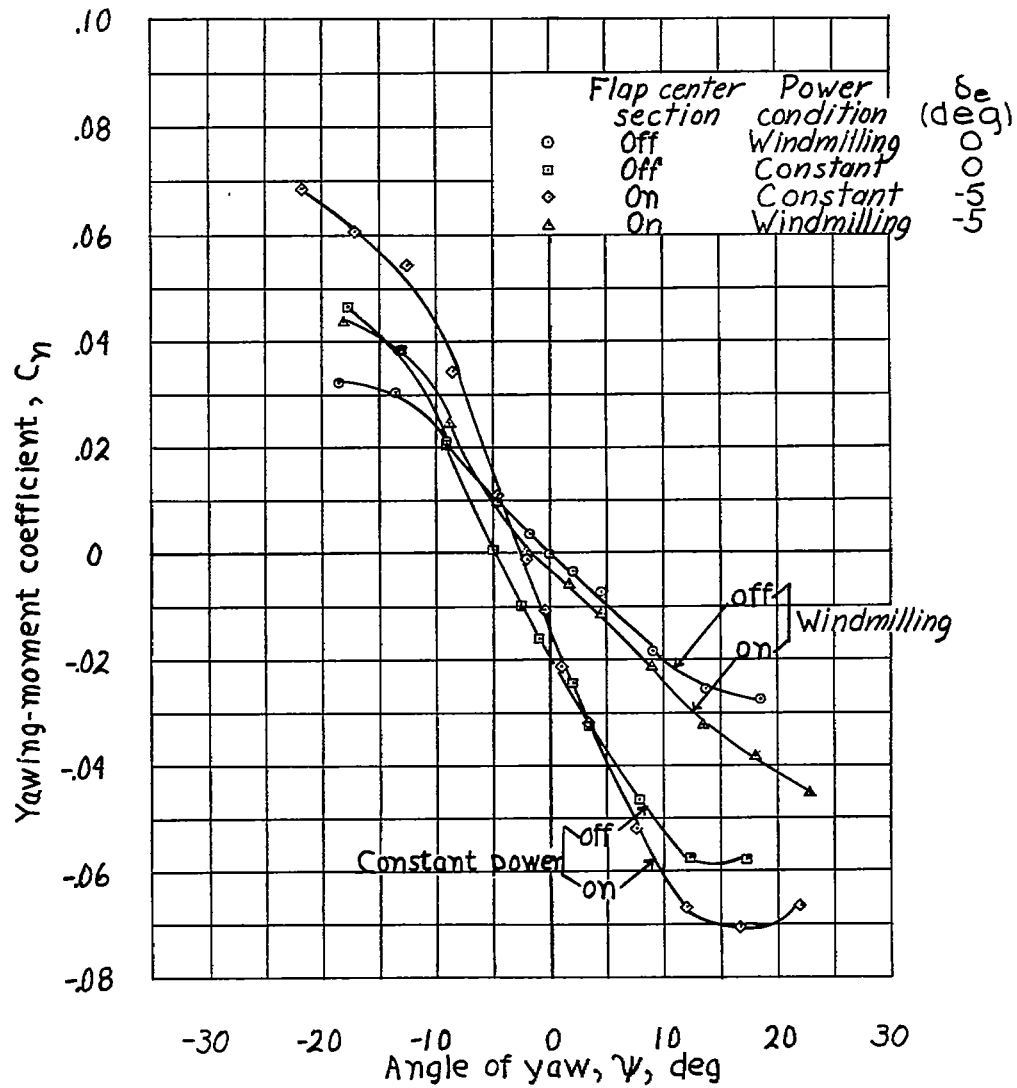
(c) Concluded.

Figure 16.- Concluded.



(a) Effect of removing the flap center section.

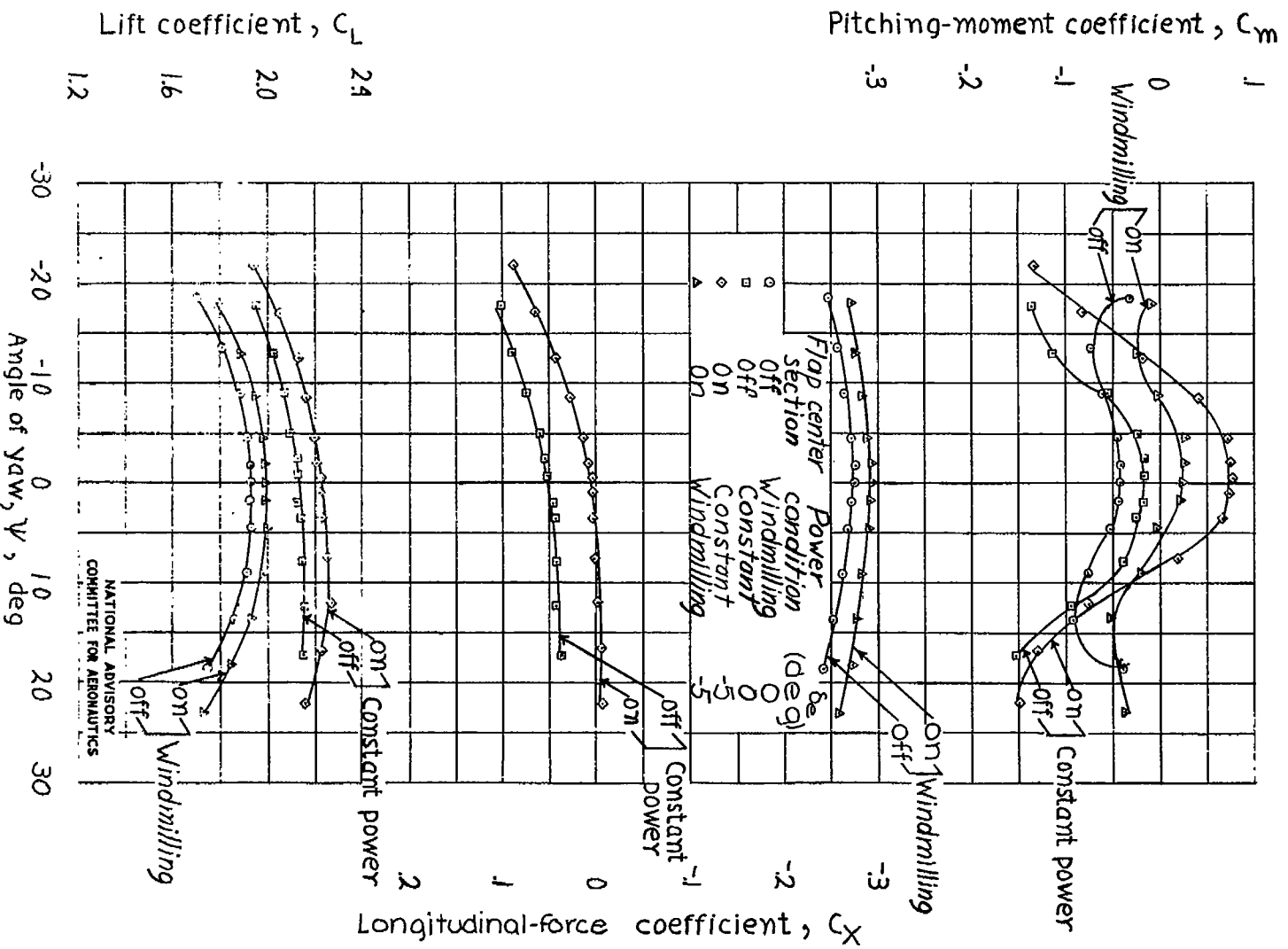
Figure 17.- Effect of model modifications on the aerodynamic characteristics of the model as a low-wing airplane with a full-span single slotted flap. $\alpha \approx 9.6^\circ$; $\delta_r = 0^\circ$.



(a) Continued.

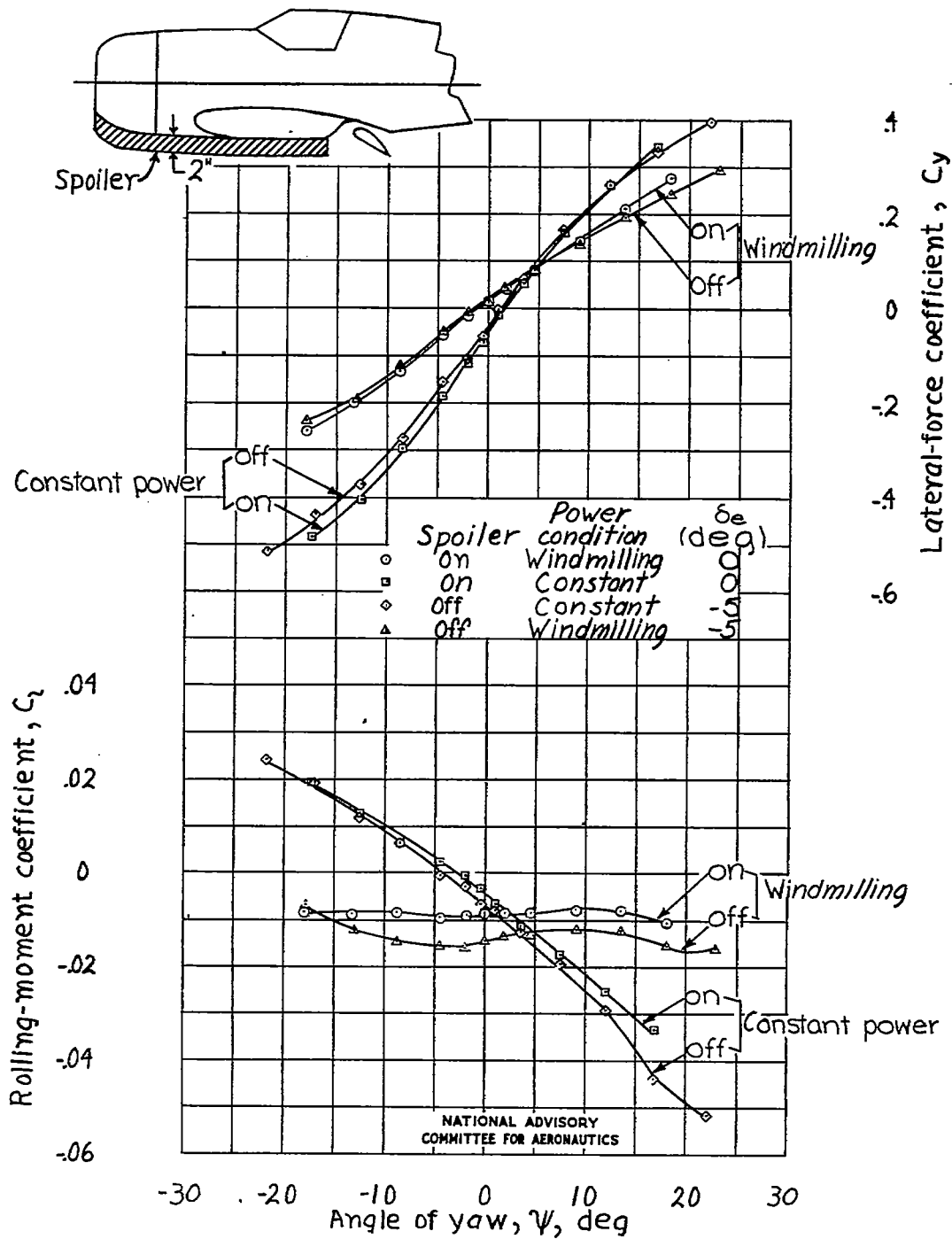
NATIONAL ADVISORY
COMMITTEE FOR AERONAUTICS.

Figure 17.- Continued.



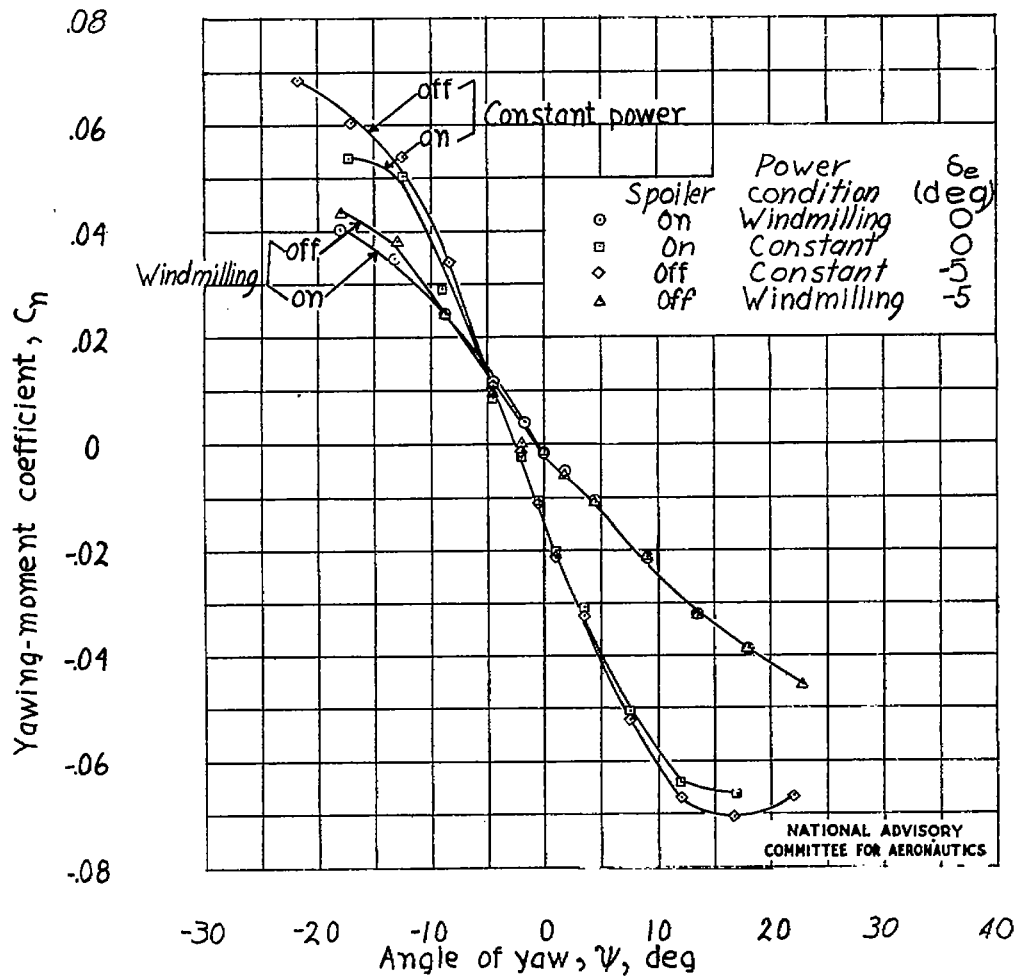
(a) Concluded.

Figure 17.- Continued.



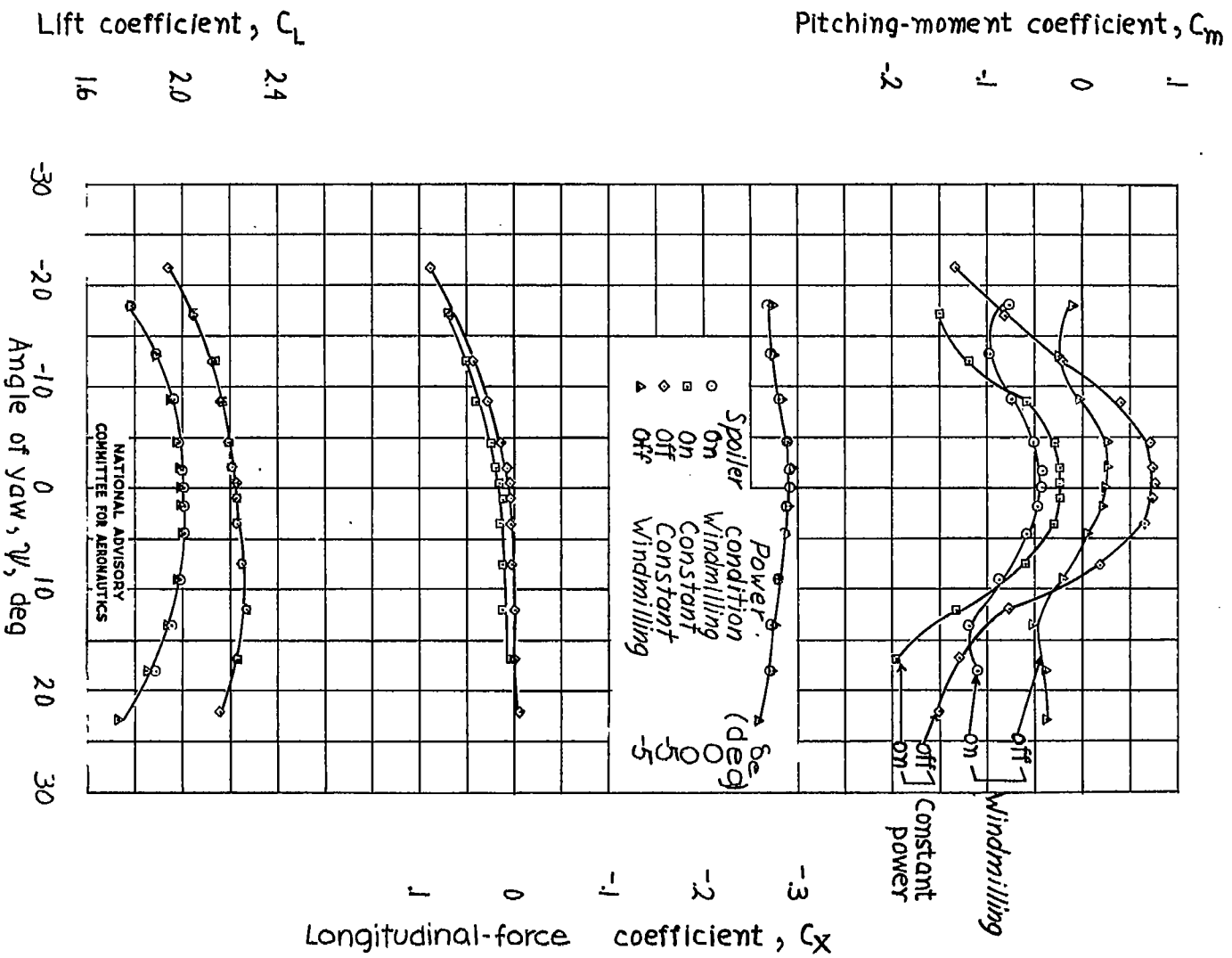
(b) Effect of adding a spoiler.

Figure 17.- Continued.



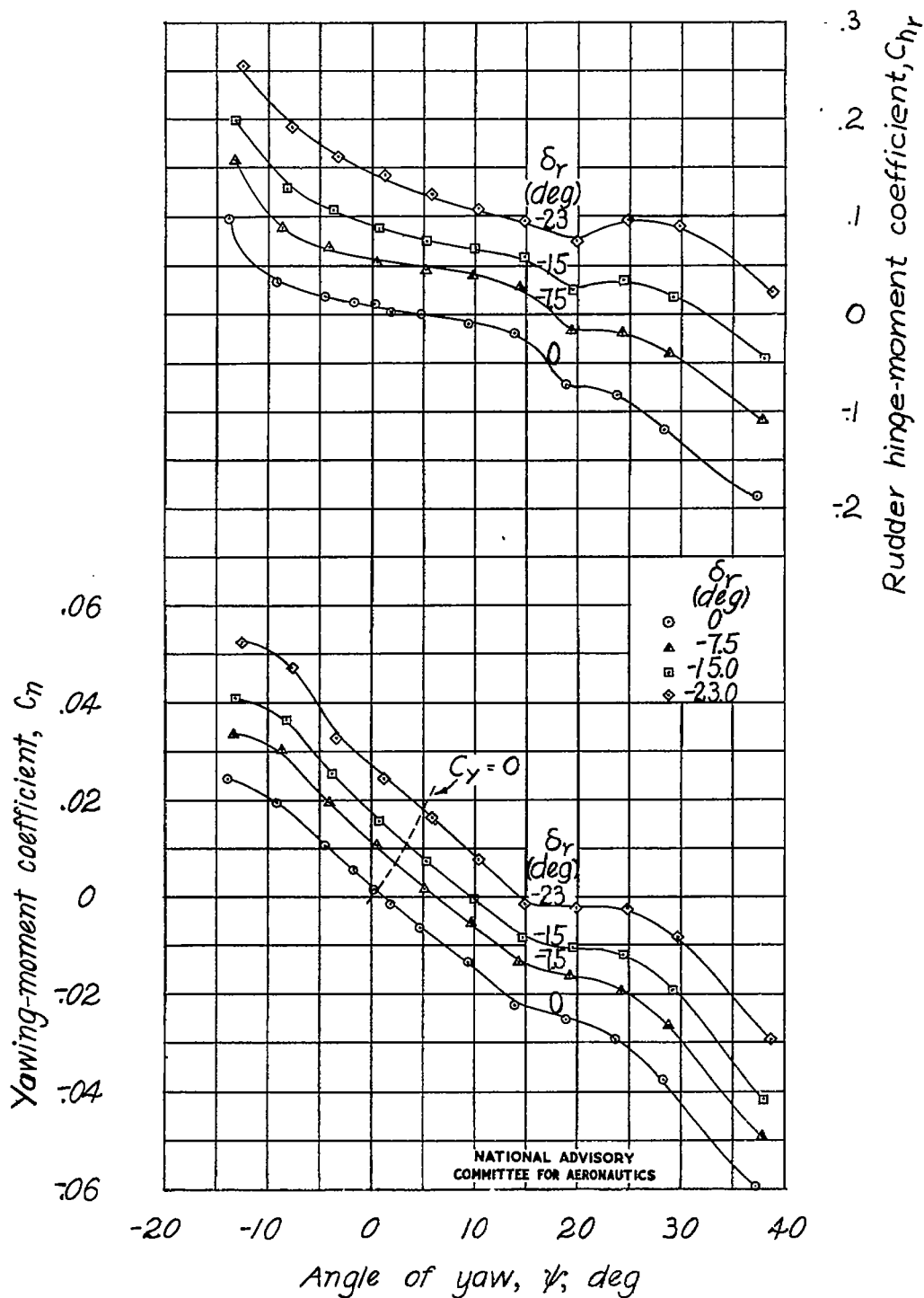
(b) Continued.

Figure 17.- Continued.



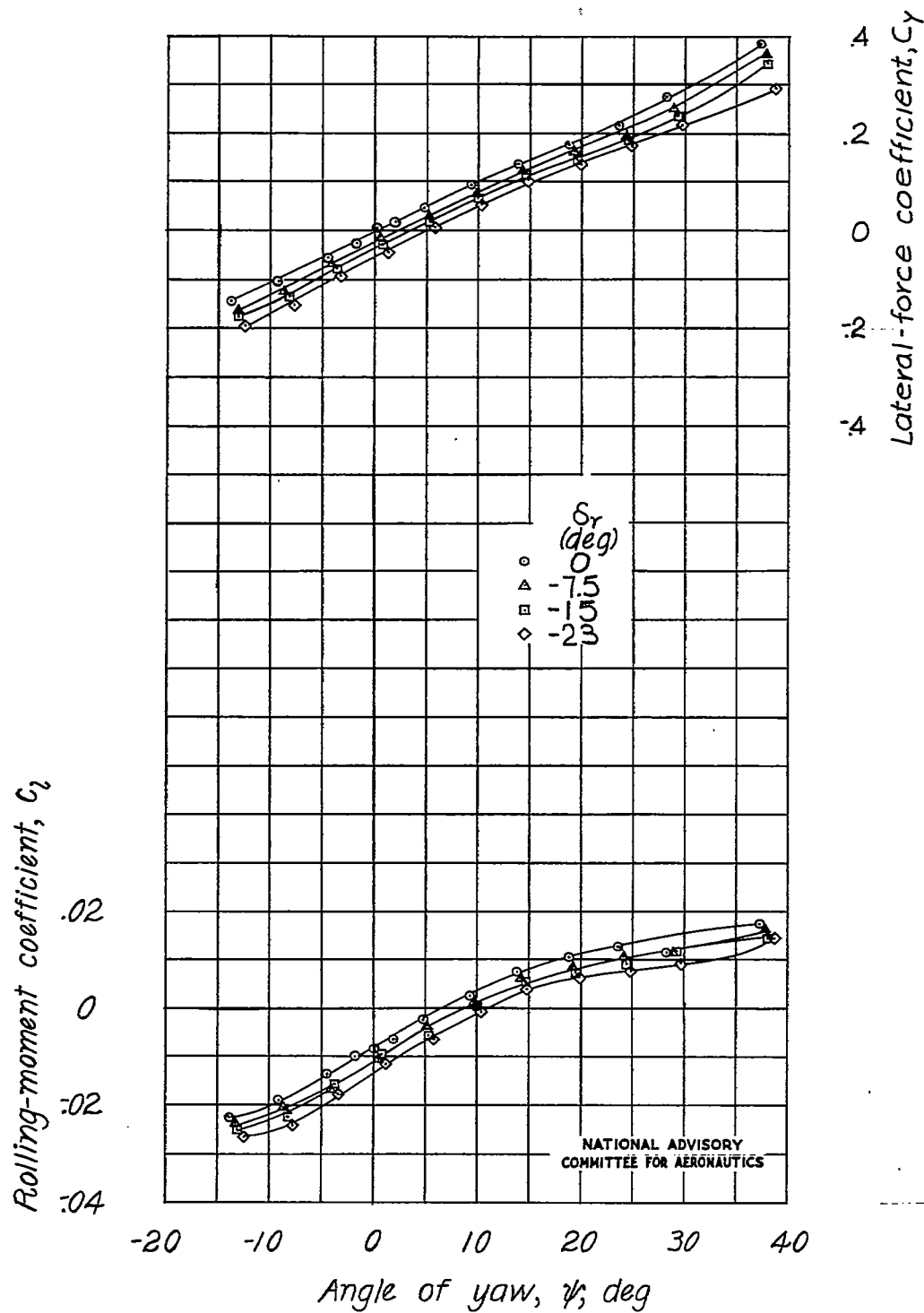
(b) Concluded.

Figure 17. - Concluded.



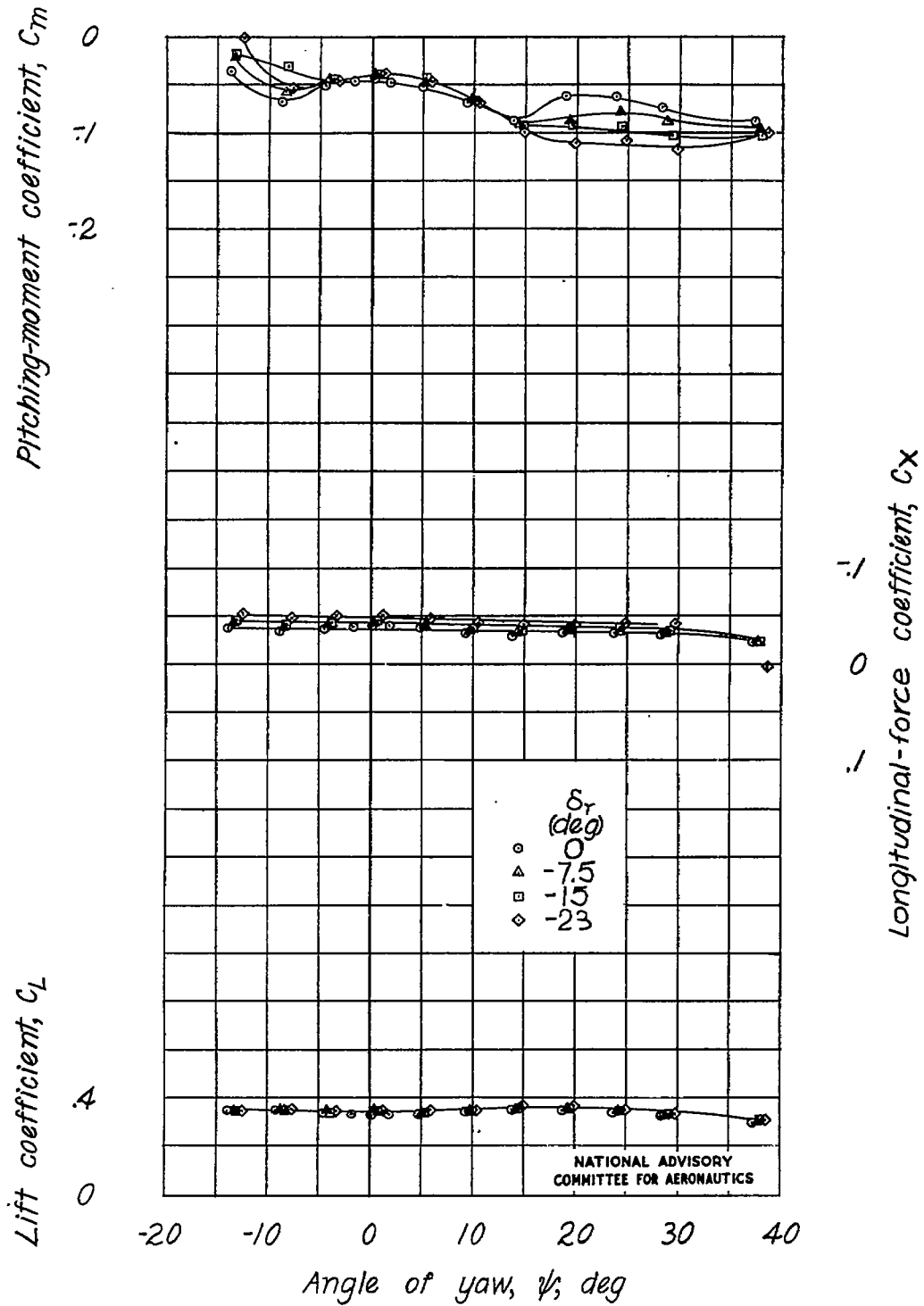
(a) Propeller windmilling.

Figure 18.- Effect of rudder deflection on the aerodynamic characteristics of the model as a low-wing airplane with flap neutral. $\alpha \approx 1.2^\circ$.



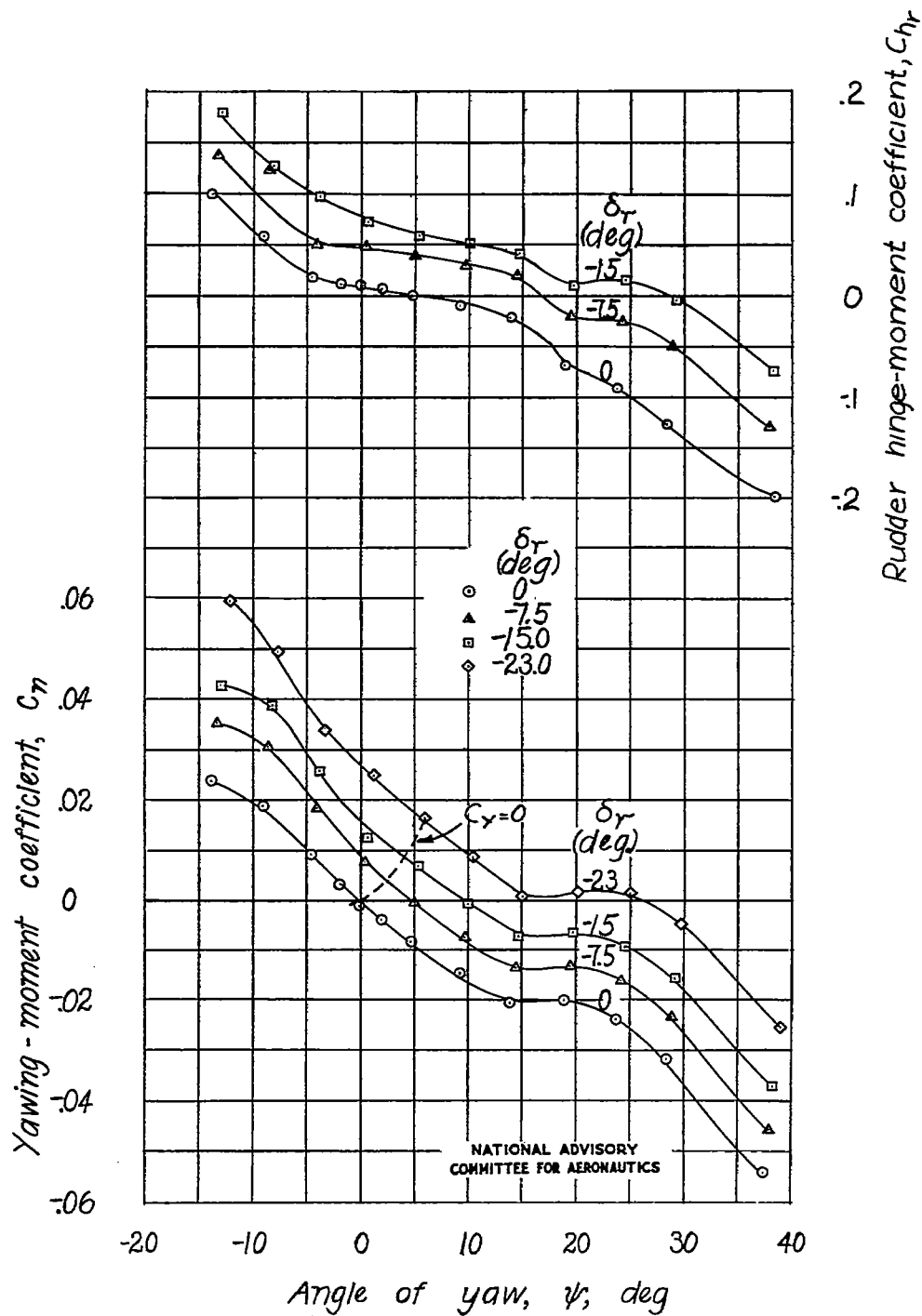
(a) Continued.

Figure 18.- Continued.



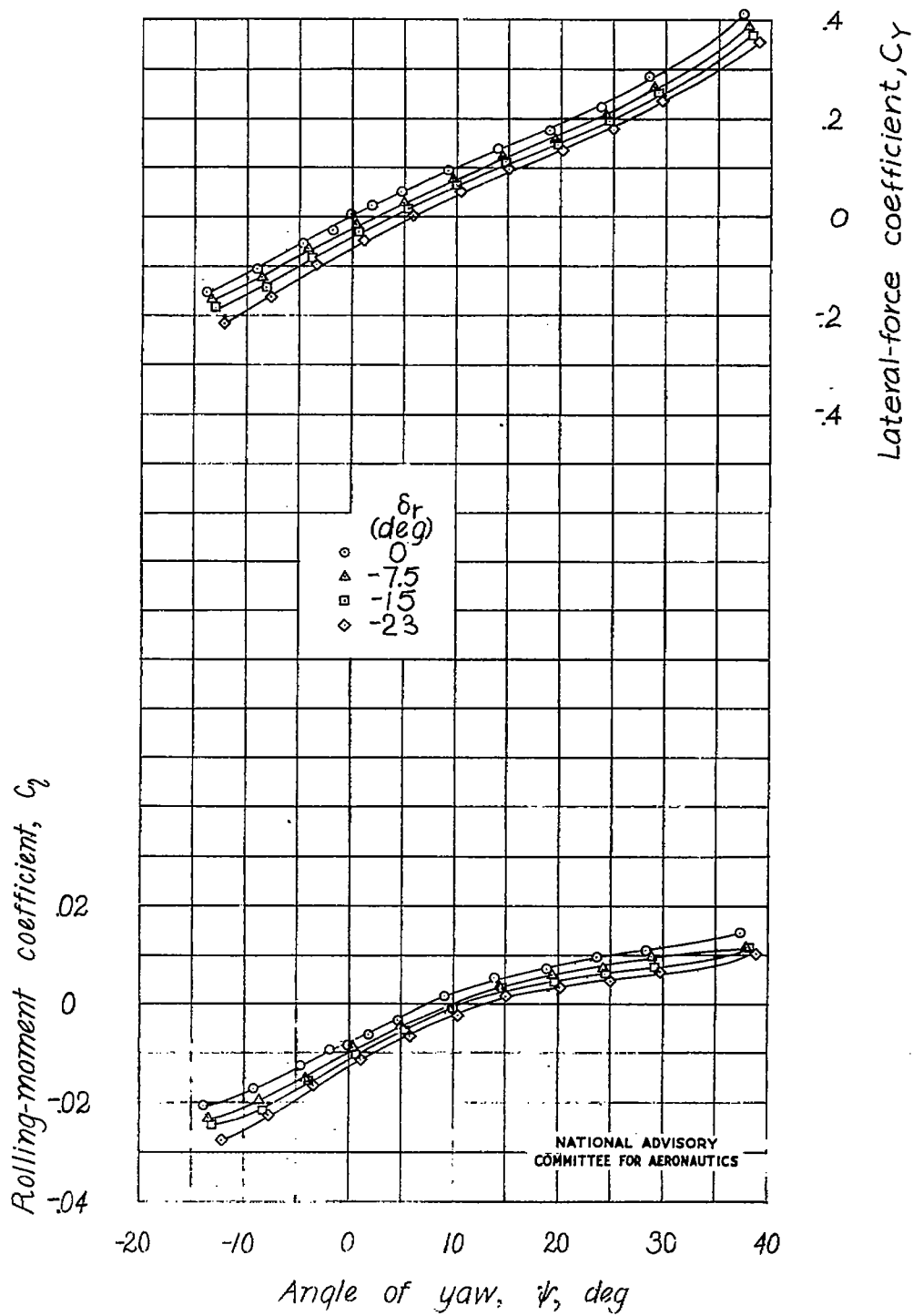
(a) Concluded.

Figure 18.- Continued.



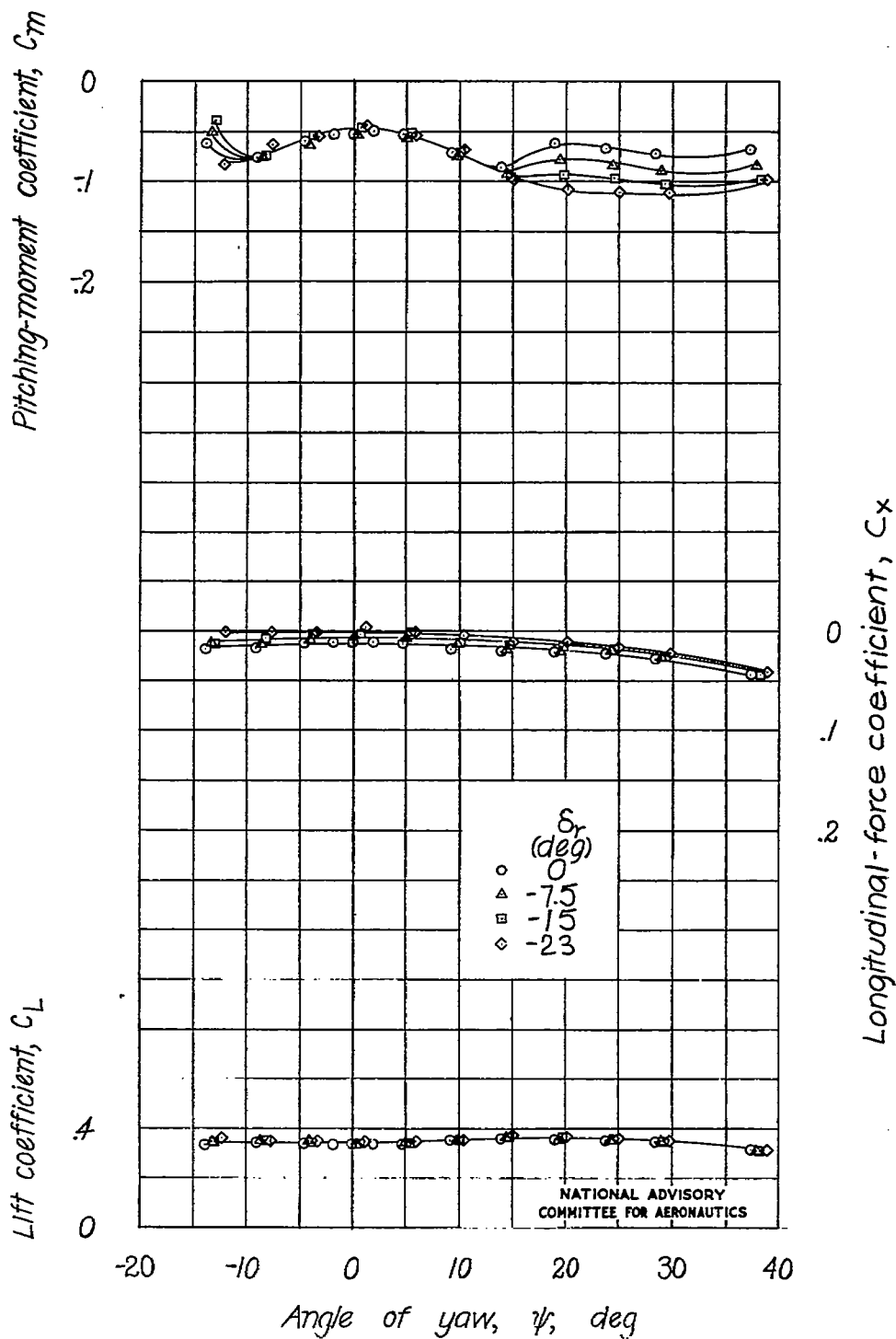
(b) Constant power.

Figure 18.- Continued.



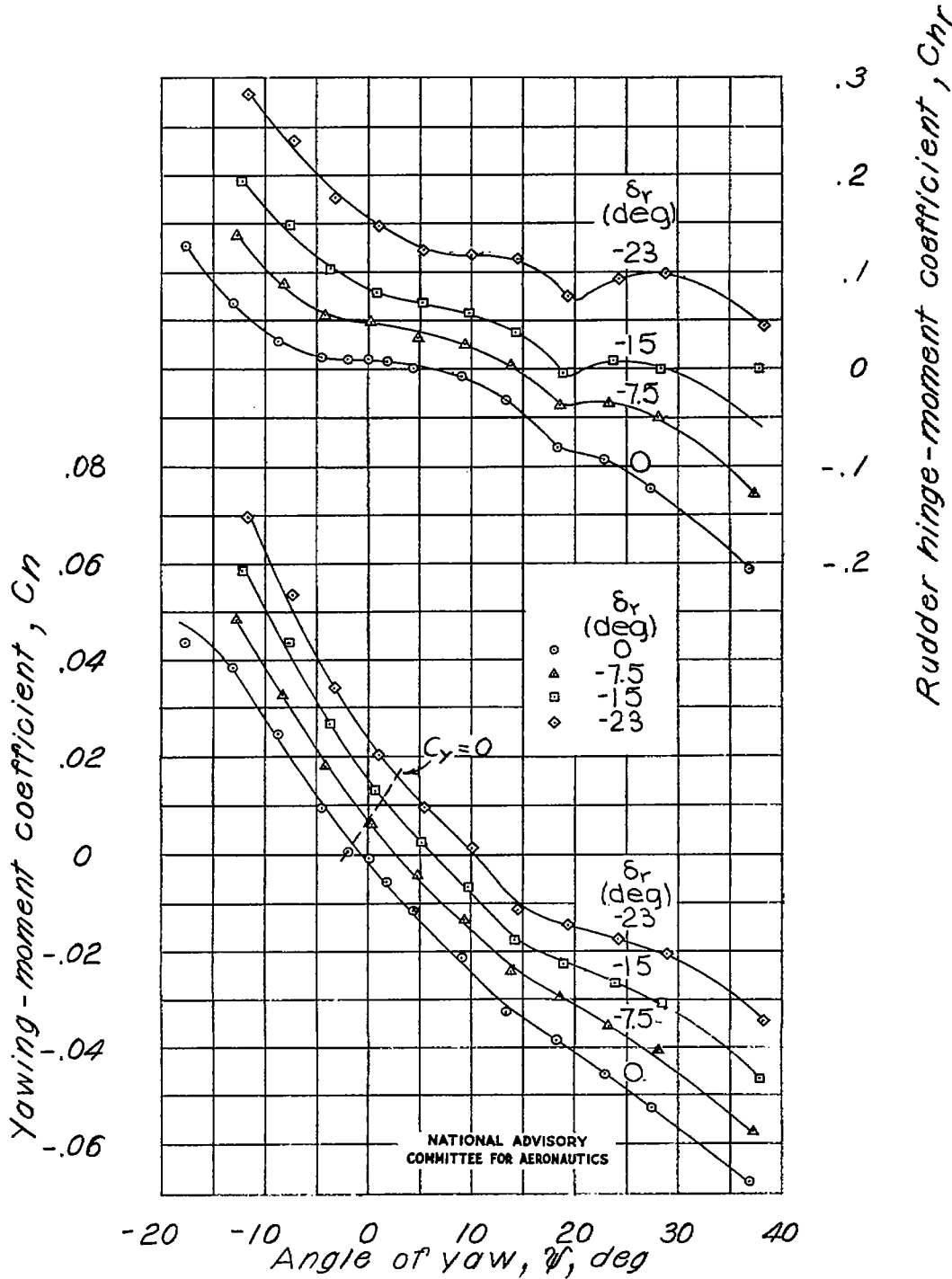
(b) Continued.

Figure 18.- Continued.



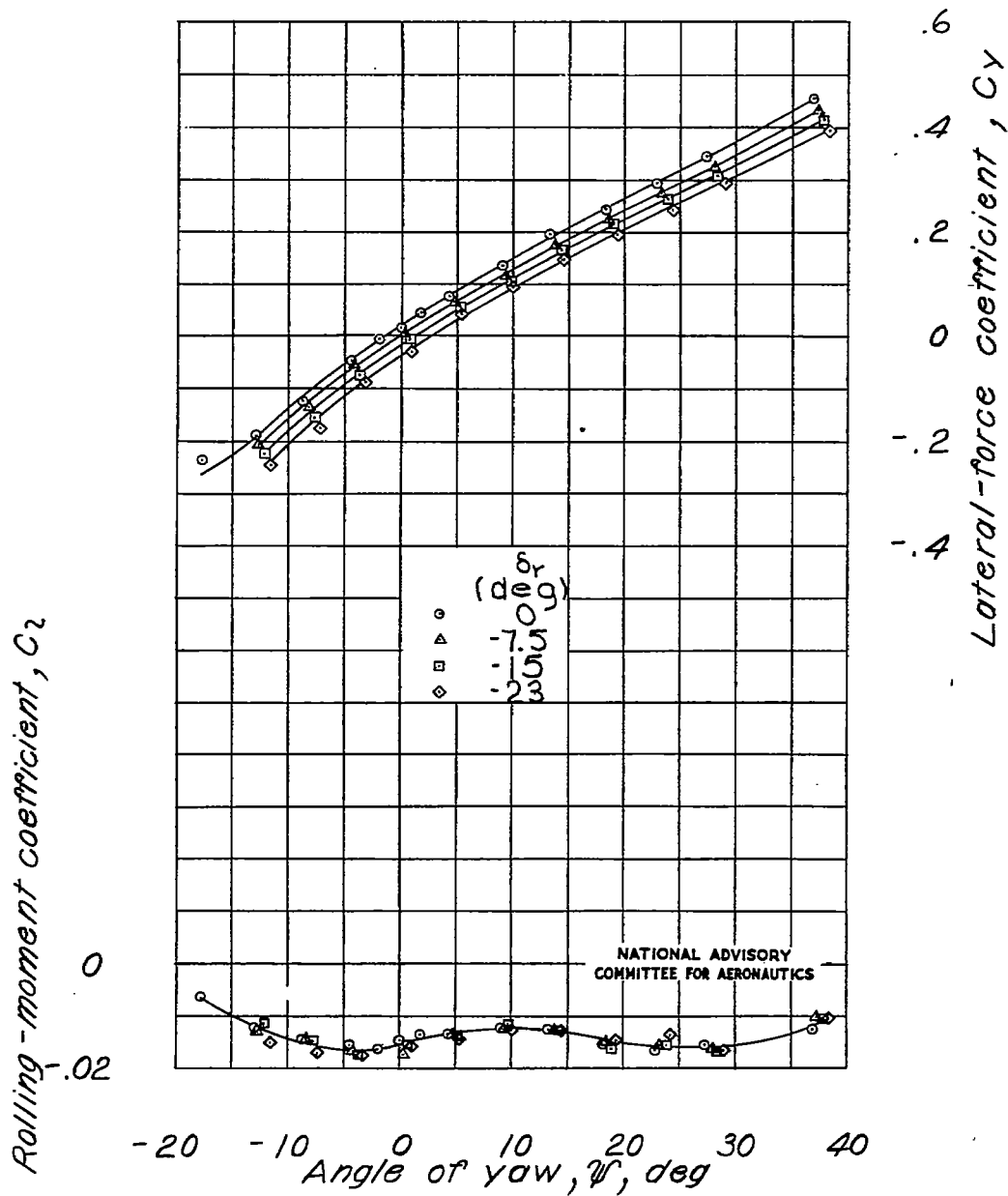
(b) Concluded.

Figure 18.- Concluded.



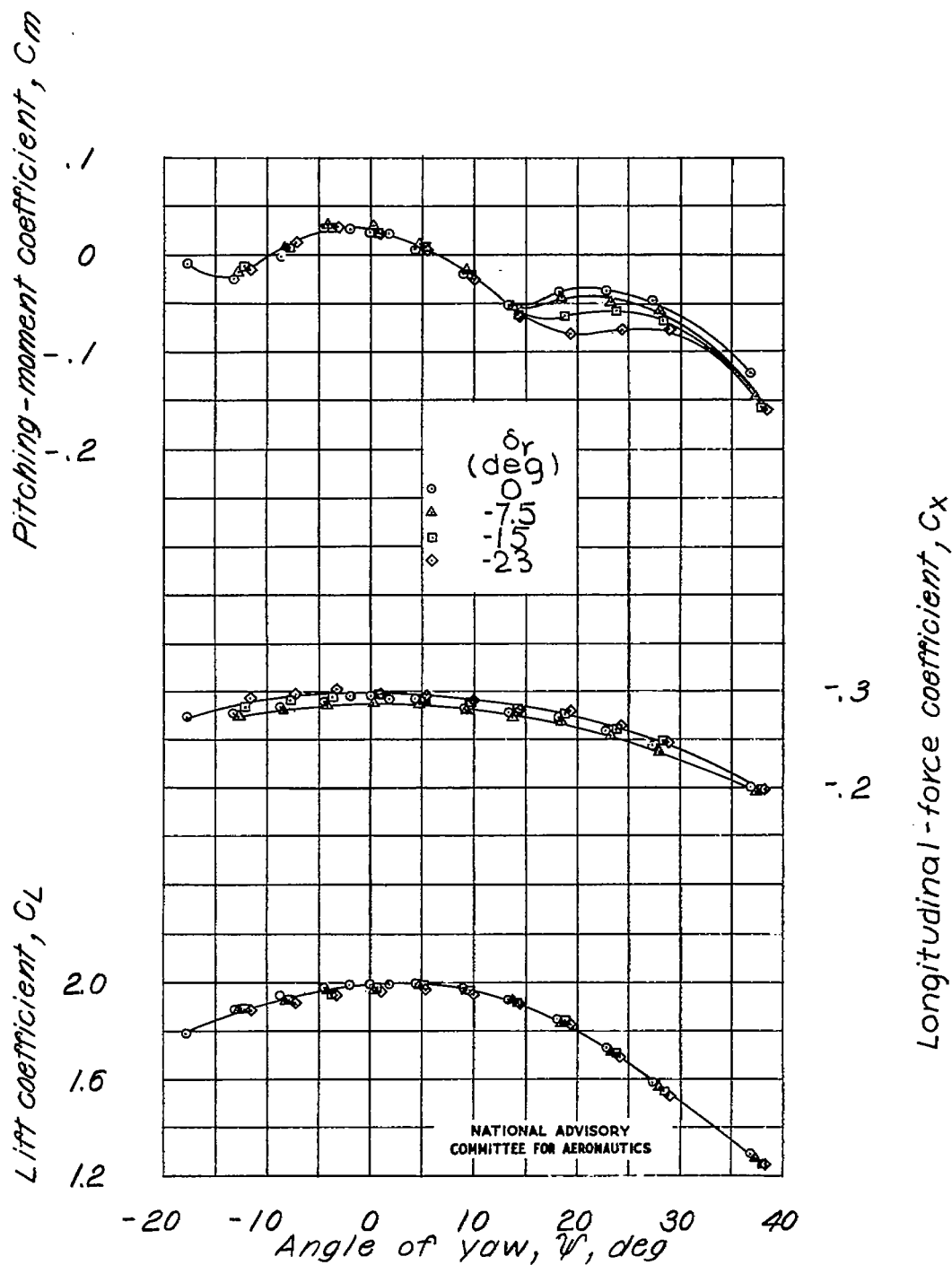
(a) Propeller windmilling.

Figure 19.- Effect of rudder deflection on the aerodynamic characteristics of the model as a low-wing airplane with a full-span single slotted flap. $\alpha = 9.7^\circ$.



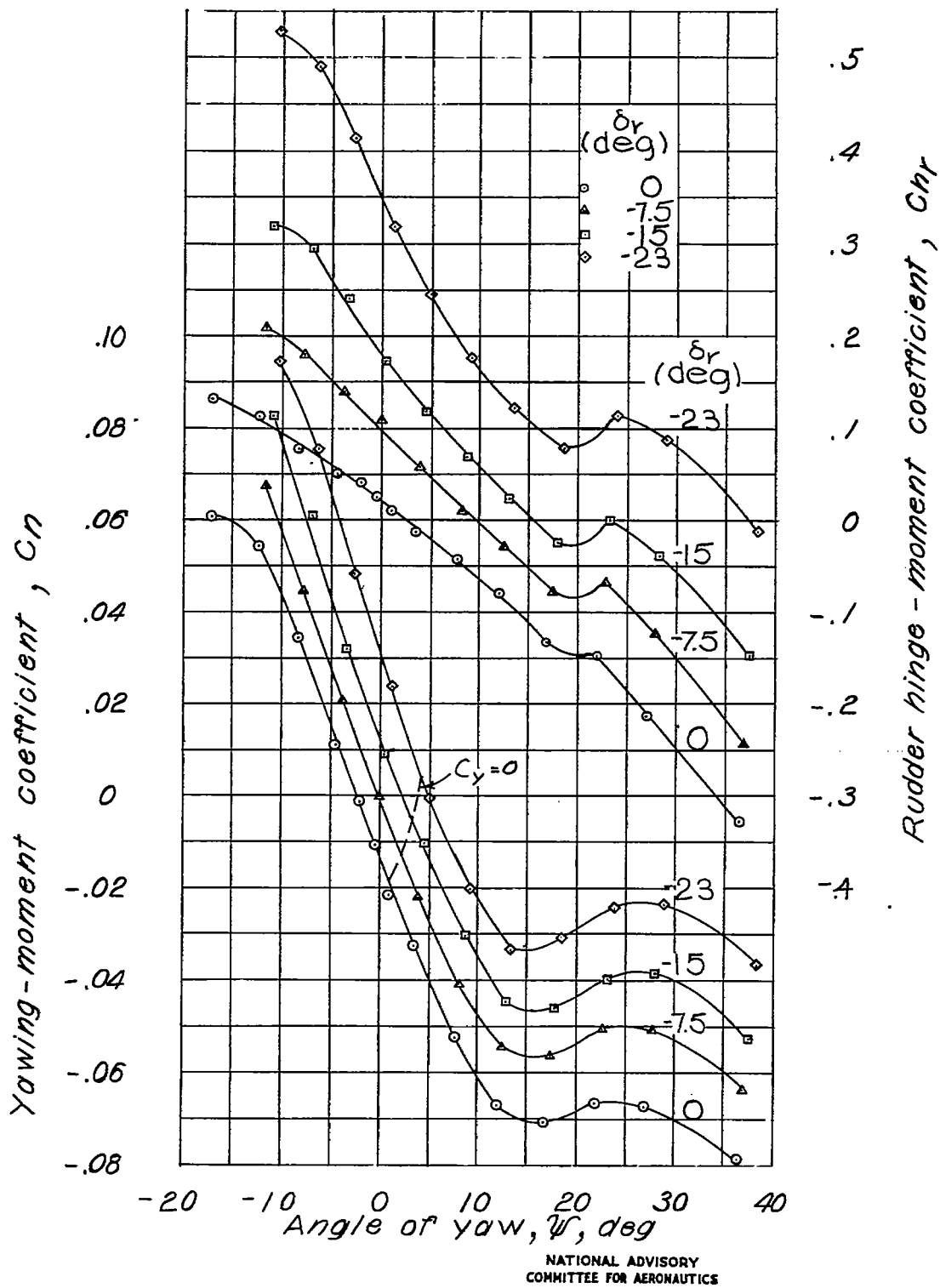
(a) Continued.

Figure 19.- Continued.



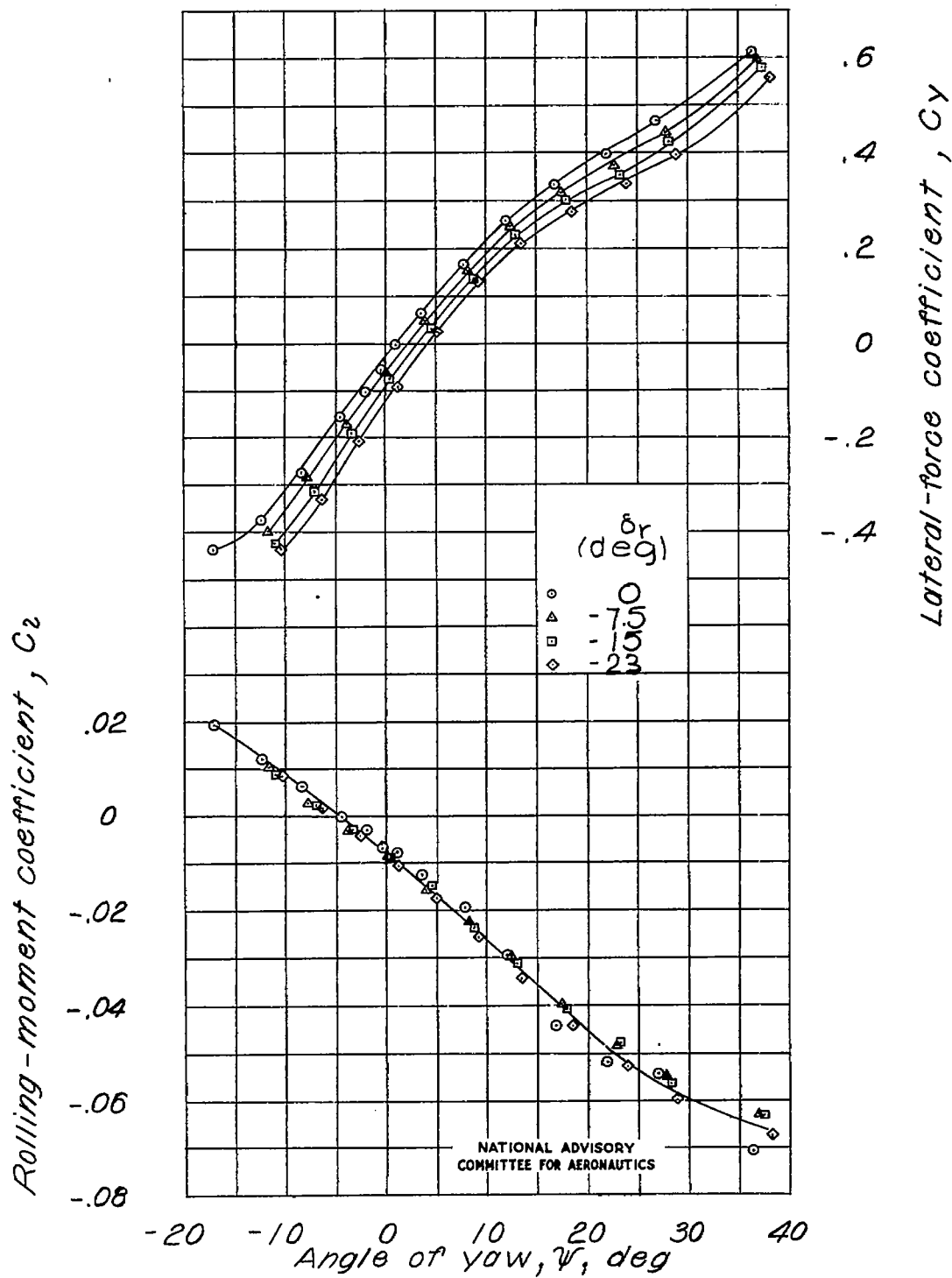
(a) Concluded.

Figure 19.- Continued.



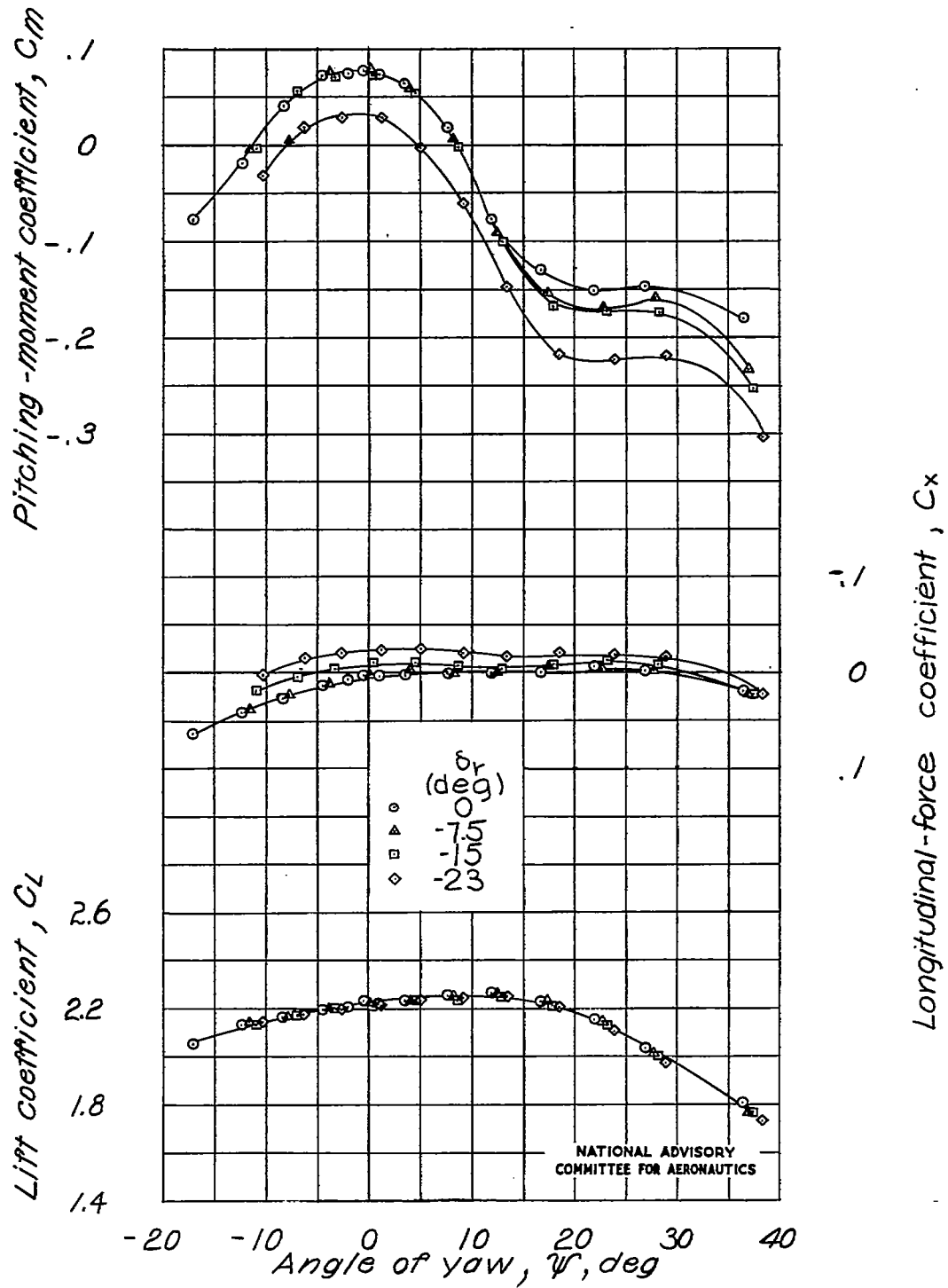
(b) Constant power.

Figure 19.- Continued.



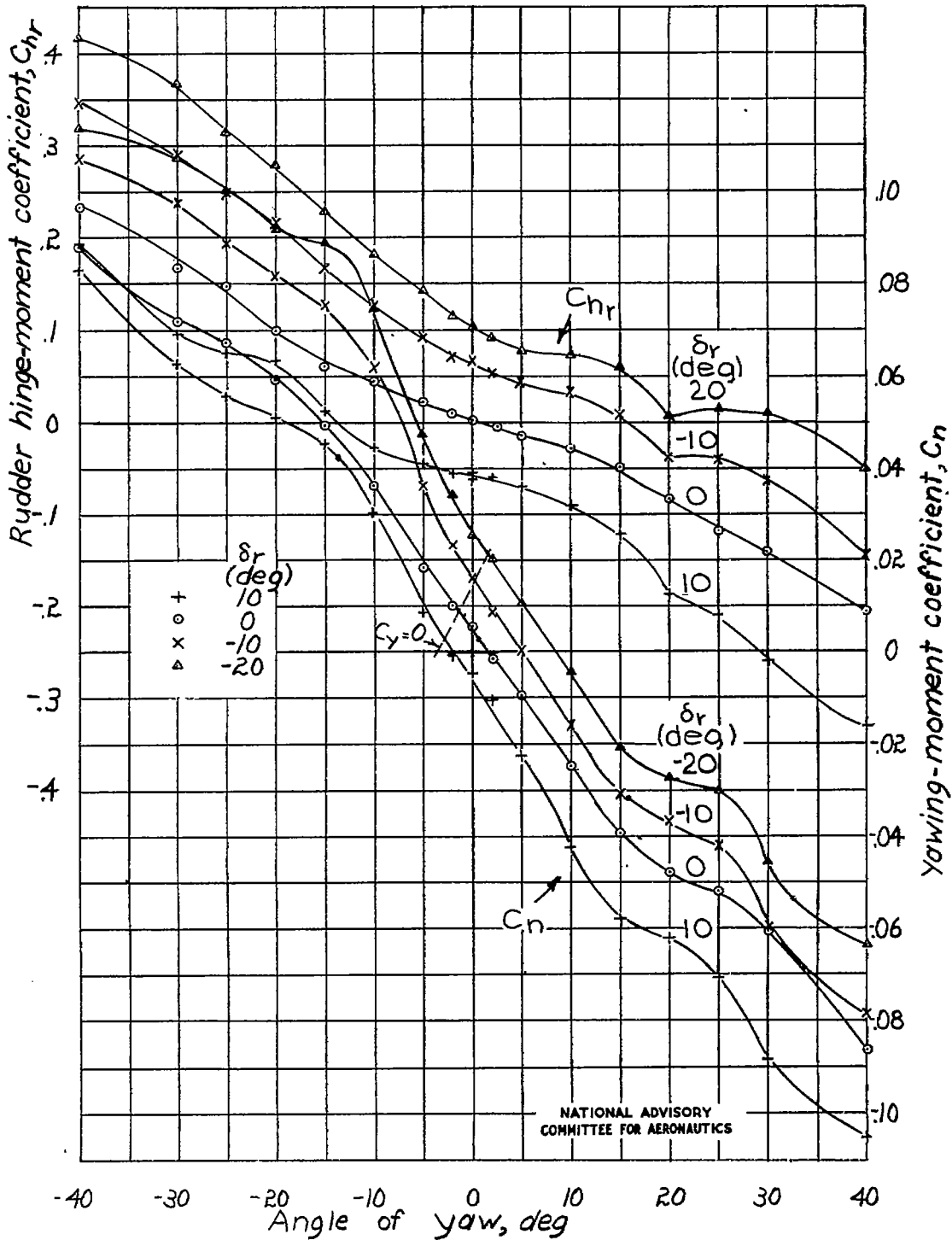
(b) Continued.

Figure 19.- Continued.



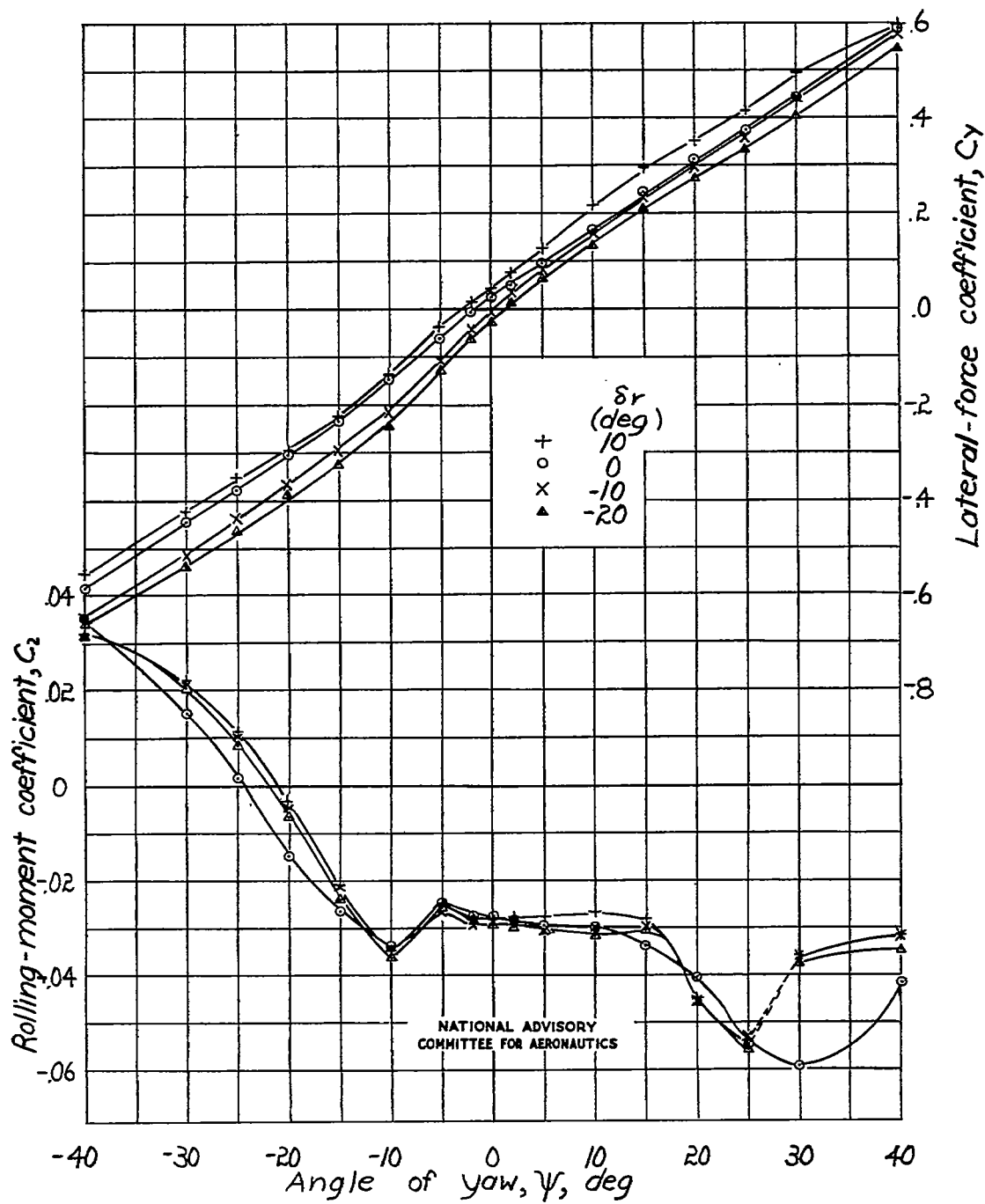
(b) Concluded.

Figure 19.- Concluded.



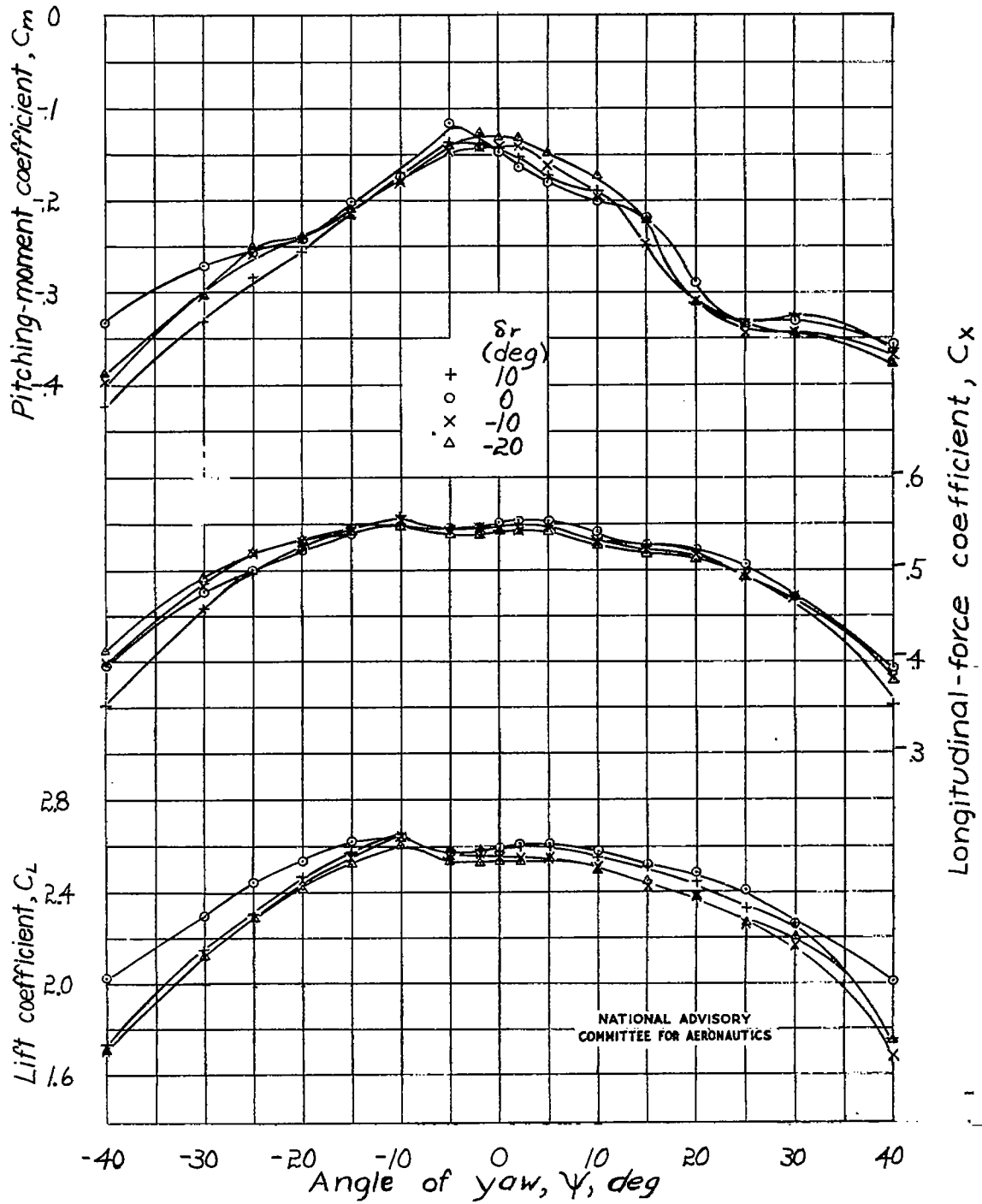
(a) Propeller windmilling.

Figure 20.- Effect of rudder deflection on the aerodynamic characteristics of the model as a low-wing airplane with full-span double slotted flaps. $\alpha \approx 7.3^\circ$.



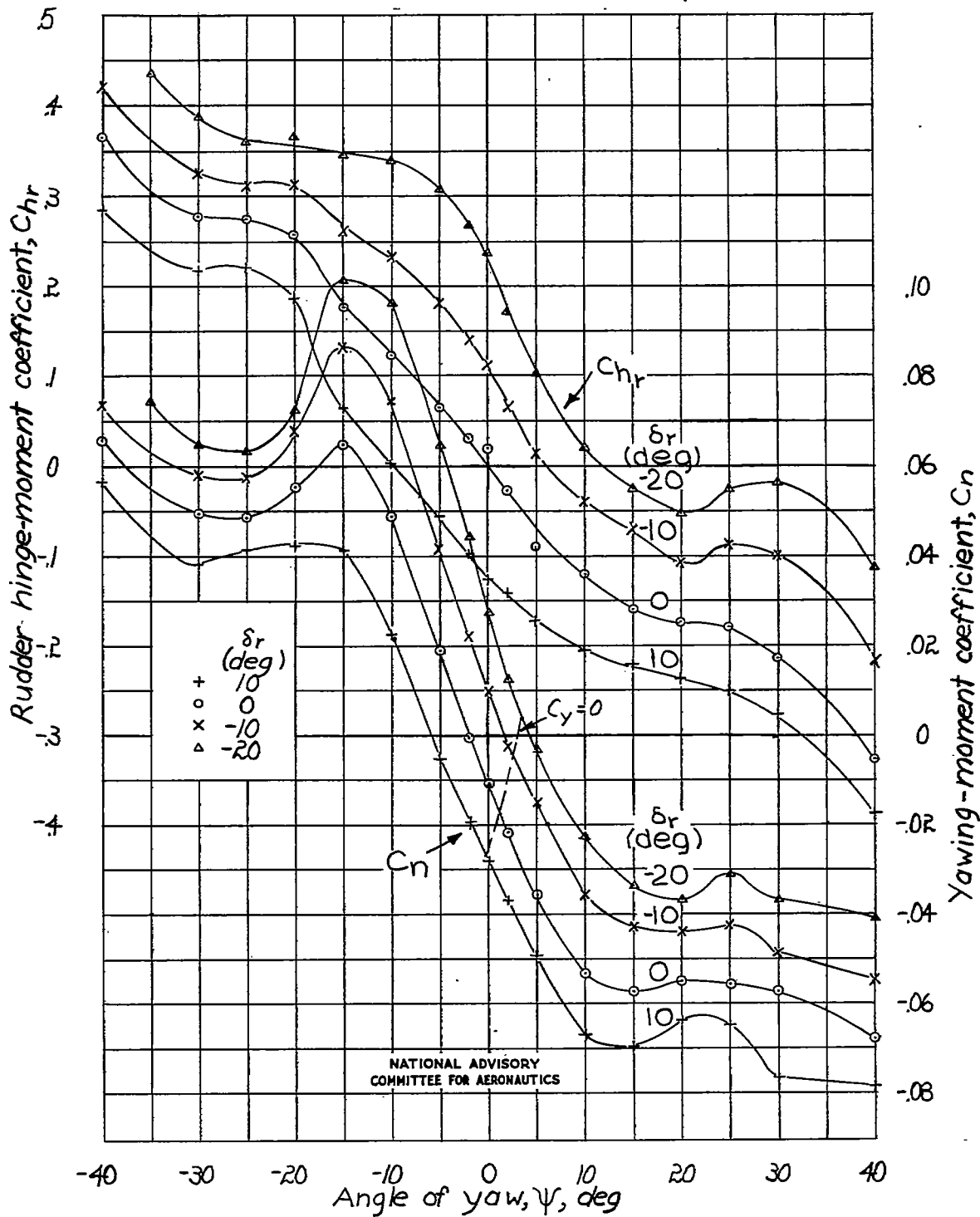
(a) Continued.

Figure 20.- Continued.



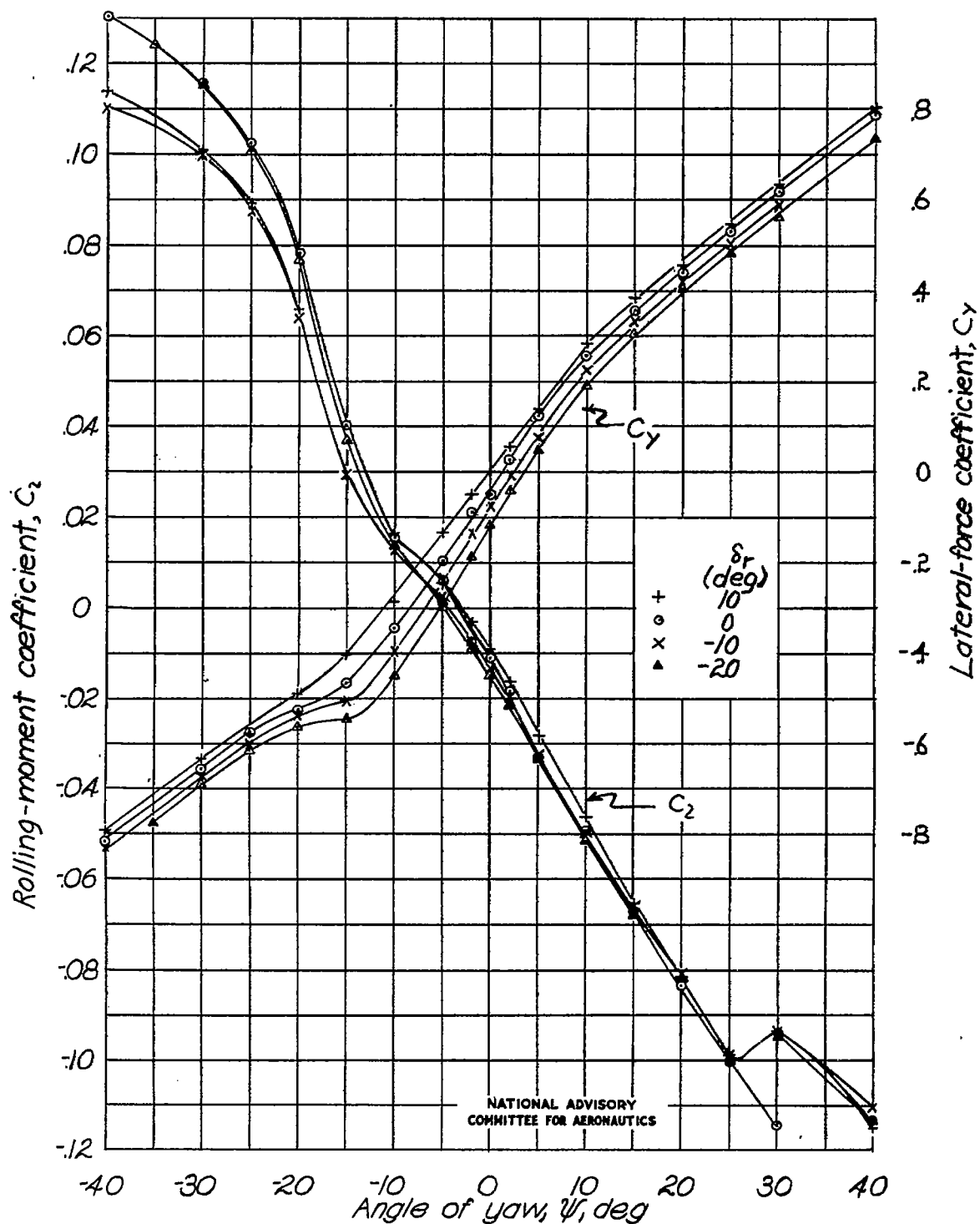
(a) Concluded.

Figure 20.- Continued.



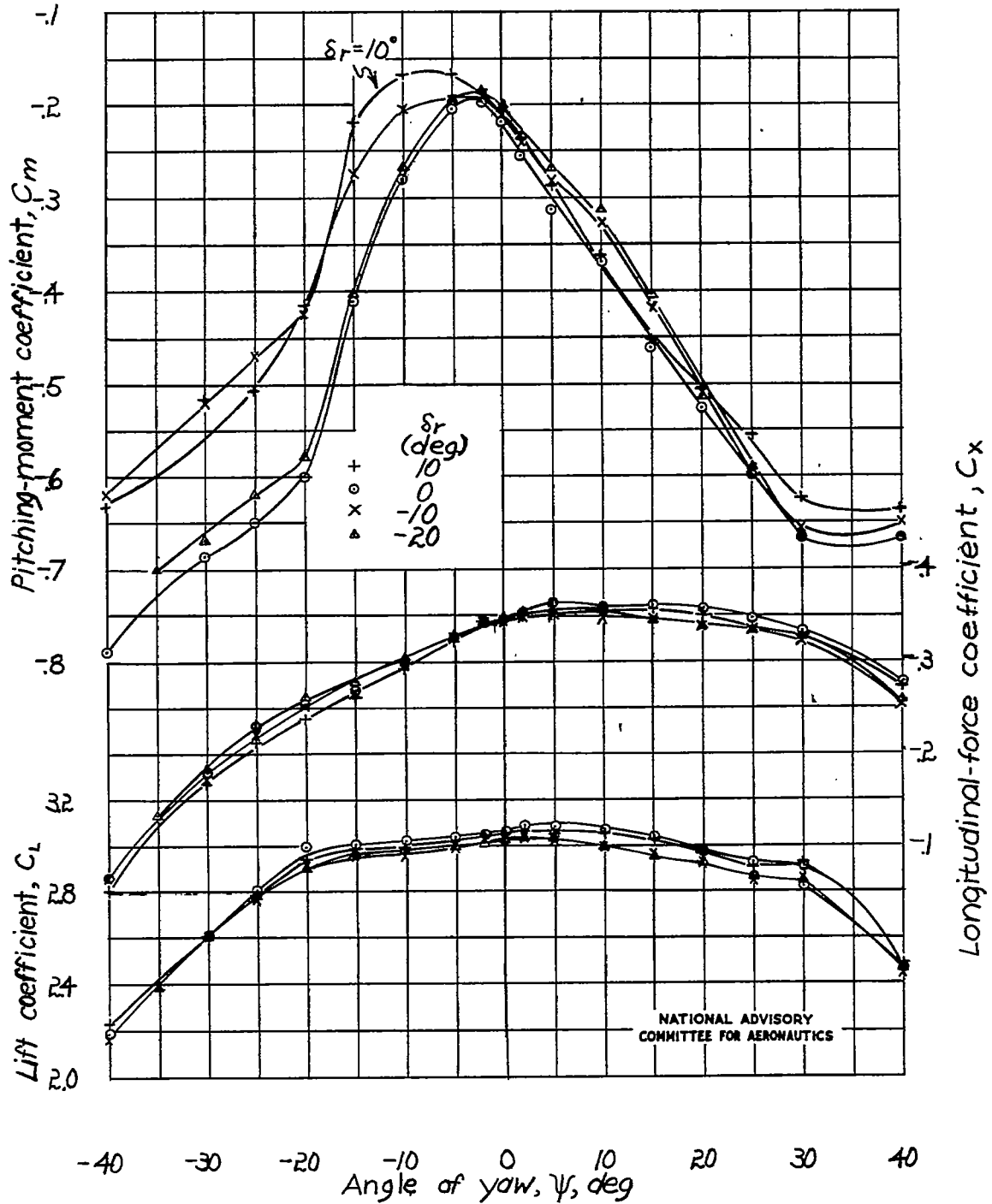
(b) Constant power.

Figure 20.- Continued.



(b) Continued.

Figure 20.- Continued.



(b) Concluded.

Figure 20.- Concluded.